METALLIC CLUSTER FORMATION IN GLASSES

BY

JOHN S. RICH

A THESIS

SUBMITTED TO THE FACULTY OF

ALFRED UNIVERSITY

IN PARTIAL FULFILLMENT OF THE REQUIREMENTS
FOR THE DEGREE OF

DOCTOR OF PHILOSOPHY

IN

GLASS SCIENCE

ALFRED, NEW YORK

FEBRUARY, 2011

METALLIC CLUSTER FORMATION IN GLASSES

BY

JOHN S. RICH

B.S. ALFRED UNIVERSITY (2006)

M.S. ALFRED UNIVERSITY (2008)

SIGNATURE OF AUTHOR (Signature on File)

APPROVED BY (Signature on File)
JAMES E. SHELBY, ADVISOR

(Signature on File)
MATTHEW M. HALL, CO-ADVISOR

(Signature on File)
ALEXIS G. CLARE, ADVISORY COMMITTEE

(Signature on File)
WILLIAM C. LACOURSE, ADVISORY COMMITTEE

(Signature on File)
S.K. SUNDARAM, ADVISORY COMMITTEE

(Signature on File)
CHAIR, ORAL THESIS DEFENSE

ACCEPTED BY (Signature on File)
DOREEN D. EDWARDS, DEAN
KAZUO INAMORI SCHOOL OF ENGINEERING

ACCEPTED BY (Signature on File)
NANCY J. EVANGELISTA, ASSOCIATE PROVOST
FOR GRADUATE AND PROFESSIONAL PROGRAMS
ALFRED UNIVERSITY

ACKNOWLEDGMENTS

I would like to thank my parents for supporting me throughout this experience. Without you both, this would not have been possible. I would like to thank my friends. You all made my time in Alfred worth remembering. And last, but certainly not least, I would like to thank Dr. Shelby for being there for me when he could.

TABLE OF CONTENTS

LIST OF TABLES

Page

LIST OF FIGURES

Page

ABSTRACT

Hydrogen reactions with glasses containing different metallic ions were investigated. Hydrogen successfully reduced Ni, Co, Cu and Pb in soda-lime-silica glasses at a range of different temperatures (500°C, 550°C, 600°C, and Tg). The tarnishing model was successfully applied to account for the increase in the "free hydroxyl" absorption band at high reaction temperatures. At lower temperatures, it was shown that nickel and cobalt absorbance data did not follow the tarnishing model, most likely due to the slow reaction rates involved with reducing these ions and a dehydroxylation mechanism. The permeability of hydrogen molecules was calculated from the absorbance data and found to be ~30 times lower than that reported in the literature. This was again explained by a dehydroxylation mechanism. A possible interaction between the metallic clusters and the glass matrix was identified for the lead containing glass. This interaction is most likely an interfacial bond between the cluster and the glass which results in a stretching of the lead lattice upon cooling.

Hydrogen also reduced indium in a series of sodium-indium-silicate glasses over a range of temperatures (500°C, 550°C, 600°C, and Tg). The indium containing glasses all exhibited an increase in the absorbance of the "free hydroxyl" band with the square root of reduction time, but the trends with temperature were inconsistent. This was explained through an enhanced dehydroxylation mechanism due to the high concentrations of hydroxyl being formed in the glass. These glasses also exhibited a clear property change (viscosity, Tg, durability, thermal expansion) at the surface due to the removal of indium leaving residual soda-silicate glass in the composition region of immiscibility. Hydrogen induced formation of alloys of nickel and copper was also demonstrated. The reaction rate had little effect on alloy formation and as long as the metals in question will form an alloy and diffuse at the treatment temperatures, an alloy composition is possible. This opens up the door for a variety of new, unexplored, bulk properties for glasses ranging from magnetism to catalysis.

1. INTRODUCTION

Nanometer sized metallic particles, commonly referred to as clusters, have been used for hundreds of years to induce colors in glass, yet they are still not completely understood.[1-3] While shades of yellow, red and brown are easily produced; the potential of metallic clusters for coloration in glasses has only begun to be realized. Colloidal solid solution alloys can potentially be tailored to absorb over different regions of the visible spectrum resulting in endless combinations of color. When glasses contain two or more reducible species, clusters may form as individual particles, layered aggregates, or solid solution alloys.[4-8] Solid solution alloys of nickel and cobalt, which exhibit a wide range of Curie temperatures and magnetic susceptibilities, have been recently created at Alfred University by a number of researchers.[4-7] Oddly enough, elements such as Bi, Pb, and In have been found to reduce when heated above their melting temperatures.[9-11] They coalesce as nanodroplets of liquid metal inside the glass, the droplets then crystallize during cooling. Germanium may be reduced in glass to form distinct colloids or a continuous semiconducting film.[12,13] Germanium colloids are also of considerable interest due to their luminescence and charge retention properties that make them useful for integration into photonic and semiconductor technologies. Phase separated glasses containing a germanium rich phase have the potential to form continuous nanowires throughout the bulk glass.

This thesis is divided into three sections based on the ions being reduced and the goal of the individual reduction experiments. Indium reduction is discussed first in terms of the tarnishing model and SEM work. The reduction of various 2^+ ions is discussed in terms of the tarnishing model and the issue of reaction rate is made apparent. The simultaneous reduction of nickel and copper is the third, and final discussion. Glasses containing these metallic ions will reduce to form alloys if the conditions are appropriate, and this redefines the accepted rules for hydrogen induced alloy formation in glasses.

2. LITERATURE REVIEW

2.1 Introduction

Metallic clusters have been used for hundreds of years to produce coloration in glasses. One of the oldest known examples of this coloration is that of gold ruby glass. This well-known brilliant ruby coloration in glasses is typically attributed to the presence of fine metallic gold particles dispersed in a glassy matrix.[9,14] The complex scattering and absorption of light by the small gold clusters is responsible for this red coloration.[15-17] The true discovery of gold ruby glass is often associated with the names of Andreas Cassius and Johann Kunckel.[18-20] Cassius and his son studied the preparation and formation of a red mixture via the addition of dilute solutions of gold chloride to stannous chloride. This mixture produces a gold hydrosol, often referred to as Purple of Cassius, which consists of stannic acid and metallic gold clusters in water. Cassius and his son added this mixture to a glass melt effectively adding gold and tin to the composition of the glass. Cassius noted that the cooled glass was colorless and that only by reheating would the glass become red. He described this in his article "De Auro" (1685). Kunckel described methods of preparation and even some properties of gold-ruby glass (1679)[2,18-20]. He was even able to make gold-ruby glass on a commercial scale prior to the 1700's and produced beautiful pieces that can be found to this day. However, Kunckel did not master the process, most likely due to an incomplete understanding of the complex chemistry behind this method of inducing color, and had to scrap a large amount of his gold-ruby glass product. Kunckel was the first recorded person to be able to develop and produce large and sometimes-complex glassware made of this gold-ruby glass. There is some limited mention of red mixtures based on gold prior to the work of Kunckel and Cassius. The writings of Glauber, Valentinus, Libavius, Roman discoveries from the 4th century (Lycurgus Cup), some Egyptian manuscripts, and even some Assyrian tablets describe the production of gold-ruby colored mixtures, and some even indicate forming gold-ruby glasses.[1,3,18,19,21] Clearly metallic clusters in glasses have been of interest for many years before our modern era.

Most metallic ions are soluble, to some degree, in a glass melt, especially at high temperatures. As the glass is quenched to room temperature, these ions generally remain in solution, but a variety of methods have been employed to nucleate and grow metallic clusters within a large variety of glass compositions.[9,11,19] For the purpose of this review, the term cluster will be used to represent a particle containing more than a single atom.

2.2 Hydrogen Diffusion

Hydrogen diffusion and reactions with glass have long been studied. To be able to fully describe all of the appropriate phenomena related to this work, it is important to address the different terminology typically used. The diffusivity (D) is often described as an atomic, or molecular, rate of movement (cm^2/s). Permeability (K) is a steady state flow rate through a material (molecules/atm-sec-cm). Solubility (molecules/cm^3-atm) is the concentration of gas that is dissolved into the interstitial free volume of a material. The permeability, by definition, is the product of the diffusivity and the solubility.[22]

Diffusion of gases through a glass membrane occurs in several steps. The process is thought to initiate with the impact of the gas molecule or atom in question with the surface of the glass membrane. This impact is followed by the adsorption of the gas molecule, or atom, through some sort of polarization of the molecules and surface species or through a weak intermolecular attraction. The gas then dissolves into the membrane at the surface and the concentration dissolved is limited by the solubility sites available in this specific glass and the partial pressure of the gas being considered. The dissolved gas in the surface begins to diffuse through the interior as atoms or molecules (or possibly ions) based on a concentration gradient. When the gas atoms reach the opposite surface, they will potentially leave the soluble sites of the glass to adsorb to the outgoing surface. This process would be followed by desorption and release of the gas in question. As the molecules fill up every site possible (that is possible under the conditions of the measurement), the gas leaving the glass membrane will begin to exit at steady-state, i.e. one molecule goes in the glass, and one molecule comes out. This flow rate of atoms in and out is related to the permeability.[23-27]

2.3 Hydrogen Reaction

Hydrogen not only diffuses through a glass structure, but it also interacts with reducible ions, gases, or defects. Any reaction is controlled by the diffusion of the hydrogen molecule through the glass network to a reaction site. Reaction sites can be anything from a species that will thermodynamically accept electrons from hydrogen to a dissolved oxygen molecule in the glass network. If hydrogen reacts with an ionic species it may effectively reduce the ion by donating electrons and produce hydroxyl groups with the remaining oxygens to balance charge. Depending on the coordination around the ion in question very different environments of hydroxyl can form. A standard reaction of a hydrogen molecule and a multivalent ion in glass is described by:

$$RO + H_2 \rightarrow R^0 + 2(Si - OH) \quad (1)$$

where R simply represents some arbitrary 2^+ ion dissolved in a silicate glass. These chemical reactions are often controlled by either the diffusivity of the hydrogen molecules to the reaction site or controlled by the rate of reaction at the site of the bound species. When the reduction rate is fast enough that the reactions are controlled by merely the diffusivity of the hydrogen molecules to the reaction site, the reaction process can be successfully described by the tarnishing model. The tarnishing model relates the thickness (X) of a moving reaction boundary with the reaction time (t), the concentration of hydrogen in the glass (C_s), the diffusivity of hydrogen in the glass (D), and the initial concentration of reaction sites (C_x), or:

$$X = \sqrt{\frac{2tC_sD}{C_x}} \quad (2)$$

Henry's Law states that the concentration of dissolved hydrogen in a glass is a product of the solubility of hydrogen in the glass in question (S) and the applied partial pressure of the gas (P). This and the fact that permeability (K) is the product of diffusivity (D) and solubility (S) allows us to rewrite the tarnishing model:

$$X = \sqrt{\frac{2tPK}{C_x}} \quad (3)$$

It is often convenient in practice to measure the concentration of the forming reaction products rather than the growing layer thickness. The fractional concentration of the reaction product can be described by:

$$\frac{C-C_i}{C_f-C_i} = \frac{2X}{L} = \sqrt{\frac{8KPt}{C_x L^2}} \quad (4)$$

Experimentally monitoring the concentration change allows for the direct determination of K. The only temperature dependent term present in this model is the permeability as the initial concentration of reaction sites rarely changes with temperature.[22,28]

Many studies have successfully related the tarnishing model to reduction rates in glasses.[6,7,10,12,13,29-35] One of the earliest is that of Johnston and Chelko.[32] Their work was designed as a study of the details of molecular hydrogen transport and reaction in solid glasses. They successfully reduced soda-lime-silica (SLS) glass fibers and slabs containing varying concentrations of either Fe^{3+}, Ce^{4+}, or Sn^{4+}. Some of their data was based on changes in the UV-Visible and IR spectral regions. Their results indicate that partial pressure of hydrogen affected the diffusivity calculated via the tarnishing model. Since diffusivity is supposed to be independent of pressure they describe their calculated diffusion coefficient as an effective diffusivity. This most likely resulted from variations in the concentrations of gas dissolved in the glass interstices as a function of pressure. Their work led to a modified tarnishing model using solubility and permeability instead of diffusivity for hydrogen reduction in glasses.

Barton and Morain[29] studied the hydrogen reduction of silver-containing SLS glasses. They studied the rate of precipitation of silver clusters through optical spectroscopic techniques. Using the appropriate Mie absorptions they were able to calculate hydrogen permeabilities for a variety of glasses. The values were typically higher than expected, and it is possible that their optical measurements should have accounted for growth of the clusters. Mie theory relates the number volume of particles and the volume of a particle to the absorption of clusters dispersed in a dielectric matrix. This implies that if the number volume or the volume of the particles increases, the absorption will increase. This could explain their higher than expected results.

Shelby and Vitko[35] studied the hydrogen reduction of Fe^{3+} to Fe^{2+} in soda-lime-silicate glasses using optical spectroscopy and electron spin resonance. In applying their

data sets to the tarnishing model, they checked all of the associated variables such as partial pressure of hydrogen, the initial concentration of reactable species, the time of the heat treatment, and the sample thickness. This study proved that the permeability was able to be extracted from the reduction data using the tarnishing model and that the glasses reduced as the tarnishing model would predict.

The tarnishing model has also been applied to systems where there are no reducible species present. Shelby[34] studied the reaction of hydrogen with hydroxyl-free vitreous silica. The tarnishing model was applied to the formation of hydroxyl in these silica glasses. Two odd findings were the lack of Si-H, which would have been a byproduct if hydrogen was breaking apart the silica network, and the reaction only progressing to a minute and finite value in these glasses. It was proposed that the reaction may be occurring with defect sites in the silica network or with dissolved oxygen molecules within the glass. Shelby was able to calculate the permeability of hydrogen molecules in these glasses based on the tarnishing model and found excellent agreement with measured permeabilities.

Kohli et al.[33] studied the coloration of glasses containing arsenic and attempted to apply the tarnishing model to this system. A broad optical absorption was observed in the visible region and the glasses changed to a dark brown color. The coloration was believed to be a result of the reduction of As^{5+} to As^{3+}, but the optical absorption changes did not fit well with the tarnishing model. This most likely was a result of the As^{5+} being reduced to an atom. These atoms would agglomerate and affect the optical absorptions, but these agglomerations and subsequent optical absorption changes would most likely be a result of diffusion based nucleation and growth mechanisms. One interesting thing to note from this study was that heat treatment in an atmosphere devoid of hydrogen following reduction, slowly reversed the coloration.

Tuzzolo and Shelby[10] studied the hydrogen induced formation of metallic clusters of arsenic, antimony, and bismuth in glasses. They noted that a darkened layer formed at the surface which progressively increased in thickness with treatment time. The coloration was related to a Rayleigh type scattering. The authors note that the particles growing must be a function of the concentration of atoms available in the glass, and a function of their atomic size and thus the rate they diffuse. They relate the darkening

rates to the initial oxidation states of the ions, the permeability of the glass, and the mobility of the atoms in the glasses.

Estournès et al.[30] studied copper reduction by hydrogen in soda-lime-silicate glasses. The authors reduced these copper containing glasses at 440-650°C. They not only studied the reduction of the glasses in question but also the changes in composition of the glass during reduction. The authors noted that the copper concentrations increased near the surface and the concentration of calcium decreased. This could imply some sort of interdiffusion mechanism. They found that copper reduced to form metallic clusters in discrete layers that grew parallel to the surface of the treated sample and increased in depth and distance apart increased with treatment times. The authors were able to extract activation energies for permeation by relating the optical absorption of metallic copper (ca. 560 nm) to a concentration reduced.

Estournès et al.[31] studied nickel reduction by hydrogen in soda-lime-silicate glasses. They measured the optical absorption of these glasses, the thickness of the reduced layer and the magnetization of the bulk glass. They only report reduction at 600°C. The thickness of the reduced layer was found to grow with the square root of time as predicted by the tarnishing model, but the absorption and magnetizations did not. They attribute these differences to these measurements being related to the sizes of the clusters forming. Since these properties are not just related to the liberation of the atoms, but subsequent growth, a diffusion related nucleation and growth term may be more appropriate.

Sturdevant and Shelby[12] studied the reduction of binary germanium silicate glasses. The reduction was attributed to the presence of GeO_2 in these glasses. They successfully applied the tarnishing model to the increases in the hydroxyl bands for these glasses. An interesting aspect of this work was the study of the dehydroxylation of these glasses. They noted that the base glasses did not lose much water through treatment in a vacuum. The rate of decrease in hydroxyl was much slower than the rate of increase during reduction. The authors attribute this to some of the hydroxyl formation by reduction being irreversible.

Youchak and Shelby[13] studied the reduction of germanium in alkali alumina germanate glasses. This study encompasses the greatest concentration of reacting species

present in a base glass seen by the author at this point with some of the glasses in this study containing 90 mol% GeO_2. The authors successfully applied the tarnishing model to the formation of hydroxyl in these glasses. Due to the high concentrations of reacting species, conductive films were able to form on the surfaces of these glasses. The authors also measured weight loss data and found that the reduction process led to mass loss. This mass loss is very likely due to dehydroxylation during the reduction process.

The most recent study pertinent to this literature survey was that of Miller and Shelby.[7] They studied the reduction of cobalt containing commercial borosilicate glasses between 625-790°C. This is believed to be the first, and only, study reported for the reduction of cobalt in a hydrogen environment. The authors were able interpret their hydroxyl formation data, optical absorption data, ESR data, magnetization data, and reduced layer thickness data using the tarnishing model, i.e. the square root of treatment time. This is also one of the first papers to note that there is a possible reaction controlled regime and a hydrogen diffusion controlled regime in the reduction experiments. This is very likely due to the thermodynamic state of cobalt in these glasses, but the tarnishing model requires that reaction be fast compared to the diffusion of gas to the reaction site for a sharp boundary to form. Either way these authors were able to calculate permeability values for hydrogen and note that their values are slightly lower than would be expected.[7]

2.4 Nucleation and Growth Theory

After the ions are reduced to the atomic state in a glass, nucleation and growth mechanisms affect the size and shapes of the growing clusters. Nucleation in glasses has been extensively studied ever since Stookey's discovery that glasses containing nucleating agents could produce glass-ceramic composites through exposure to controlled heat treatment.[36] Nucleation is vital to the formation of crystals within a glass, however nuclei being present does not mean crystal growth must follow.

Nucleation in a glass has been divided into three subcategories:[37]

(1) The nucleation of a gas inside a glass

(2) The nucleation of a liquid inside a glass

(3) The nucleation of a crystal inside a glass

For the purposes of this literature survey, the second two will be of primary concern as some of the metals reduced in this study were reduced above their melting temperatures, and others were not. This would lead to the formation of liquid droplets and metallic crystals and therefore the nucleation of both must be understood.

Some of the known complications with regards to nucleation theory in solid materials are the unknown surface/interfacial energy terms, heterogeneous nucleation, slow material transport, and potential stresses which result from phase transformation.[38] Classical nucleation theory (CNT) has been successfully applied to homogeneous nucleation in a glass, but it is very difficult to directly confirm evidence of nucleation experimentally. The theory assumes the formation of spherical nuclei equally distributed throughout the bulk of a glass, or at the surface, and has been described by numerous authors.[9,11,16,37-45] For this review, it is assumed that any localized grouping of atoms is symbolized properly by the term nuclei, even though nuclei existing in certain size ranges may be unstable.

Nucleation is typically described as a process governed by the transport of atoms to a nucleus over time. The formation of nuclei is hindered by both thermodynamic and kinetic barriers. The volume nucleation rate is a function of the collision frequency of atoms/ions with the developing nuclei, the concentration of critical nuclei, and the number of atoms/ions surrounding the critically sized nuclei. Thus the rate of homogeneous crystal nucleation (I) at steady state as a function of temperature (T) can be expressed by:

$$I = A\ exp[-(\Delta W^* + \Delta Q)/kT] \tag{5}$$

where ΔW* represents the change in free energy, or work, associated with the formation of a critical nucleus in a glass phase, ΔQ is the kinetic barrier to nuclei formation (i.e. the change in activation energy associated with material transport occurring from the glass phase to the forming nucleus whether it be controlled by a viscous or a diffusion based mechanism), and k is Boltzmann's constant. The pre-exponential term (A), was approximated by Turnbull and Fisher,[46] as:

$$A = 2n_v V^{1/3}(kT/h)(\gamma_{is}/kT)^{1/2} \tag{6}$$

where n_v is the quantity of formula units of the crystallizing phase in a unit volume of the glass matrix phase, V is the volume per formula unit of the crystallizing phase, h is Planck's constant, and γ_{ls} is the interfacial energy between the glassy matrix and the crystalline nucleus. This term is often experimentally determined to be temperature independent.

The derivation used to determine the pre-exponential constant (A) assumes that fairly large nuclei have formed and that long range diffusion did not influence the nucleation process. The remaining term in equation (5) is ΔQ, or the kinetic barrier to nucleation. There are typically two main contributions considered to properly describe the changes in the free energy of a system due to the formation of spherical nuclei. There is a decrease in the volume free energy of crystallization due to the supercooled liquid locally arranging to form lower energy crystalline nuclei, and an increase in the surface energy due to the formation of an interface between the crystal and the supercooled liquid. The competition between these two terms defines the change in free energy, or work, necessary to create a spherical nucleus:

$$\Delta W = (4/3)\pi r^3 \Delta G_v + 4\pi r^2 \gamma_{ls} \quad (7)$$

where r represents the radius of the nuclei, ΔG_v is the change in free energy of the system caused by the transformation of a certain volume of glass to a certain volume of the crystallizing phase and is negative for all temperatures below the melting temperature, and γ_{ls} is the surface energy associated with the interface between the crystal and the melt per unit of area. The change in free energy is plotted against radius (Figure 1) to emphasize the competition between surface energy and free energy of crystallization at various radii and how the change in free energy, or the sum of these terms, is affected.

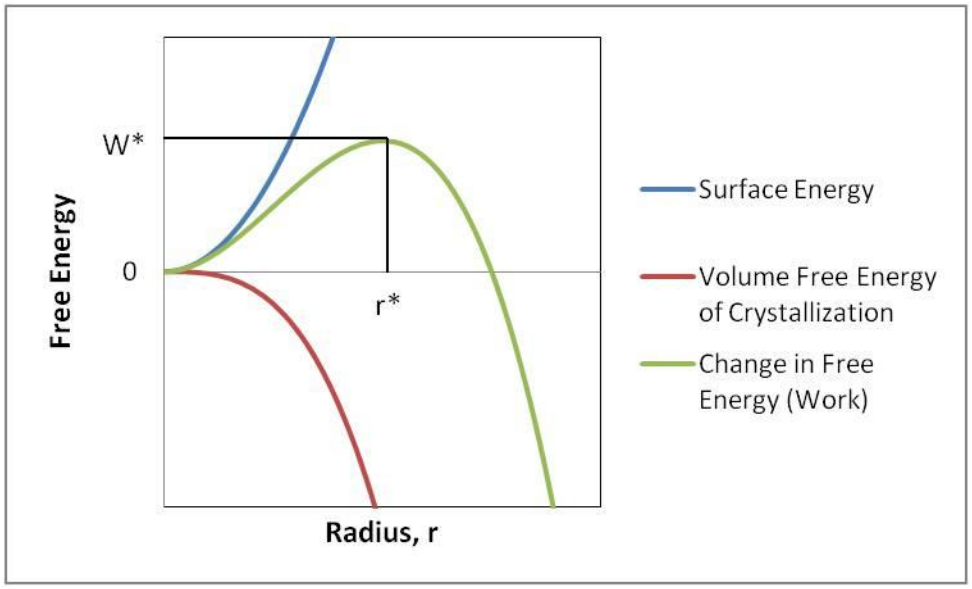

Figure 1. A representative plot depicting the change in free energy of nuclei formation as a function of nuclei radius.[11]

The free energy of the system increases when small nuclei are introduced due to the surface energy term dominating. This means that very small nuclei are energetically unstable and will redissolve into the supercooled liquid. When nuclei develop past a critical radius size (r*), the change in the free energy of the system decreases due to the volume free energy of crystallization term dominating. This means that above a critical radius the forming nuclei are energetically stable.[9,11,16,36-55]

The nucleation of a liquid from a glass is more commonly known as phase separation, or liquid-liquid immiscibility.[9,16] Typically, phase separation is discussed in terms of the Gibbs free energy. The Gibbs free energy is related to the interface between two phases. One of the simplest theories used to describe the free energy of a system is referred to as the regular solution model.[56] This model assumes that pure components are being mixed, that the components are randomly distributed, and that each component is surrounded by a fixed number of neighbors. This model describes phase separation by considering the molar free energy of mixing (ΔG_m):[9,16]

$$\Delta G_m = \Delta H_m - T\Delta S_m \tag{8}$$

where ΔH_m and ΔS_m are the enthalpy and entropy of mixing respectively, and T is temperature. For a regular solution, the entropy of mixing is described by the expression:

$$\Delta S_m = -R(X_A \ln X_A + X_B \ln X_B) \quad (9)$$

where X_A and X_B are the mole fractions of components A and B respectively. The enthalpy of mixing is given by:

$$\Delta H_m = \alpha X_A X_B \quad (10)$$

where α is attributed to the various possible bond energies in the solution, the coordination around the various molecules in the solution, and the total concentration of molecules in the solution. A simplistic example of α for a two component regular solution is described by the expression:

$$\alpha = -Zc\left(E_{AB} - \frac{E_A + E_B}{2}\right) \quad (11)$$

where Z is the number of nearest neighbors around the components A and B, and c is the total concentration of atoms/ions in the mixture. The bond energies for atoms/ions of A-A, B-B, and A-B are E_A, E_B, and E_{AB} respectively. Using the above thermodynamic equations, calculated plots were created for an example two component system to show the Gibbs free energy changes with composition.(Figure 2)[11] Plot (a) is an example of a regular solution in which the addition of both components (A and B) lowers the free energy of the overall mixture which forms a thermodynamically stable homogeneous phase at all temperatures plotted. Plot (b) is an example of immiscibility. At 300K, the free energy of this solution exhibits a saddle and this creates a tendency for the mixture to form two distinct phases. As the temperature increases it is clear that the saddle is no longer present indicating that the free energy has surpassed the critical temperature and the mixture will form a single homogeneous phase.

It must be acknowledged that in a glass the simple solution model discussed above is not completely accurate. There have been various attempts[57,58] to redefine ΔS_m and α as the regular solution model is far too simple to accurately describe the complex nature of glass. It is also important to note that lower temperatures limit diffusion based processes, which could inhibit phase separation.[9] The mechanism of primary concern here is the nucleation of droplets of a distinct phase in another glassy phase due to these thermodynamic terms.

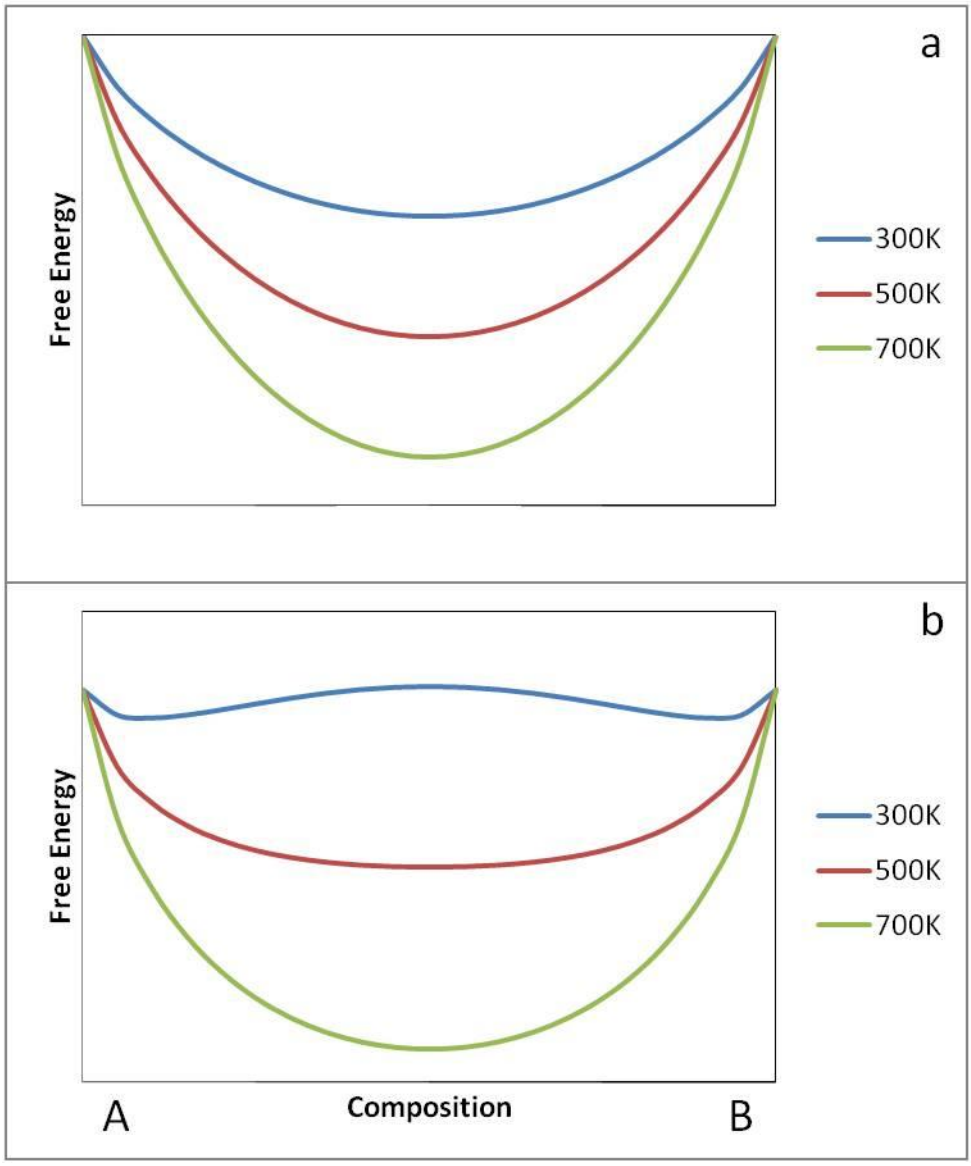

Figure 2. Representative examples of Gibbs free energy vs. composition for a two component mixture at various temperatures which exhibits (a) complete miscibility and (b) separation into two phases at low temperatures.[11]

Crystal growth occurs in glasses subsequent to the formation of nuclei, and is very temperature dependent, similar to nucleation. Dependant upon temperature, nucleation may occur and the nuclei will be incapable of measureable growth until higher temperatures are achieved, or nucleation may occur and the nuclei will simultaneously grow at the same temperature. Typically, growth occurs at higher temperatures in comparison to nucleation, and similar to nucleation, growth occurs below the liquidus, or

melting, temperature. This implies that if a glass is held within its crystallization temperature regime, yet above its nucleation temperature regime, crystallization will only occur if nuclei are present. Crystallization is covered in many sources and will only be briefly discussed here.[9,11,16,59,60]

Crystallization in a glass is typically discussed in terms of a growth rate (U):[11]

$$U = a_o(\upsilon_1 - \upsilon_2) \tag{12}$$

where υ_1 is the jump frequency of atoms from the glass to the crystal, υ_2 is the jump frequency of atoms from the crystal back into the glass, and a_o is on the size scale of an atomic/molecular diameter or the distance that the interface between the glass and the crystal moves (sometimes simply described as an interatomic separation distance per net jump). The atomic frequency of atoms jumping from the glass to the growing crystal (υ_1) is described by:

$$\upsilon_1 = \upsilon\, exp(-N_A \Delta E/kT) \tag{13}$$

where υ is a general frequency of atomic jumping from site to site at the interface between the glass and the crystal, N_A is Avogadro's number, ΔE is the activation energy for atomic motion, and k is Boltzmann's constant. The atomic jump frequency from the crystal back into the glass (υ_2) is described by:

$$\upsilon_2 = \upsilon\, exp(-N_A(\Delta E - \Delta G_v)/kT) \tag{14}$$

where ΔG_v is the change free energy of the system caused by the transformation of a certain volume of glass to a certain volume of the crystallizing phase and is negative for all temperatures below the melting temperature (this is the same as the free energy term used for nucleation in a glass discussed earlier). By inserting Eqs. 13 and 14 into Eq. 12 a more general expression for crystal growth rate (U) in a glass can be compiled as:[9,11]

$$U = a_o \upsilon \exp(-N_A \Delta E/kT)[1 - \exp(-N_A \Delta G_v)/kT)] \tag{15}$$

Turnbull and Cohen[61] introduced the concept that the activation energy needed for atomic motion in crystallization could be the same as that for diffusion in ionic transport experiments. This effective diffusion coefficient (D) is typically described by:

$$D = a_o^2 \upsilon \exp(-N_A \Delta E/kT) \tag{16}$$

Since the effective diffusion coefficient in a glass can be related to viscosity through the Stokes-Einstein equation, when growth is viscosity controlled, the crystal growth rate (U) can be described as:[9,11]

$$U = (kT/3\pi a_o^2\eta)[1 - exp(N_A\Delta H_m(\mathrm{T_m} - \mathrm{T})/kTT_m)] \quad (17)$$

This equation is only applicable to normal growth. Normal growth is considered to occur on a rough interface, atomically speaking, and the interface is said to contain a large fraction of growth sites. There are more complex models[59,60] that use another pre-exponential term to account for growth on pre-existing screw dislocations present on atomically smooth interfaces, and others that assume an atomically smooth interface where nuclei can develop and allow for growth. The same basic issues discussed earlier for nucleation theory apply here.

2.5 Redox Equilibria in Glasses

It is well known that compositionally complex systems have the potential to chemically react. A common example is the simultaneous oxidation and reduction of metals. Oxidation refers to a transfer of electrons from a metal to an oxygen atom, or a bonding to the oxygen atom in highly covalent cases, and reduction is the exact opposite. This reaction can occur without any changes in the number of atoms contained within the overall system. Typically, redox reactions are written in terms of an equilibrium constant (K). This is related to the moles of products over reactants. Since all chemical species discussed in this thesis are dissolved in a glass, it will be stated as activity rather than moles, as activity is an effective concentration due to intermolecular interactions. In general, glasses are very difficult to discuss in terms of activities, since many of the constituents in a glass have unknown activities, and equilibrium can be kinetically difficult to determine. Thus, determining an equilibrium constant for a melt is a very difficult process.[62,63]

Paul[63] mentions that redox states of ions in glasses will stop changing due to kinetic limitations once the temperature has dropped below T_g.[63] Since redox kinetics are controlled by the diffusion of oxygen through the melt, and oxygen diffusion is very slow at temperatures near most glass T_g's, it is possible that redox is not seen to change below T_g due to the slow diffusion rates of a reactable species. This supports hydrogen

reduction data. As hydrogen molecules are much smaller than oxygen molecules, and have much higher diffusion coefficients, it is possible that redox is limited by the diffusion of a reactive species to a reaction site below T_g.[63,64]

It is well established in literature that redox equilibrium changes dramatically in a system when more than one reducible ion is dissolved in that system.[63] It is often stated that one of the species is an oxidizer for the other species in the glass. Regardless, this complicates the situation dramatically. Paul and Douglas[63] were able to estimate the heats of reaction for the individual oxides and found that the reducible oxide mixtures exhibited heats of reaction equivalent to the sum of the individual oxides. They also determined that typical redox tables were valid for alkali silicate glasses but did not hold true for alkali borates.[63-65]

2.6 Instrumentation Background

A variety of experimental techniques were used throughout this study and the primary ones will be discussed in more detail here. Almost all of the data collected was directly related to optical spectroscopy, IR spectroscopy, grazing incidence X-Ray diffraction (GIXRD), and scanning electron microscopy (SEM). All the techniques but SEM required some calculation or modeling and will be discussed here.

2.6.1 Spectroscopy

Radiation can interact with a material in a variety of ways including reflection, refraction, scattering, absorption, and transmission. The three most important to this work are scattering, absorption, and transmission. The attenuation, or absorption, of radiation passing through a material is described by:

$$I = I_o * exp(-\alpha x) \tag{18}$$

where I represents transmitted intensity, I_o is the incident intensity, α is the linear absorption coefficient (1/cm), and x is the sample thickness (cm). Most of the data recorded and presented in this thesis is plotted as absorbance (A) which is also known as optical density (OD):

$$A = OD = log_{10}(I/I_o) \tag{19}$$

which implies that an absorbance of one corresponds to 10% transmission, an absorbance of two corresponds to 1% transmission, and an absorbance of three would correspond to 0.1% transmission. Beer-Lambert's Law relates the optical density to the concentration of a species (C) through an extinction coefficient (ε):

$$A = \varepsilon C x = \alpha x \tag{20}$$

This applies to both IR and optical spectroscopy data. In order to determine concentrations of species in a glass the extinction coefficient must be known for the specific glass system in question.

2.6.2 Optical Spectroscopy

All oxide glasses exhibit an ultraviolet edge (UV-edge) where wavelengths of higher energy light cannot be transmitted. This is typically attributed to transitions of valence electrons of anions (typically oxygen) to excited states. Non-bridging oxygen in a glass structure would need less energy for this type of electronic transition than a bridging oxygen. This means that shifts of the UV-edge to longer wavelengths (lower energies) occurs with increases in the non-bridging oxygen content of a glass. The UV-edge can often be masked by charge transfer bands where the energy of light is sufficient to cause an electron to transfer from a cation to a neighboring anion.[9,11,66]

Most of the absorptions in this study are related to ligand field coloration. Transition metals dissolved in glass are surrounded by different coordinations of ligands, or oxygens anions. The 3d electronic energy levels are split due to the field strength, coordination, and arrangement of nearby ligands. Coloration in glasses containing these transition metals is explained by absorptions due to electronic transitions of these 3d electrons into the various energy levels formed due to this splitting.[9,11,15,17,19]

The other source of color in the glasses used in this study is related to Mie scattering. The two most common examples of scattering are Mie and Rayleigh. Rayleigh scattering is commonly related to particles smaller than the wavelength of light. This scattering is proportional to λ^{-4} which implies that shorter wavelengths scatter light much more than longer wavelengths. Mie scattering is a complex scattering that is related to larger particles, of approximately the wavelength of light. When the particles become 2x the wavelength of light in size, it has been shown that at specific angles,

different colors can be scattered, termed polychroism. When conducting particles dispersed in a dielectric matrix become very small, less than ~40 nm in diameter, they can also absorb radiation. This absorption is often described as a result of free electrons in the conducting particles acting as a bound plasma, and the absorption band is called a plasma resonance band. The light is described as penetrating fully into the particles due to their small size, and this suggests that all of the conduction electrons are involved with this absorption process. With such small particles the scattering component of the complex Mie scattering relationship is negligible. The absorption coefficient of small (<40 nm) metallic particles dispersed in a dielectric matrix is given by:[17]

$$\gamma = NV\frac{\left(36\pi nk{n_o}^3\right)}{\lambda\left(\left(n^2-k^2+2{n_o}^2\right)+4n^2k^2\right)} \tag{21}$$

where N is the number of particles per unit volume, V is the volume of the particles, n_o is the refractive index of the glass, and n and k are optical constants of the metal. This will be referred to as an attenuated Mie absorption due to it being a shortened version of the complex Mie scattering equation.[2,9,11,15,17,66] Doremus and many others have shown that this Mie absorption can be calculated for a variety of conducting spheres of silver, gold, and copper. Their theoretical calculations agree well with experimental measurements.[67-73]

2.6.3 IR Spectroscopy

Infrared spectroscopy is often described as a low energy spectroscopy in which absorptions are related to vibrational transitions of the structure, the IR-edge or multiphonon edge, or impurity absorptions due to gases. The frequency of an absorption in the IR is often described through Hooke's Law, or that the frequency is proportional to the square root of the force constant of a bond over the reduced mass of a molecule.

This work is very focused on structural vibrations, in particular that of hydroxyl, or OH. Three typical bands are reported due to the existence of hydroxyl in the range of 4000-2000 cm^{-1}. The band located at ~3500 cm^{-1} is typically attributed to "free" hydroxyl, i.e. hydroxyl that is not hydrogen bonded to anything nearby in the structure. The band located at ~2700 cm^{-1} is typically attributed to "hydrogen bonded" hydroxyl, and a third band within the shoulder at ~2300 cm^{-1} is typically attributed to stronger "hydrogen bonded" hydroxyl. "Hydrogen bonded" hydroxyl is typically thought to be

indicative of nearby non-bridging oxygens. The extinction coefficients for these bands have been measured and are readily available for certain glass compositions. One method for determining the amount of water in a glass, or hydroxyl, was conceived by Scholze: [74-81]

$$C_{OH} = \frac{17000}{xd}\left(\frac{A_{3500}}{\varepsilon_{3500}} + 4/3\,\frac{A_{3500}}{\varepsilon_{3500}}\right) \tag{22}$$

where C_{OH} is the concentration of hydroxyl in ppm, x is the sample thickness (cm), d is the glass density in (g/cm^3), A is the intensity of the absorbance of the band in question, and ε is the related extinction coefficient.[74-81]

2.6.4 GIXRD

X-Ray diffraction was crucial to the identification of metallic clusters as well as to attempt to measure the particle sizes of the clusters. Particle size calculations are inherently based on broadening, and particle size refers to that of the grain, not necessarily the particle. Broadening of X-Ray peaks is typically a result of small particle size (less than 1 μm grains), instrumental effects, and strain. If the instrumental broadening can be calculated, and strain can be either ruled out or calculated, then it is possible to determine particle size based on this broadening. The Scherrer equation is typically used to relate peak broadening to a mean crystallite size:

$$\tau = \frac{K\lambda}{\beta cos\theta} \tag{23}$$

where K is a shape factor (typically about 0.9), β is the full width at half max of a peak, τ is the mean crystallite size, λ is the incident x-ray radiation, and θ is the Bragg angle. In consideration of the current research, spherical particles should be strained if there is any interaction with the lattice. However, this strain would most likely be uniform due to the spherical shape of metallic clusters. Uniform strain will shift the peak due to stretching or compressing the interatomic dimensions, but it should not broaden it. Non-uniform strain will cause a broadening, but it is doubtful that this is a factor in these measurements.[82-84]

3. EXPERIMENTAL PROCEDURE

3.1 Melting/Annealing

All of the glasses used in this study were batched from reagent grade mixtures of Na_2CO_3, CaO, In_2O_3, NiO, CuO, Pb_3O_4, Co_3O_4, and SiO_2. The glasses were prepared to yield 15 g of glass after any decomposition reactions and the powders were dry mixed prior to melting in silica pestles using a stainless steel spatula to shear and mix the powders thoroughly. The glasses were all melted in a 50 ml 90Pt/10Rh crucible in air in a resistance furnace for 1-4 hours at 1400-1600°C. After melting the glasses were quenched to remove them from the crucible as cleanly as possible.

The glass transition temperature (T_g) was determined using a differential scanning calorimeter (DSC) and analyzing the heat flow data by the onset intercept method for each glass. The DSC was heated at 20°C/minute in platinum pans and a flowing nitrogen atmosphere. All samples were annealed by heating to 10°C above the measured T_g for 30 minutes followed by a cooling rate of -3°C/min to room temperature. The T_g was found to be accurate within ±3°C.

3.2 Cutting/Polishing

All of the glasses were prepared in a similar fashion for heat treatment and data collection. After annealing the glasses were mounted and cut into plates ~1 mm thick using a slow speed saw and a diamond blade. A kerosene water mixture was used to lubricate the saw blade. The plates were ground using SiC paper followed by polishing using a cerium paste. After polishing the samples were ultrasonically cleaned in ethanol to remove any remaining cerium. The thickness of every sample was determined using a micrometer to within ±0.01 mm.

3.3 Hydrogen Reduction

All samples were treated in 700 torr (0.92 atm) of H_2 at 500°C, 550°C, 600°C, or Tg of the glass in question. Throughout the reduction heat treatments, the samples were

periodically removed for measurement. The hydrogen treatment system was custom built for these studies and is shown in Figure 3. The sample was loaded into a large silica ampoule that was sealed via a compressed rubber O-ring to the filling apparatus. The sample was placed in a smaller silica tube to preserve the integrity of the outer silica ampoule. An internal shielded thermocouple was placed directly above the sample to monitor the temperature during reduction. A roughing pump was used to evacuate the system, and a tube furnace was centered over the sample in the silica ampoule. At approximately 200°C a quick hydrogen flush was initiated to remove any adsorbed gas species and ensure that the pressures read were due to as much hydrogen gas as possible. When the approximate treatment temperature was achieved, the roughing pump was isolated from the sample atmosphere. The silica ampoule was filled to the desired pressure of hydrogen gas, and then sealed so as to minimize tubing and stainless steel connections being in contact with the reducing atmosphere as much as possible to minimize leaking. Two furnaces were used in this study, and to ensure that the pressures were relative between the two, hydrogen reduction rates in commercial glasses were monitored and they were in close agreement. At the end of the desired reduction time, the furnace was removed and the samples were allowed to quickly cool to room temperature before exposing the sample to atmospheric gases.

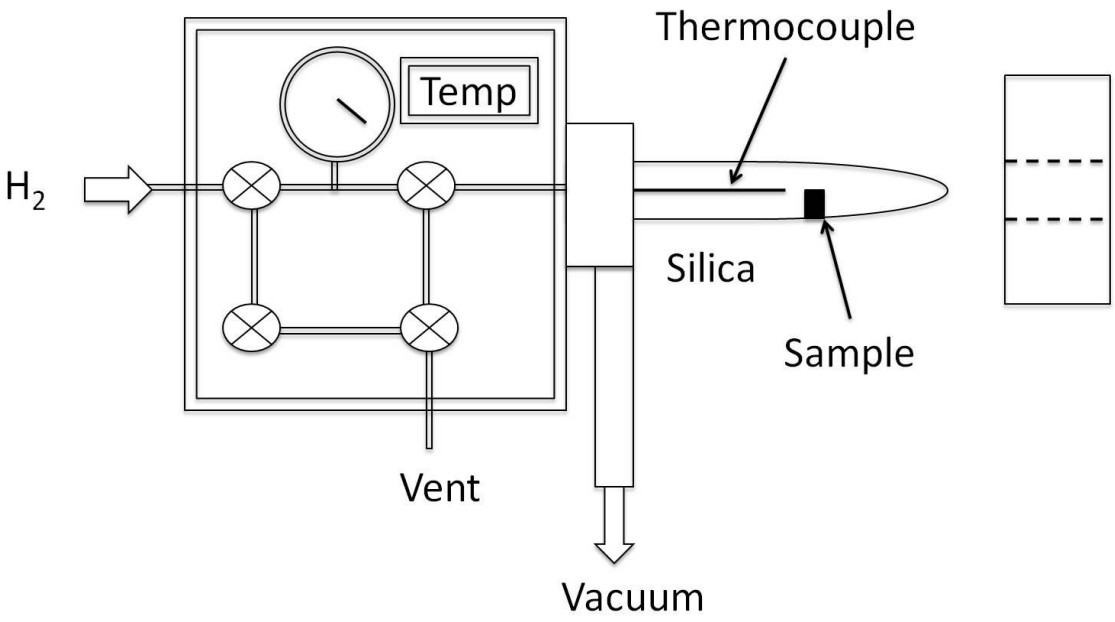

Figure 3. Schematic of custom build hydrogen reduction furnace used in this study.

3.4 Spectroscopy

UV-Vis absorption spectra were recorded before and after treatments in a single beam Perkin Elmer Lambda 40 spectrometer. The atmosphere in the spectrometer was ambient. A scan range of 200-1100 nm with a 1 nm resolution was used for all data. IR absorption spectra were recorded before and after treatments in a single beam Thermo Nicolet Avatar 360 FT-IR with a scan range of 4100-2000 cm^{-1} and a resolution of 1.93 cm^{-1}. The spectra were collected as an average of 32 scans to minimize background. There are typically three sources of error involved in these measurements. The samples need to have parallel surfaces since any degree of tilt will affect the data. The determination of the sample thickness can also affect the data. Lastly noise, instrument quality, and scan conditions will also affect this data. When comparing different samples, the homogeneity of the glass the samples were taken from is also an issue. A measured relative error for the IR spectrometer, based on seven samples of commercial glass was determined to be ± 0.004 mm^{-1}. A measured relative error for the UV-Vis spectrometer used based on seven samples of commercial glass was determined to be ± 0.13 mm^{-1}.

3.5 X-Ray Diffraction

Diffraction data was collected using a Siemens Kristalloflex D-5000 Grazing incidence X-Ray Diffractometer (GIXRD) with an initial angle of 2° to the surface of the glass. A level sample surface was introduced into the chamber and the patterns were obtained for the metallic clusters dispersed in the surface of the treated glasses. Scans were recorded with a 0.04° step size and a 20 second dwell time from 10° to 70° 2θ for phase identification, and crystallite size identification.

4. SODIUM INDIUM SILICATES

4.1 Introduction

Indium is known to exist in octahedral sites in sodium silicate glasses. Very little literature exists for glasses in this series. To the author's knowledge, the only reported evidence of indium being reduced is in sodium-indium-silicate glasses studied at Alfred University by VanCott and Shelby. This work noted that indium was reduced at temperatures near the glass T_g. Indium crystals were confirmed through SEM, EDS, XRD, and even DSC results. No spectroscopic data was reported, and no study of the reaction mechanisms or rates. A more in depth study of the effect of temperature, composition, and heat treatment time is needed to better understand hydrogen reduction of indium in glasses.[85,86]

4.2 Experimental

This chapter consists of two separate studies. The glasses used throughout this chapter are listed in Table I for the two types of experiments conducted. The samples for the SEM work were rough ground and polished in the same fashion as described in the Experimental Procedures section. Six polished plates of a 10 In_2O_3–15 Na_2O–75 SiO_2 (mol%) glass were used. The glass transition temperature (Tg) is approximately 720°C as determined via the DSC slope onset method mentioned in the Experimental Procedures section. Two thin sections were treated in a hydrogen atmosphere (700 torr or 0.92 atm) for 100 hours at 670°C (50°C below Tg), 720°C (Tg), and 770°C (50°C above Tg) yielding 6 samples for this portion of the study. One of the two samples from each treatment temperature was broken, mounted in epoxy, and again polished to create cross sections for analysis. The cross sections were coated with a gold/palladium mixture to minimize charging, while the remaining samples were carbon coated to minimize charging while imaging the surfaces. The cross sections were imaged in the traditional high vacuum mode while the surfaces were imaged in low vacuum environmental mode.

Table I. Experimental Treatment Temperatures for the Two Parts of this Chapter

	Spectroscopy Treatment Temperatures (°C)			SEM Treatment Temperatures (°C)		
Composition	**500**	**550**	**600**	**670**	**720**	**770**
$15Na_2O$-$2In_2O_3$-$83SiO_2$	X	X	X			
$15Na_2O$-$5In_2O_3$-$80SiO_2$	X	X	X			
$15Na_2O$-$7In_2O_3$-$78SiO_2$	X	X	X			
$15Na_2O$-$10In_2O_3$-$75SiO_2$	X	X	X	X	X	X
$20Na_2O$-$10In_2O_3$-$70SiO_2$	X	X	X			
$30Na_2O$-$10In_2O_3$-$60SiO_2$	X	X	X			

4.3 Results

4.3.1 Microscopy

The three cross sections were imaged using backscattered electrons (BSE) in order to show atomic number contrast (Figure 4). It is well established that the backscattered electron signal is dependent upon the atomic number with only a slight dependence reported for density. Heinrich reports a simple relationship between the backscattered coefficient (η) and the atomic number of the elements (Z)[87]:

$$\eta = (\ln Z/6) - (1/4) \quad Z \geq 10 \tag{24}$$

Indium metal, having the greatest atomic number, has the brightest contrast as expected when compared to the other constituents present in all of the micrographs taken using the SEM (Table II). Since the aforementioned equation is for elements, a rule of mixtures

approach based on weight fractions was used to estimate backscattered electron coefficients for the oxide glasses imaged in this study.

Table II. Calculated Backscattered Electron Coefficients and the Contrast Between Them for the Glasses Imaged Assuming Density has a Negligible Effect

Component 1 (mol%)	**Component 2 (mol%)**	**η_1**	**η_2**	**Contrast (%)**
Pure In	$15Na_2O$-$10In_2O_3$-$75SiO_2$	0.40	0.26	34.92
Pure In	$16.7Na_2O$-$83.3SiO_2$	0.40	0.15	63.59
$15Na_2O$-$10In_2O_3$-$75SiO_2$	$16.7Na_2O$-$83.3SiO_2$	0.26	0.15	44.06

Representative micrographs of cross sections of the treated glasses are shown in Figure 4. A depleted region is present at the surface of all three cross sections indicating a glassy phase with a much lower concentration of indium than the pretreated glass. The boundary between the indium depleted region and the still indium rich region of the glass is very broad for the glasses treated at 720°C and at 770°C. The boundary between the two regions is much more defined for the glass treated at 670°C. Some extracted statistical data for particle size and the depleted region thickness is displayed in Table III. All measurements were conducted using a minimum of 15 samplings.

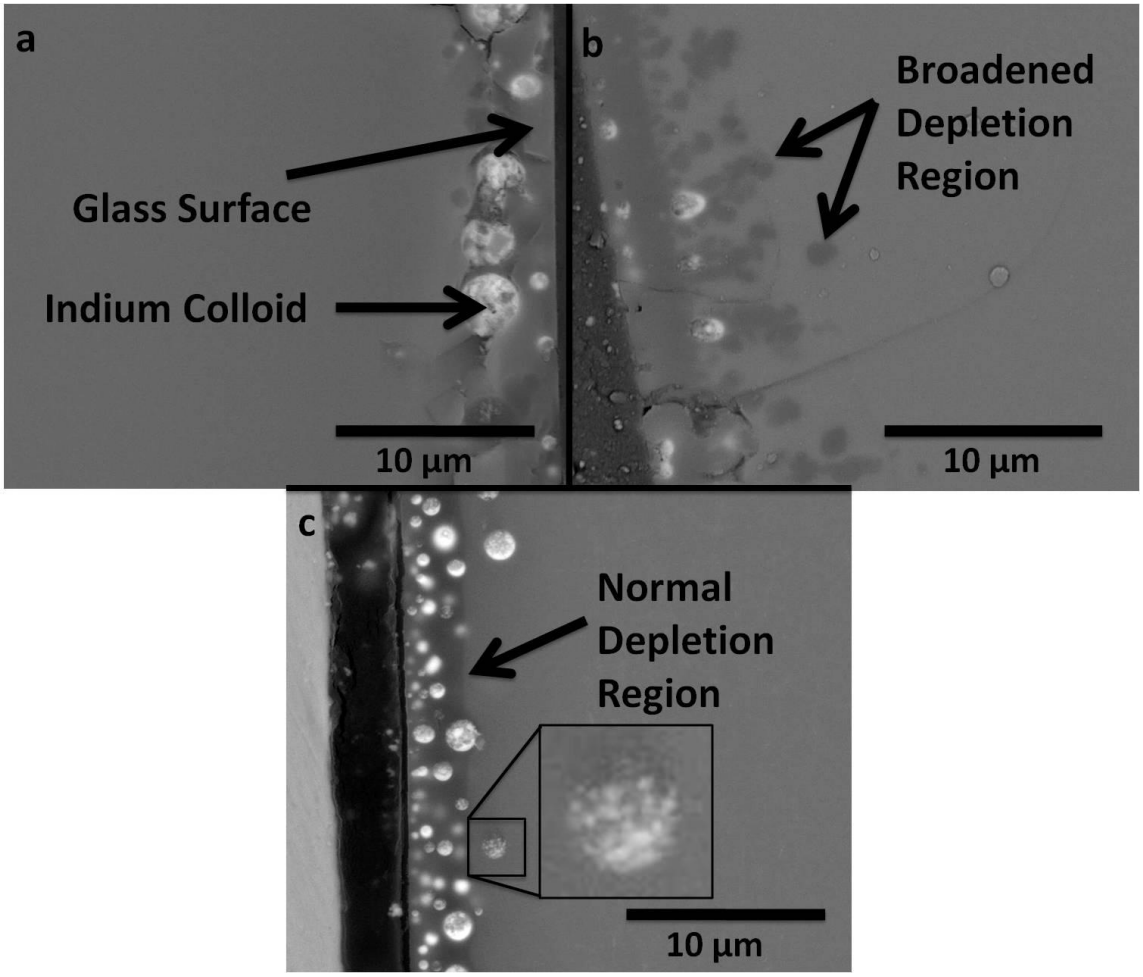

Figure 4. Representative ESEM micrographs taken using BSE of cross sectioned samples treated at a) 720°C, b)770°C, and c) 670°C.

Table III. Measurements Depicting Average Sizes of Features in Micrographs with Standard Deviations in Parenthesis

Temperature (°C)	**Depth of Typical Depleted Region (µm)**	**Depth of Abnormal Depleted Region (µm)**	**Diameter of Metallic Clusters (µm)**	**Number Density of Clusters (cm^{-3})**
670	3.05 (0.10)	-	0.67 (0.37)	3.62E+08
720	3.42 (0.73)	6.92 (0.17)	1.17 (0.88)	1.04E+08
770	3.03 (0.23)	6.72 (1.85)	0.89 (0.44)	1.29E+08

The sample treated at 670°C (50°C below Tg) exhibits the smallest average cluster size as well as the smallest standard deviation (Table III). The calculated number density of clusters per volume of glass is also found to be the largest of the three samples imaged. The indium clusters are very spherical in nature and appear to get larger with increasing distance from the sample surface (Figure 4(c)). Very few clusters were found to exist outside of the depletion region. Some of the larger clusters appear to exhibit a darker contrast region within which could represent particles of the depleted glass phase or voids in the cluster itself. At the bottom of the micrograph of this cross section, just outside of the depleted region, a cluster in the middle of some sort of growth process can be found. This large spherical cluster appears to consist of many much smaller clusters very close together yet still separated by a glassy phase. The indium depleted region is very similar in depth to that of the sample treated at 770°C; however, there was no broadening of the depletion zone as is found in the cross sections of the samples formed at the other two temperatures.

The sample treated at 720°C (Tg) exhibited the largest clusters and, as would be expected, the smallest number density of clusters per volume of glass (Table III). Even though this sample has the largest clusters, it also has some of the smallest as denoted by the large standard deviation reported. The indium clusters were very spherical as in the sample treated at 670°C; however, the clusters formed at this temperature exhibit a very rough texture in their bulk, and some even appear to contain pieces of depleted glass (Figure 4 (a)). This texture may be apparent at this temperature due to the large size of the particles and the resolution of the ESEM. The depleted glass chips could be an artifact of polishing as the depleted region did appear to crack away relatively easily during the polishing procedure. The clusters again appear to be larger at greater distances from the surface of the sample. The indium depleted region is very inconsistent across the surface of the treated sample. The average depletion region penetrated further than in any other sample but it appeared to penetrate much deeper still in specific regions. This broadening of the depletion zone occurred across the surface to variable depths within the sample, but the regions are somewhat periodic in nature and in no way consistent. This led to the use of the term “broadened depletion region”. This sample exhibited, on average, a deeper broadened depletion region than could be found in the sample treated at

770°C. This by no mean implies that there is a greater degree of broadening for this sample than the sample treated at 770°C. This sample did not exhibit as much broadening in comparison to the sample treated at 770°C. Typical EDS spectra for indium in the different regions of contrast in the micrographs are shown in Figure 5. The unmarked peaks are due to gold and palladium. It is obvious that the clusters consist of more indium than the bulk glass which also contains slightly more indium than the depleted region. The bulk glass also possibly contains more sodium than the depleted region although, due to the potential for sodium to migrate, this needs to be confirmed. It must be noted that the interaction volume of the beam and the sampling volume of X-Ray collection is on the order of microns and therefore considerable amounts of glass and other particles are contributing to the spectra making any quantitative analysis difficult.

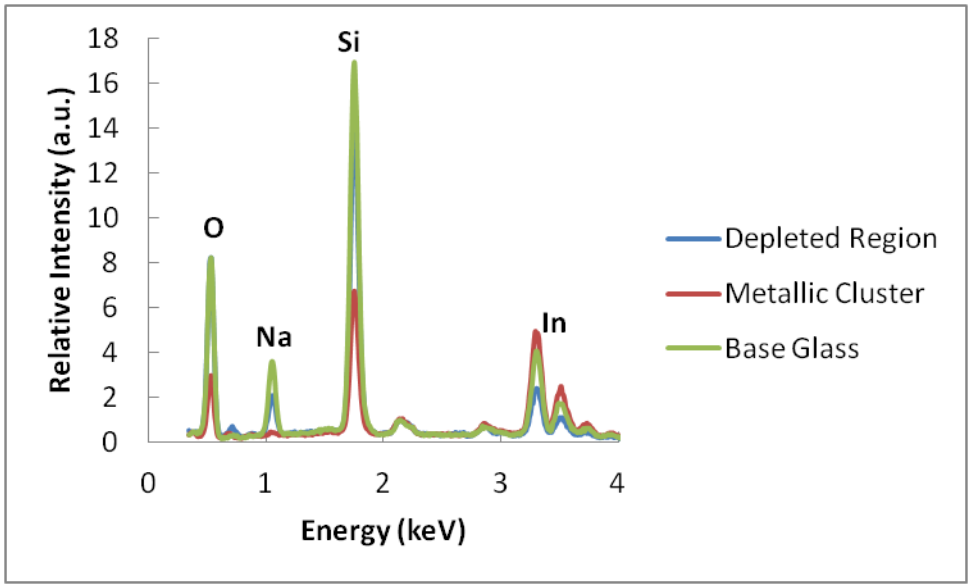

Figure 5. Representative EDS spectra for the various regions present in the micrographs.

The sample treated at 770°C (above Tg) is the most difficult to analyze due to the large amount of sample deformation that occurred during the treatment. Large voids were found within the bulk possibly due to some sort of gaseous evolution during the reduction. This sample also exhibits a large degree of crystallization at the surface and within the bulk (Figure 6 (a&b)). The crystals at the surface and within the bulk both consist of large amounts of indium as indicated by EDS analysis and by the contrast of

BSE. The larger crystals located near the surface appear to be surrounded by an indium depleted region, and the crystalline phase is very dendritic in nature. The contrast and EDS spectra indicate that this crystalline phase is some sort of sodium-indium-silicate. There even appears to be an indium depleted region at the surface of the glass sample above the crystalline phase. This dendritic surface crystalline phase average thickness was measured to be 57.16 ± 7.84 μm. This is much thicker than any of the measured indium depletion zones. The EDS spectra from the crystalline phase and the depleted zone near the crystalline phase are shown in Figure 7. The crystalline phase has a higher concentration of indium, possibly sodium, and much less silica in comparison to the composition of the depleted region. The unlabeled peaks are attributed to carbon, gold, and palladium which are all artifacts of sample preparation. Again, care must be taken when discussing sodium due to the ease of migration in glass due to an electron beam.

The bulk crystals are small and needle-like in appearance, and do not appear to be surrounded by an indium depleted region, possibly due to the size of the small crystals and the resolution of the instrument at this magnification. These smaller crystals appear to consist primarily of indium but are too small to be able to confirm any real difference with EDS due to the interaction volume of the beam and the sampling depth of the X-Rays. These small bulk crystals measured an average particle length of 0.68 ± 0.18 μm. These crystals are similar in length to the diameter of the spherical metal clusters measured near the surface of the sample at this temperature.

Metallic clusters were found only in regions with little crystallinity, and typically only within the depleted glass phase (Figure 4 (b)). Some of the clusters are very spherical while others have a stretched, oblong spherical shape. The clusters again appear to get larger deeper from the surface. They are, on average, smaller than those formed at 720°C and larger than those formed at 670°C and the number density follows the same trends. The clusters exhibit the inconsistent appearance possibly containing voids or pieces of depleted glass similarly to the clusters formed at the other two temperatures. Again the clusters are present in a region of darker contrast indicating a depletion zone.

The depleted zone is very similar to the sample treated at 670°C; however, this sample exhibits the broadening of the depletion zone. This broadening is on average

slightly less than the sample treated at 720°C, but this sample exhibits regions where the depletion zone reaches much further into the glass than in any of the other two samples. This broadened depletion zone was much more consistent than in any of the other samples. The depleted zone was found across the entire sample where there was no dendritic crystallinity below the surface. The interior of the bubbles were investigated as well and interestingly enough the surface was covered with small octahedral crystals of indium metal (Figure 6(c)). The contrast and EDS indicate that these octahedral formations are composed primarily of elemental indium. These indium crystals appear to be growing out of the surface of the glass and in a very high concentration. The size of these particles is somewhat difficult to establish due to orientation, but they appear to be approximately 3 - 4 μm in length. This is a much larger length than measured for any of the spherical clusters measured below the surface for any treatment temperature. These octahedral crystals appear to have a very consistent size.

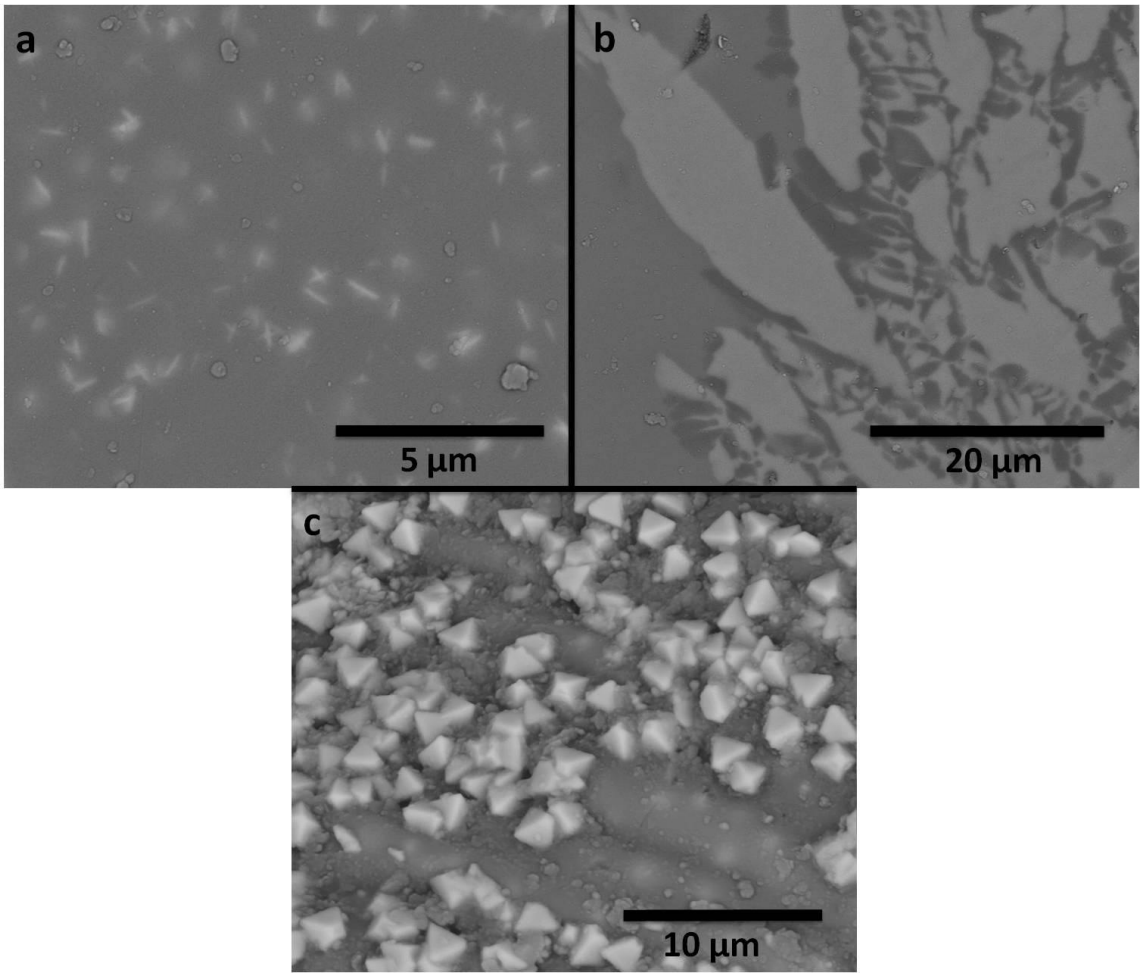

Figure 6. Representative micrographs of sample treated at 770°C taken using BSE of a) bulk crystallinity, b) surface crystallinity, and c) interior of a bubble formed during the treatment.

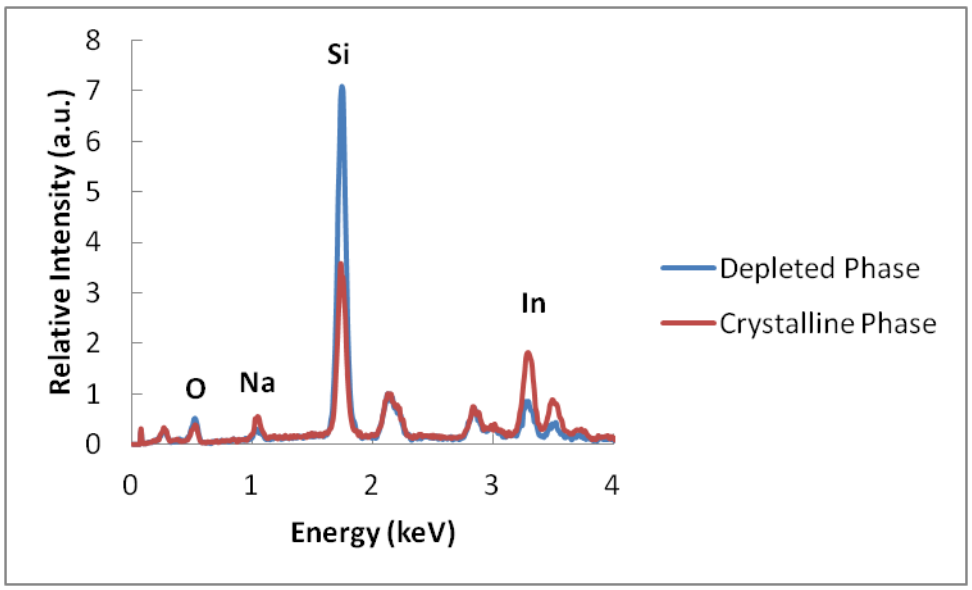

Figure 7. Representative EDS spectra of surface dendritic crystals and the indium depleted phase near the crystals.

The three remaining samples for surface imaging were carbon coated and imaged in a low-vac mode in the ESEM to minimize charging. The surfaces were imaged in BSE mode to enhance elemental differences. Representative micrographs of the surfaces can be found in Figure 8. There is an obvious contrast difference at the surface of all three samples which is again related to atomic number differences. The percentage of the bright contrast phase decreases with increasing treatment temperature. The dark contrast phase appears to have a droplet shaped morphology while the light contrast phase appears to be the matrix. The darker contrast droplets are much larger for the sample treated at 720°C than for either of the other treatment temperatures. The sample treated at 770°C appears to have the grainiest appearing bright contrast phase. A series of representative micrographs at a higher magnification are shown in Figure 9. Nearly every darker contrast phase has large cracks that look similar to crazing. The brighter contrast phase appears very well defined and appears to consist of an uncracked region with a very high concentration of very bright particles. The sample treated at 770°C was anomalous in this series. The brighter contrast phase was not nearly as defined as found with the samples from the other two treatment temperatures, and the bright particles appear to be more spread out and larger. The brighter contrast phase does appear to exhibit cracking

which was not seen in any of the samples treated at lower temperatures. The darker contrast phase does appear to contain bright particles just in a much lower density than in the brighter contrast phase. Representative EDS of the bright phase is shown in Figure 10. The indium signal increases as the treatment temperature decreases. The indium signals were only slightly lower for the darker contrast phase so they are not shown. A sodium signal was not detectable for any of the samples.

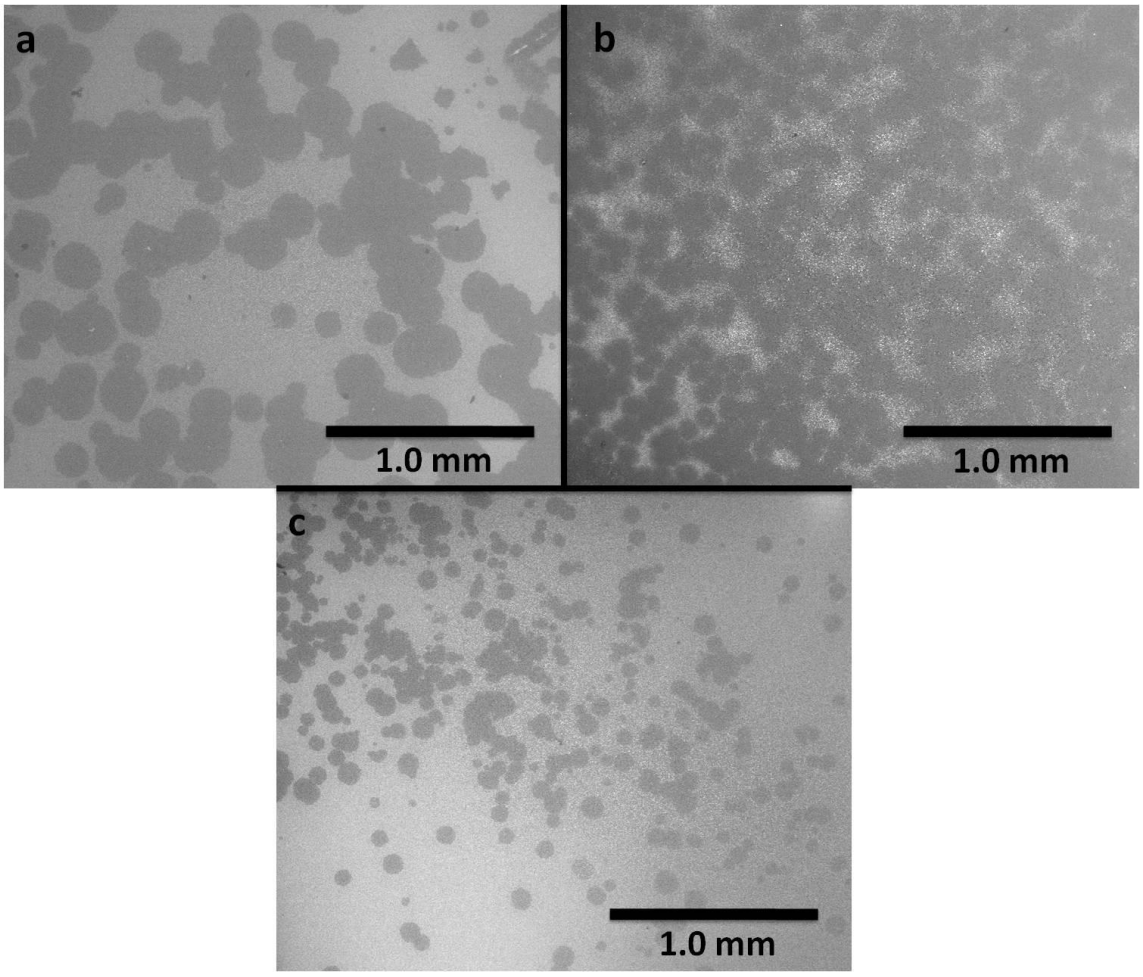

Figure 8. Representative low magnification ESEM micrographs taken using BSE of surfaces of samples treated at a) 720°C, b)770°C, and c) 670°C.

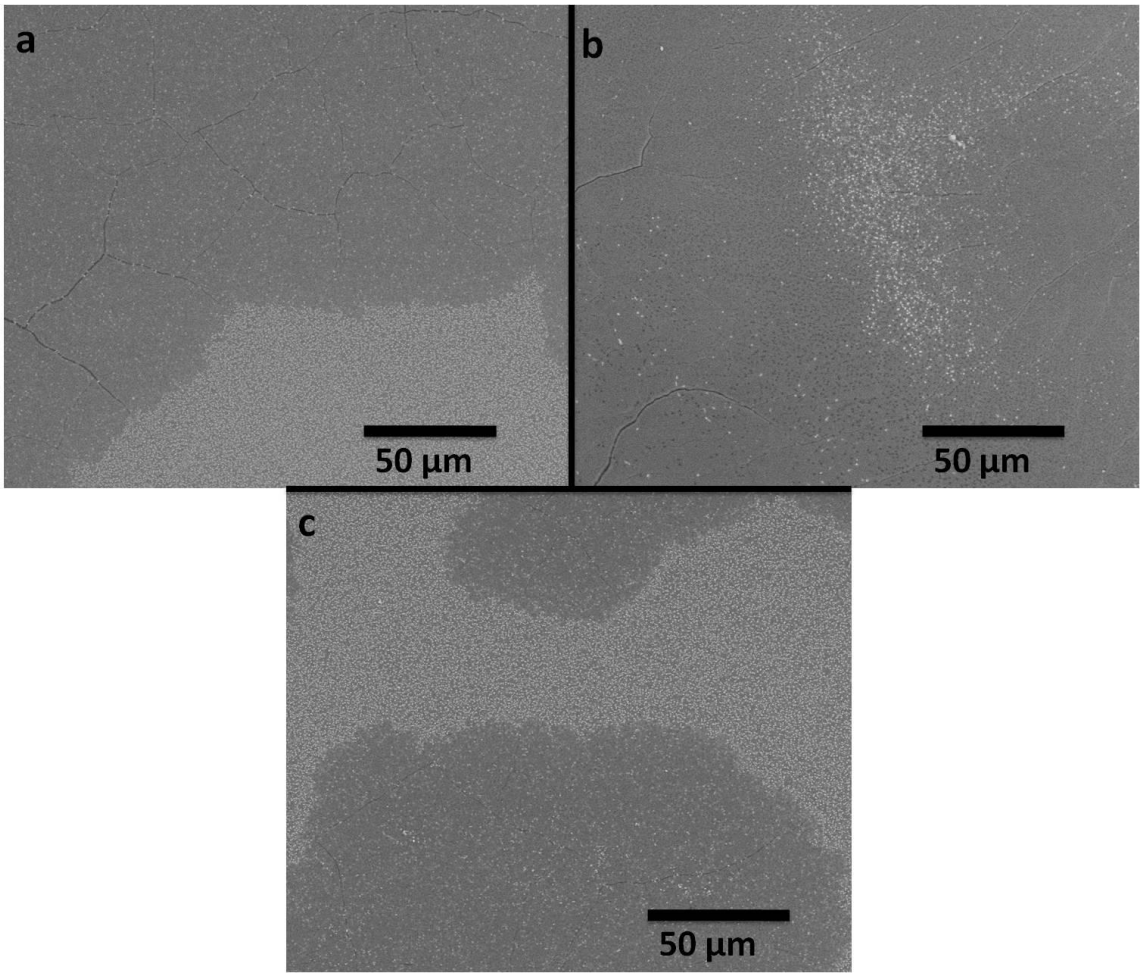

Figure 9. Representative ESEM micrographs taken using BSE of surfaces of samples treated at a) 720°C, b)770°C, and c) 670°C.

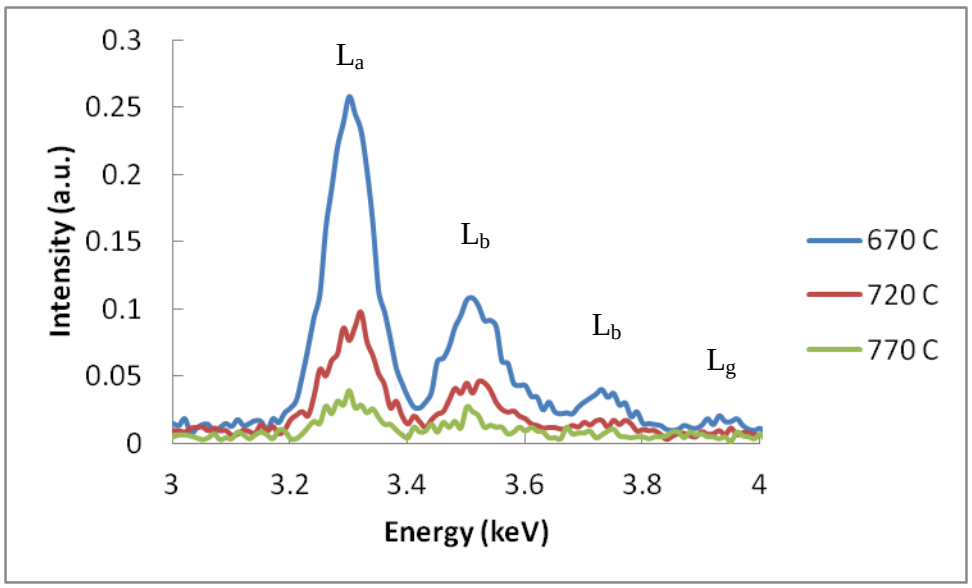

Figure 10. Representative EDS spectra of the relative indium concentration for the surfaces of the samples treated at different temperatures.

Representative higher magnification micrographs depicting the difference between the light and dark contrast phases for all sample treatment temperatures are shown in Figure 11. For the samples treated at 670°C and 720°C, the lighter contrast micrographs depict clusters that are below the surface. This makes size analysis difficult, but the visible clusters appear to be similar in size to those measured from the cross sections for the two lower treatment temperatures. The metallic clusters found at the surface of the sample treated at 770°C are larger than imaged in the cross sections, and they are larger than the clusters formed at the other two lower temperatures. The clusters are smaller for the sample treated at 670°C than for the sample treated at 720°C. The clusters are spherical in nature and the sample treated at 670°C exhibits a higher concentration of particles per volume. Some of the clusters imaged at 670°C appear to be somewhat elongated into cylindrical shapes but this could be an artifact of particle orientation and alignment below the sample surface. The metallic clusters appear to exist only at the actual surface of the sample treated at 770°C. The other two treatment temperatures have metallic clusters visible below the actual surface much more commonly than at the surface. The clusters found at the surface of the sample treated at 770°C are not as spherical as seen for the other samples. Some of the particles exhibit a

visible meniscus with the glass void that contains it. This phenomenon may be occurring at the other treatment temperatures, although it is difficult to determine due to the particles only existing slightly below the surface.

The samples treated at each temperature exhibit dark spherical shaped regions, similar in size to the metallic clusters, in the darker contrast phase. These dark spheres appear to be voids where metallic clusters once existed. There are some dark voids mixed with the brighter clusters in the brighter contrast phase of the sample treated at 770°C, but this is not seen for any of the samples treated at lower temperatures. The cracking, or crazing, that was found in the darker contrast phase at the surface is also seen in the brighter contrast phase for the sample treated at 770°C, but for none of the lower treatment temperatures. There was evidence across the surfaces of all three samples of the cracks being bridged by indium metal. The metal clearly wets the glass crack surface and has possibly been stretched upon cooling.

Grazing Incidence X-Ray Diffraction (GIXRD) measurements were performed to confirm that metallic indium is forming as a result of the hydrogen treatment, and that the clusters being imaged are indium. At 670°C, all of the peaks shown are indicative of indium metal. There is a very low intensity peak present at ~22 degrees 2θ which has been attributed to the possible presence of cristobalite. This cristobalite peak increases in intensity with increasing treatment temperature so much that it dominates the diffraction pattern collected for the sample treated at 770°C. The surface of the sample treated at 720°C also exhibited a moderate cristobalite peak, but it also has a very consistent peak shift of ~ 0.2 degrees 2θ to lower angles for all of the peaks associated with indium metal (Figure 13). The surface of the sample treated at 770°C was identified as containing a large amount of cristobalite, a small amount of indium metal, and a crystalline phase of composition $NaInSi_2O_6$ (Figure 14). The majority of unlabeled peaks in the diffraction pattern are due to this crystalline phase with only a minor contribution from the cristobalite phase diffraction pattern.

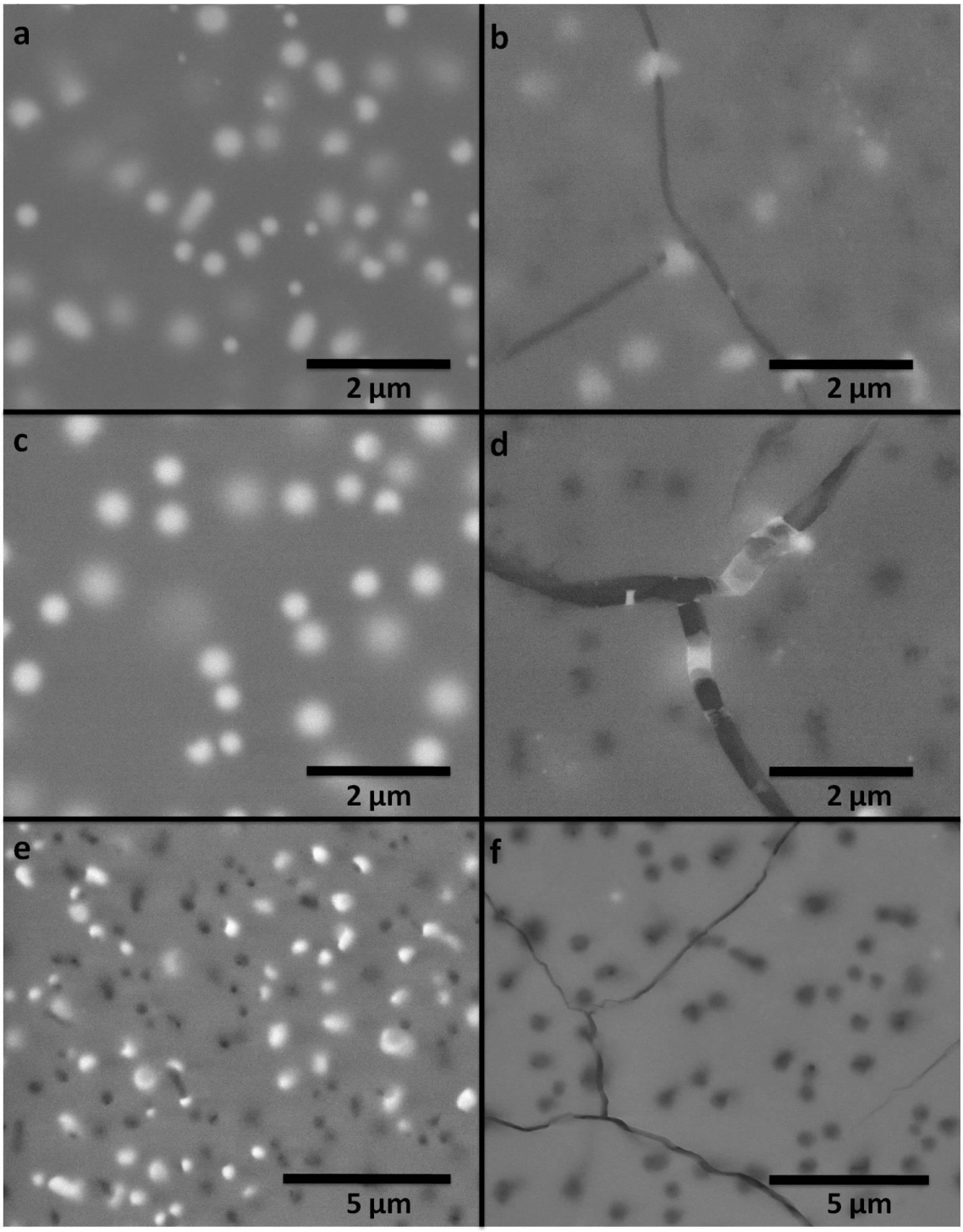

Figure 11. Representative micrographs taken using BSE of the surfaces of the samples treated at 670°C a) light region, b) dark region, treated at 720°C c) light region, d) dark region, and treated at 770°C e) light region, f) dark region.

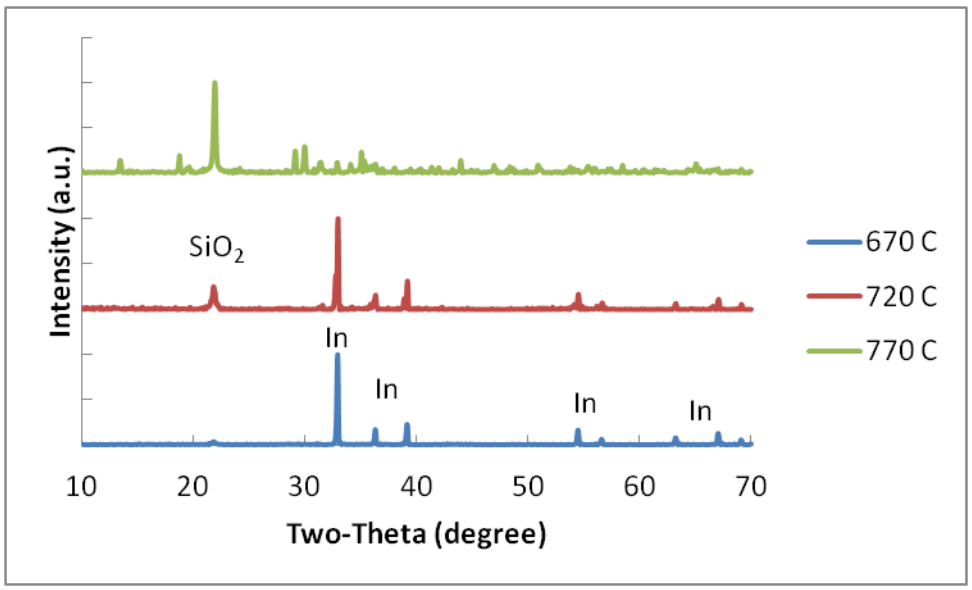

Figure 12. Representative GIXRD patterns for samples treated at various temperatures.

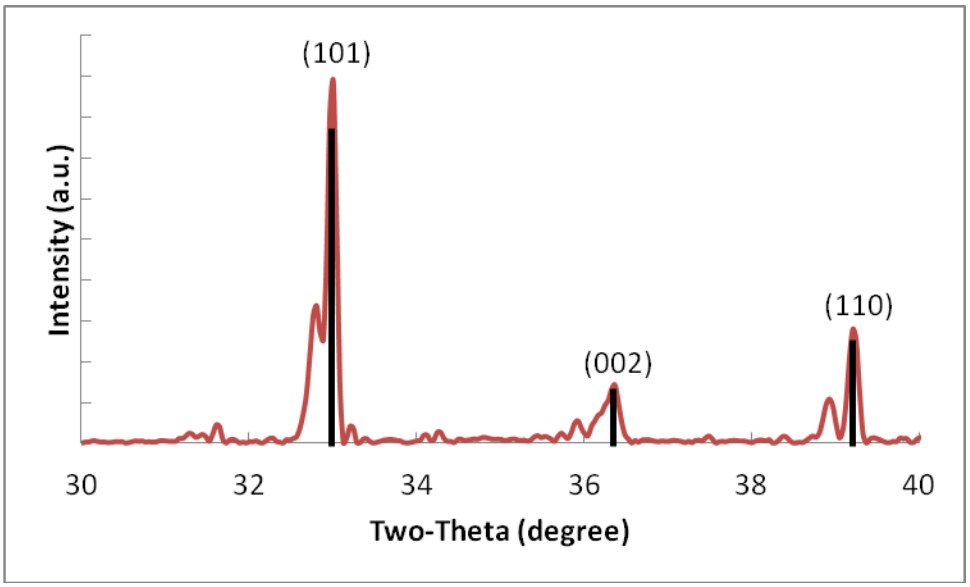

Figure 13. Magnification of the GIXRD pattern for the sample treated at 720°C.

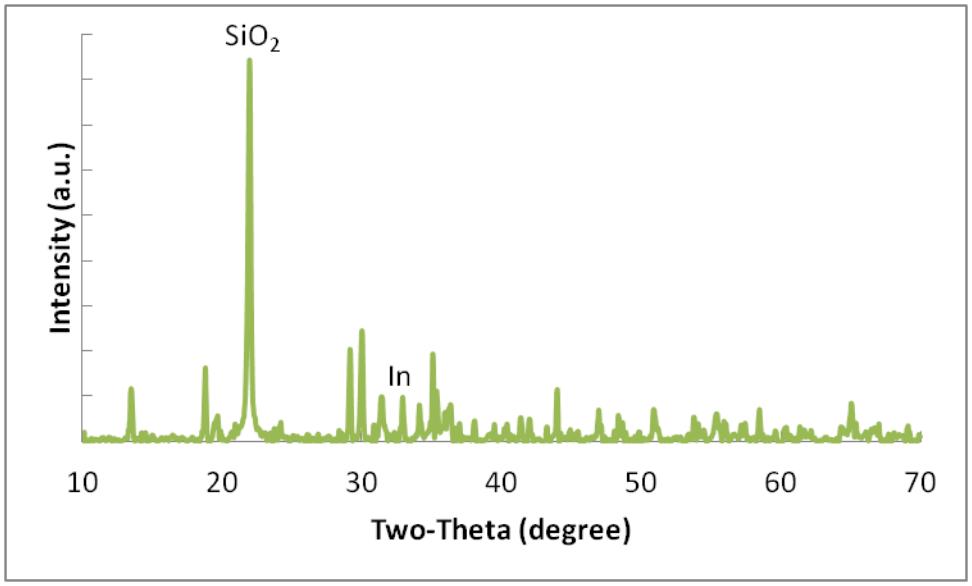

Figure 14. Representative GIXRD pattern for sample treated at 770°C.

4.3.1.1 Spectroscopy

The glasses used for this portion of work are all based on various compositions of Na_2O – In_2O_3 – SiO_2 glass. The glasses were all treated in 0.92 atm of hydrogen at 500°C, 550°C, 600°C, or at the Tg of the respective glass. IR spectra were collected for a series of glasses with varying concentrations of In_2O_3 and are shown in Figure 15. Without deconvolution the band changes are difficult to analyze, so the discussion will be limited to the large bands present in the spectra. The spectra show two easily distinguishable bands at roughly 3550 cm^{-1} and 3000 cm^{-1}. A third band within the IR edge is prominent in some of the spectra. These three bands are typically attributed to hydroxyl (-OH) in the structure of the glass. The IR edge is shifting to lower wavenumbers with increasing amounts of In_2O_3. Whether this is related to the third band within the edge cannot be determined from the data. The spectra for the samples containing 0 and 2 mol% In_2O_3 appear to have a different shape than the other spectra, especially for the band located near 3000 cm^{-1} for the rest of the glasses. These two glasses exhibit a large broad band very near to the IR edge and no distinguishable band near 3000 cm^{-1}. In general, the band near 3550 cm^{-1} increases in intensity with increasing additions of In_2O_3, and the band near 3000 cm^{-1} decreases in intensity with increasing

additions of In_2O_3. The ratios of the intensities of the two bands can be found in Table IV. The maximum intensity of the 3000 cm^{-1} band shifts to higher wavenumber values with increasing additions of In_2O_3 (Table IV).

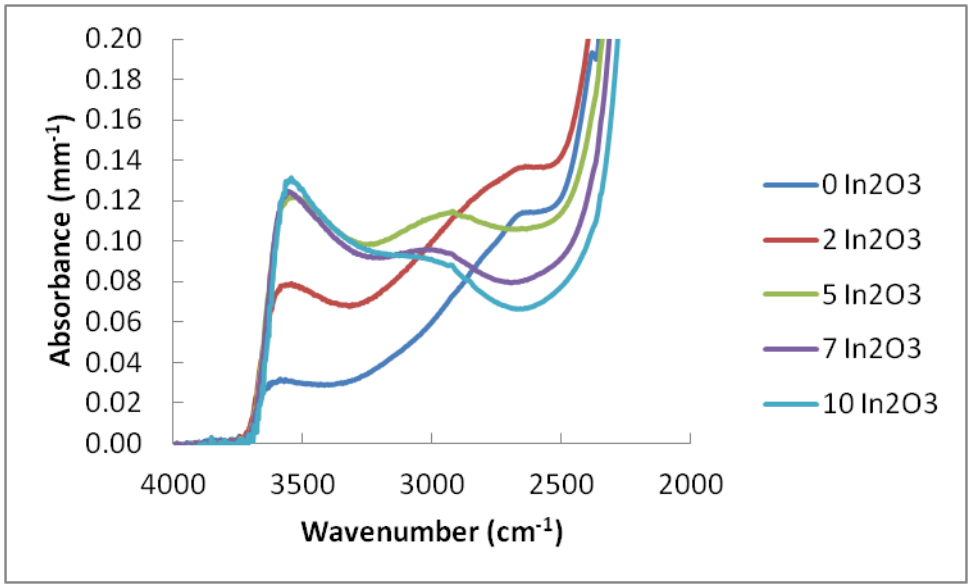

Figure 15. Representative IR spectra for glasses of composition 15 Na_2O–(x)In_2O_3–(85-x) SiO_2 (mol%).

IR spectra were also collected for a series of glasses with varying concentrations of Na_2O and are shown in Figure 16. Increasing amounts of Na_2O in the glass increases the intensity of the band located at ~3550 cm^{-1} as well as the band located at ~3000 cm^{-1}. The intensity ratio between the two bands decreases with increasing soda content (Table IV). An increase in the shoulder of the IR edge also appears to occur with increasing soda content. The shape of the band located at ~3550 cm^{-1} also appears to broaden with increasing soda content. IR spectra of a Na_2O–Al_2O_3–SiO_2 glass series with varying Al_2O_3 content are shown in Figure 17 for comparison to the indium containing glass and it is clear that the spectra have a different shape as well as intensity ratio. The glass containing 10 mol% Al_2O_3 has a distinct shoulder near the IR edge which is located near ~2660 cm^{-1} similar to the sodium silicate glass. Any band present near 3000 cm^{-1} is not defined as clearly as in the glass containing 10 mol% In_2O_3. The band located at ~3550

cm^{-1} is much broader for the glass containing alumina and the intensity ratio between this band and the shoulder near 2660 cm^{-1} is 1.13.

Table IV. IR Band Locations and Intensity Ratios for the Entire Series of Indium Containing Glasses with Standard Deviations in Parenthesis

	Approximate Band Locations		
Composition	**3500-3600 cm^{-1}**	**2600-3100 cm^{-1}**	**I_{3550}/I_{3000}**
$15Na_2O$-$85SiO_2$	3600	2660	0.27 (0.02)
$15Na_2O$-$2In_2O_3$-$83SiO_2$	3600	2660	0.54 (0.02)
$15Na_2O$-$5In_2O_3$-$80SiO_2$	3550	2920	1.12 (0.03)
$15Na_2O$-$7In_2O_3$-$78SiO_2$	3550	3000	1.34 (0.03)
$15Na_2O$-$10In_2O_3$-$75SiO_2$	3550	3070	1.45 (0.05)
$20Na_2O$-$10In_2O_3$-$70SiO_2$	3550	3000	1.09 (0.02)
$30Na_2O$-$10In_2O_3$-$60SiO_2$	3550	2920	1.00 (0.03)

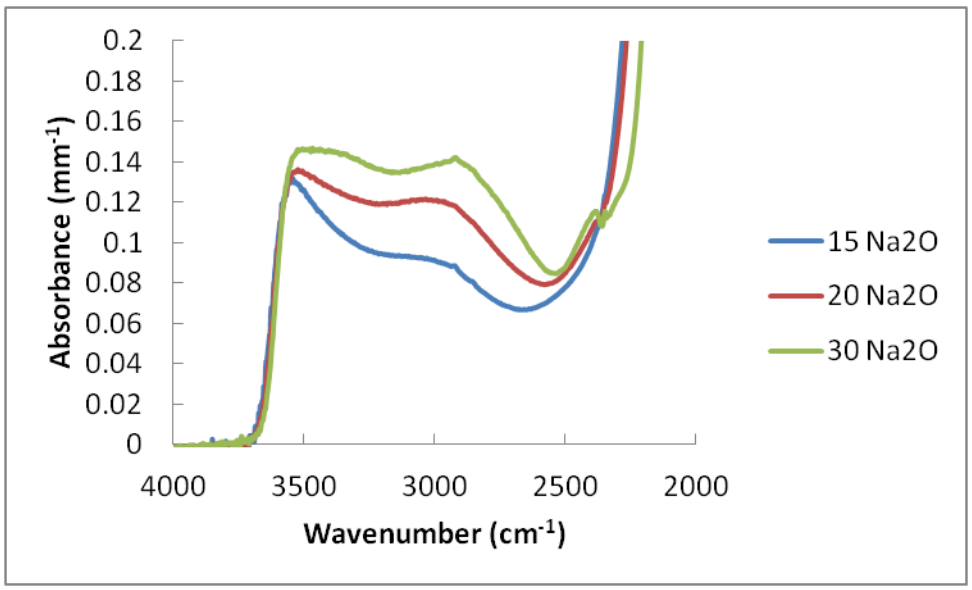

Figure 16. Representative IR spectra for glasses of composition (x) Na_2O–10 In_2O_3–(90-x) SiO_2 (mol%).

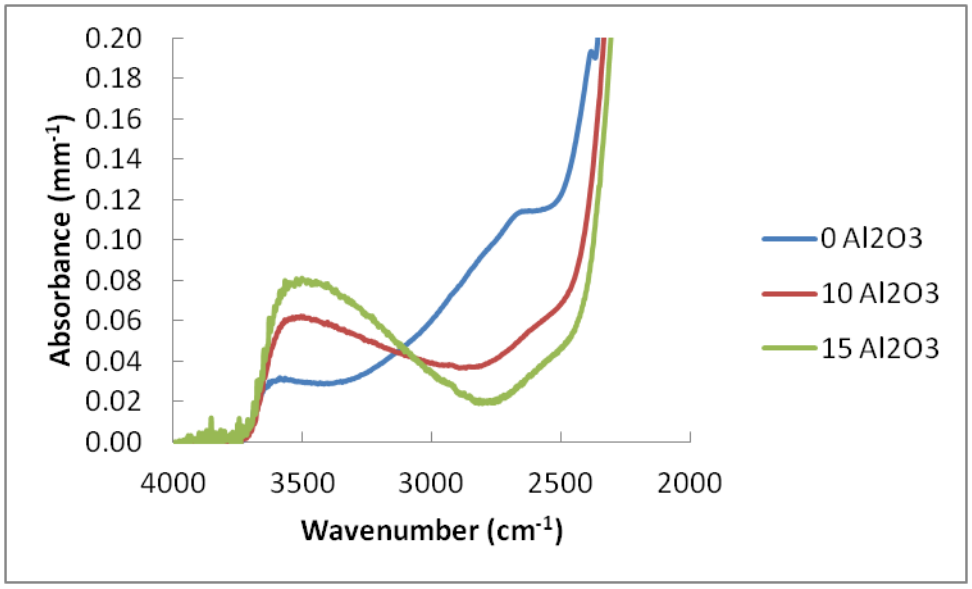

Figure 17. Representative IR spectra for glasses of composition 15 Na_2O–(x) Al_2O_3–(85-x) SiO_2 (mol%).

The IR spectra for all of the samples were monitored throughout the various reduction treatments. All of the spectra collected showed a relative increase in the height

of the bands located at approximately 3500-3600 cm^{-1} and 2750-3100 cm^{-1} (Figure 18). Some of the spectra exhibit a decrease in the intensity near the IR edge around 2500 cm^{-1}.

The relative changes are more easily monitored by creating difference spectra i.e., the baseline absorbance subtracted from the absorbance at a given treatment time. These difference spectra were also used to correct the background which is discussed more in Appendix A-1. Typical plots for a 500°C treatment of the 5 mol% In_2O_3 containing glass is shown in Figure 19. The difference spectra in this plot show 3 discrete bands located at approximately 3550, 2950, and 2350 cm^{-1}. The band at 2350 cm^{-1} is located within the IR edge and therefore is quite difficult to analyze as the edge is also changing during these reduction experiments. This band also has a very inconsistent appearance due to the presence of CO_2 bands in the same wavenumber region of the spectrum which further complicate analysis. The bands located at 3550 and 2950 cm^{-1} appear to be quite similar in appearance and location to the baseline spectra collected before the reduction experiments which are shown in Figure 15. The difference spectra for the glasses containing 2 mol% In_2O_3 are again different from the spectra taken for the rest of the samples (Figure 20). The appearances of the various difference spectra (i.e. the band shapes and locations) are very similar to that of the base spectra. A plot showing the band shapes of four glasses with different amounts of indium after reduction, can be found in Figure 21.

The main difference between the reduced and base glass spectra lies in the intensity ratios of the two main bands. In all of the glasses investigated the intensity of the band located at 3500 – 3600 cm^{-1} increases more rapidly than the band located at 2950 cm^{-1} except for the glass containing 2 mol% In_2O_3 and the glass containing 30 mol% Na_2O. The intensity ratios for all of the glasses after 225 hours of treatment in hydrogen at 500°C are shown in Table V. No other ratios were calculated due to the background correction used for the spectra collected for the rest of the treatment temperatures affecting the 2950 cm^{-1} band at a greater rate than the 3550 cm^{-1} band. For every indium containing glass composition reduced, the intensity ratio (I_{3550}/I_{3000}) increases after reduction except for the glass containing 30 mol% Na_2O (Table VI). It should be noted that the backgrounds for these indium containing glasses were much different than for any of the other spectra collected by the author and there is some

question as to the validity of the correction mentioned in the Appendix (A-1) for these glasses. At this point the correction used is an improvement but this does not mean it is valid for all conditions.

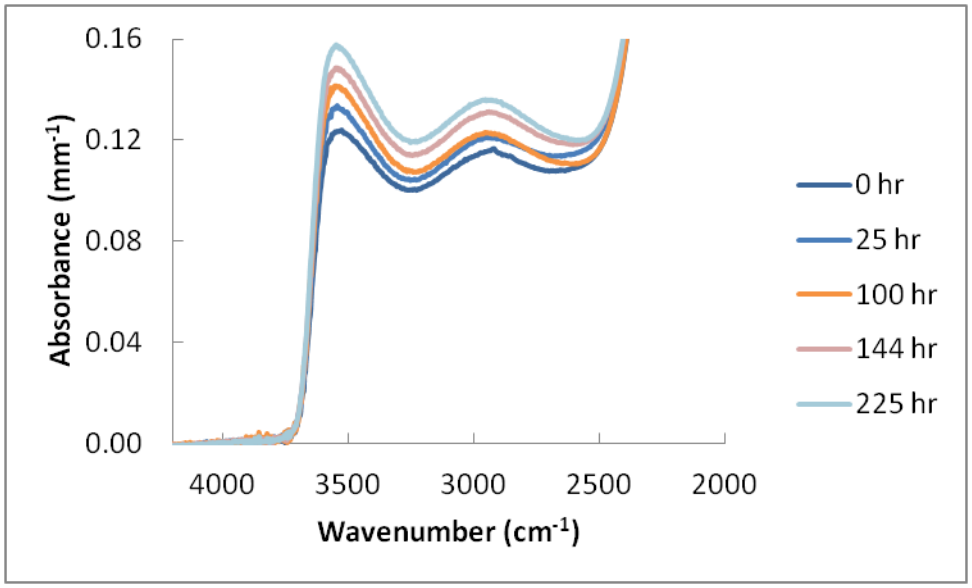

Figure 18. Representative IR spectra of 5 mol% In_2O_3 containing glass after specific treatment times in H_2 gas at 500°C.

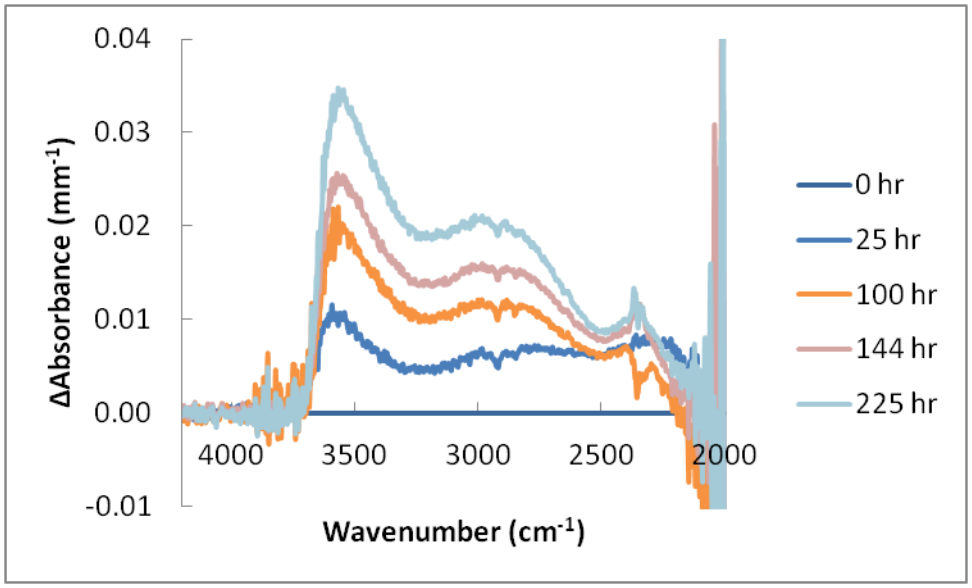

Figure 19. Representative IR difference spectra of 5 mol% In_2O_3 containing glass after specific treatment times in H_2 gas at 500°C.

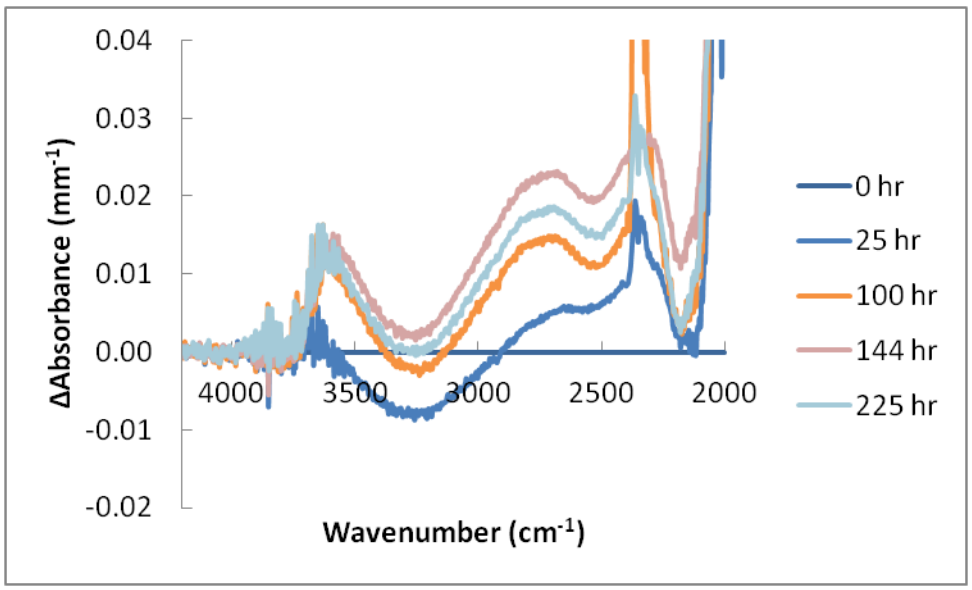

Figure 20. Representative IR spectra of 2 mol% In_2O_3 containing glass after specific treatment times in H_2 gas at 500°C.

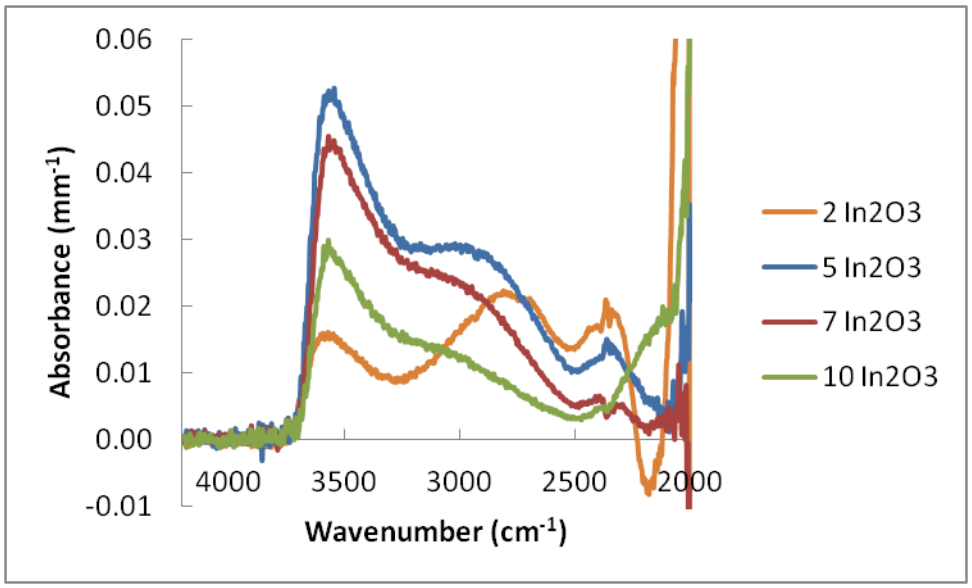

Figure 21. Representative IR difference spectra of glasses containing different concentrations of In_2O_3 after 100 hours of treatment in H_2 gas at 550°C.

Table V. Difference IR Spectra Band Locations and Intensity Ratios for the Entire Series of Indium Containing Glasses Treated at 500°C with Standard Deviations in Parenthesis

	Approximate Difference Spectra Band Locations After Reduction		
Composition	**3500-3600 cm^{-1}**	**2600-3100 cm^{-1}**	**I_{3550}/I_{3000}**
$15Na_2O$-$85SiO_2$	-	-	-
$15Na_2O$-$2In_2O_3$-$83SiO_2$	3600	2750	0.70 (0.03)
$15Na_2O$-$5In_2O_3$-$80SiO_2$	3550	2920	1.76 (0.09)
$15Na_2O$-$7In_2O_3$-$78SiO_2$	3550	3000	1.87 (0.07)
$15Na_2O$-$10In_2O_3$-$75SiO_2$	3550	3060	2.26 (0.10)
$20Na_2O$-$10In_2O_3$-$70SiO_2$	3550	3000	1.24 (0.07)
$30Na_2O$-$10In_2O_3$-$60SiO_2$	3550	2940	0.85 (0.05)

Table VI. Comparison between the base spectra intensity ratio to the difference spectra of the reduced glass intensity ratio for various indium containing glasses reduced at 500°C

	Intensity Ratios (I_{3550}/I_{3000})	
Composition	**Base**	**Reduced (Difference Spectra)**
$15Na_2O$-$2In_2O_3$-$83SiO_2$	0.54 (0.02)	0.70 (0.03)
$15Na_2O$-$5In_2O_3$-$80SiO_2$	1.12 (0.03)	1.76 (0.09)
$15Na_2O$-$7In_2O_3$-$78SiO_2$	1.34 (0.03)	1.87 (0.07)
$15Na_2O$-$10In_2O_3$-$75SiO_2$	1.45 (0.05)	2.26 (0.10)
$20Na_2O$-$10In_2O_3$-$70SiO_2$	1.09 (0.02)	1.24 (0.07)
$30Na_2O$-$10In_2O_3$-$60SiO_2$	1.00 (0.03)	0.85 (0.05)

Some of the spectra did exhibit overall absorbance decreases at very short treatment times. This decrease occurs within the first four hours, after which the three bands associated with the composition begin to increase normally. This phenomenon was most prevalent in glasses with the lowest concentrations of indium and not present at all for the glasses with the highest concentrations of indium. The decrease noted in the spectra is typically very broad exhibiting a maximum near 3350 cm^{-1}. The decrease does appear to exist from 3550 cm^{-1} to 2100 cm^{-1}, or to the IR edge of the glass.

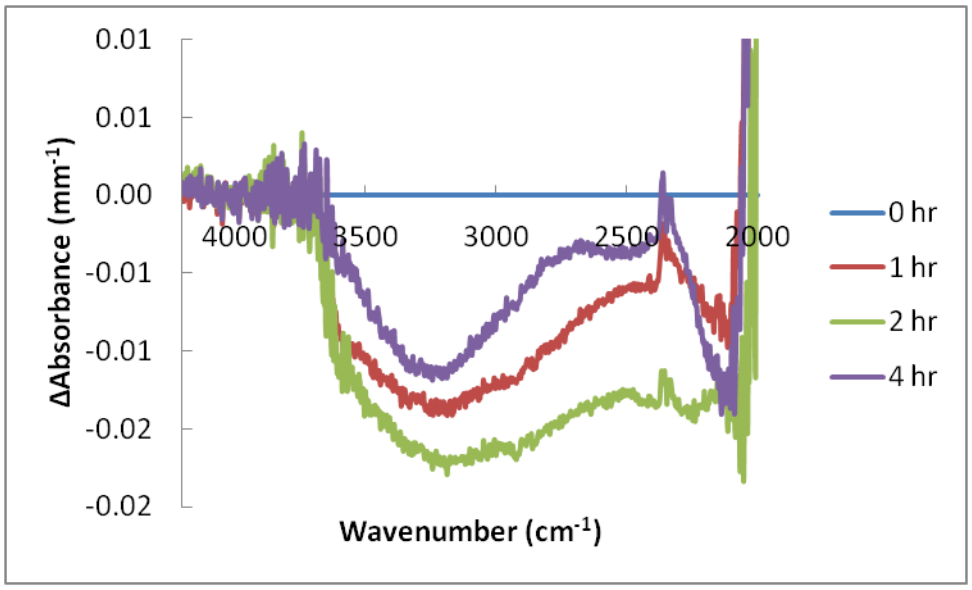

Figure 22. Representative IR difference spectra of 2 mol% In_2O_3 containing glass after specific treatment times in H_2 gas at 500°C.

The tarnishing model predicts a parabolic relationship between the reaction of ionic indium dissolved in the glasses and time, and also depends upon the permeability of hydrogen, pressure of hydrogen, and the concentration of indium present in the glass. None of the glasses treated in this study reached the completion of the reaction, and this does not allow for a direct comparison between glasses of different composition. It is possible to compare glasses of a single composition that have been treated at different temperatures. Tarnishing plots were constructed for a number of different indium containing glasses and fit with a best fit linear regression that was anchored to a y-value of zero. The glass containing 2 mol% In_2O_3 was treated at four temperatures, and a

representative tarnishing plot of the change in absorbance of the 3600 cm^{-1} hydroxyl band can be found in Figure 23. The glass treated at 500°C exhibits a very poor linear regression fit to the data points which may be a result of the considerable initial decrease that pre-empted any increase in hydroxyl for this temperature. The data for the remaining treatment temperatures were much more linear in comparison. There is a general increase in the slopes for the glasses treated with increasing temperature. The only glass that did not fit this trend is the glass treated at 600°C. It must be noted that 588°C was the measured glass transition temperature for this glass. The fit slopes and R^2 values for the glasses used in this plot and any subsequent indium tarnishing plots are shown in Table VII. The relative changes in absorbance for the data of this glass composition are the smallest recorded in this study.

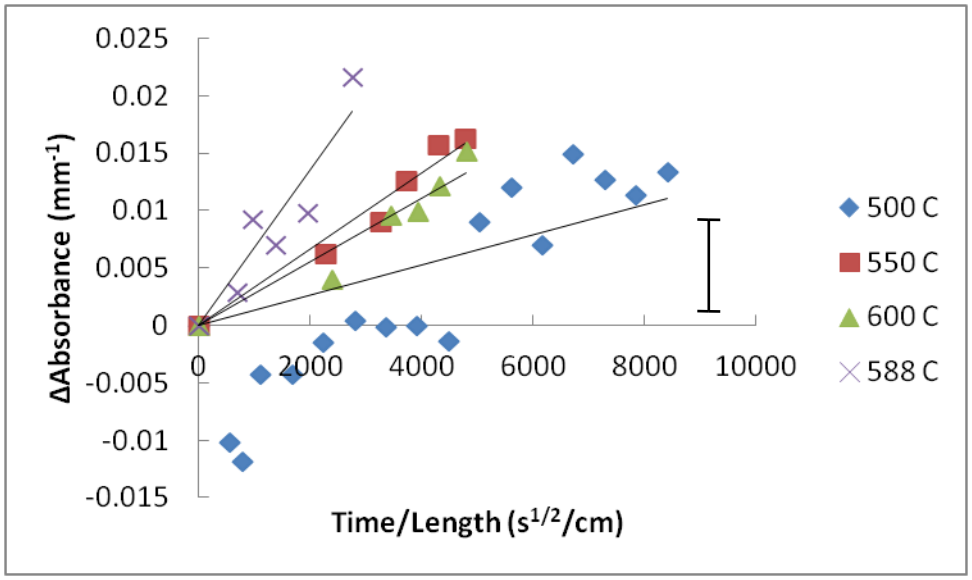

Figure 23. Plot of the change in absorbance of the 3500-3600 cm^{-1} band against the reduction time and the length of the sample for 2 mol% In_2O_3 containing glasses at various temperatures.

The glass containing 5 mol% In_2O_3 was treated at 500, 550, 600, and 662°C, and a representative tarnishing plot of the change in absorbance of the 3550 cm^{-1} hydroxyl band can be found in Figure 24. Unlike the previous data for the 2 mol% In_2O_3 sample, the data points for every treatment temperature of the 5 mol% In_2O_3 containing glasses were

fit very well, with only slight scatter, with a linear regression. The fit slopes for the data from different treatment temperatures increase with temperature. The difference between the 550°C and the 600°C data fits is small.

The glass containing 7 mol% In_2O_3 was treated at 500, 550, 600, and 694°C, and a representative tarnishing plot of the change in absorbance of the 3550 cm^{-1} hydroxyl band can be found in Figure 25. The data points for the 500°C and the 694°C treatments exhibit very poor linear regression fits due to scatter. The higher temperature data had much more considerable background correction issues and this could contribute to the scatter. The only fit slope that does not increase with the treatment temperature appears to be the slope for the 500°C treatment data.

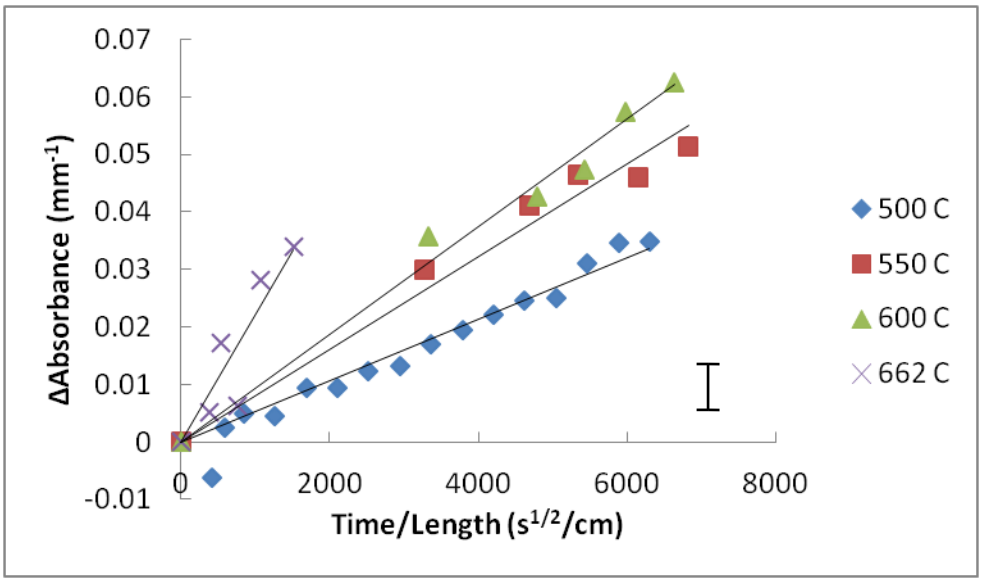

Figure 24. Plot of the change in absorbance of the 3500-3600 cm^{-1} band against the reduction time and the length of the sample for 5 mol% In_2O_3 containing glasses at various temperatures.

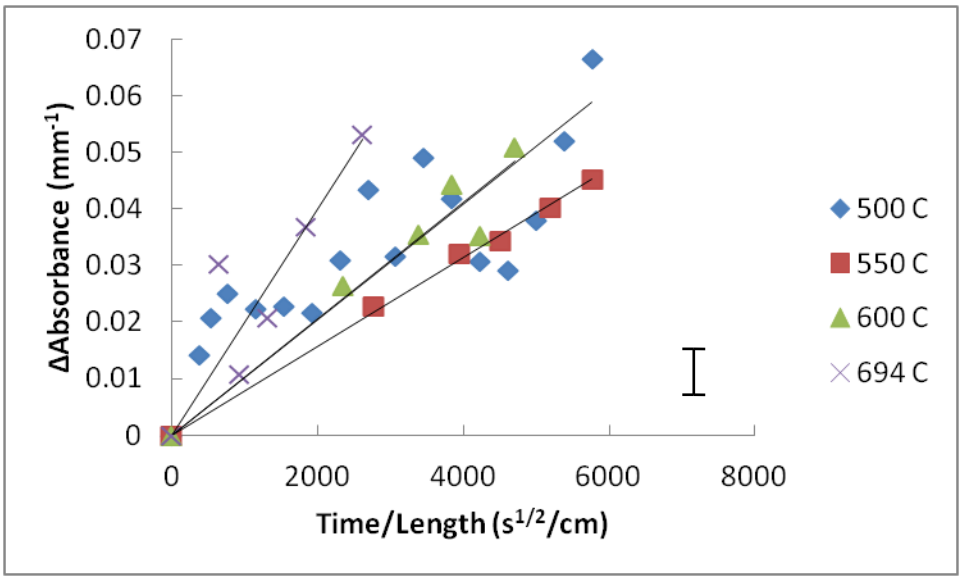

Figure 25. Plot of the change in absorbance of the 3500-3600 cm^{-1} band against the reduction time and the length of the sample for 7 mol% In_2O_3 containing glasses at various temperatures.

The glasses containing 10 mol% In_2O_3 and 15 mol% Na_2O were treated at four temperatures, and a representative tarnishing plot of the change in absorbance of the 3550 cm^{-1} hydroxyl band can be found in Figure 26. All the data points for every treatment temperature of the 15 mol% Na_2O containing glasses were fit very well, with only slight scatter, with a linear regression. Similar to the 7 mol% samples, the linear regression fits were out of the expected order, with the 500°C treatment temperature data having a larger slope than the 550°C treatment temperature data. Otherwise the slopes of the data behave as expected and increase with treatment temperature.

The glasses containing 10 mol% In_2O_3 and 20 mol% Na_2O were treated at four temperatures, and a representative tarnishing plot of the change in absorbance of the 3550 cm^{-1} hydroxyl band can be found in Figure 27. All the data points for every treatment temperature of the 20 mol% Na_2O containing glasses were fit very well, with only slight scatter, with a linear regression. Only two data points exist for the 698°C treatment due to the complex background of the spectra, and all of the slopes increase with increasing treatment temperature as predicted by the tarnishing model.

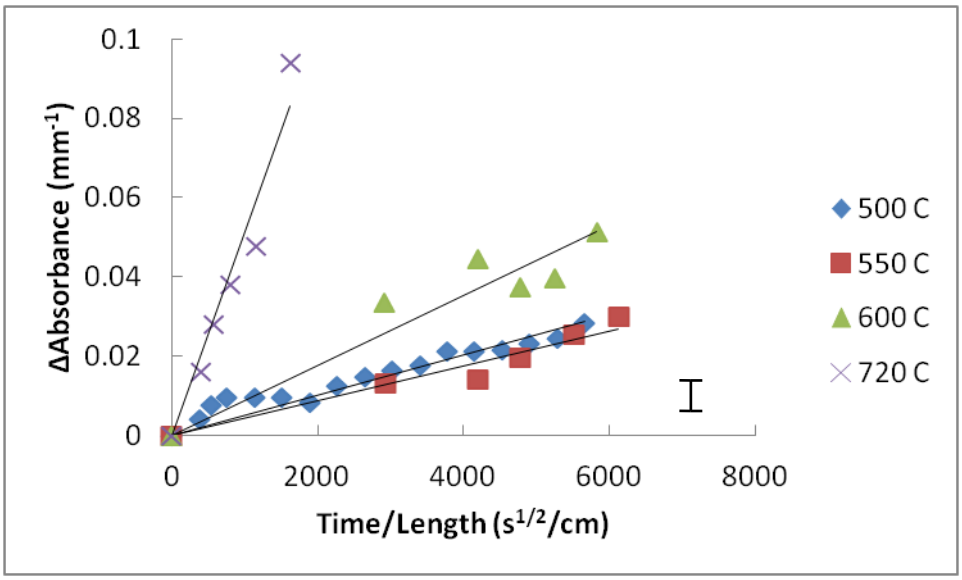

Figure 26. Plot of the change in absorbance of the 3500-3600 cm^{-1} band against the reduction time and the length of the sample for 10 mol% In_2O_3 containing glasses at various temperatures.

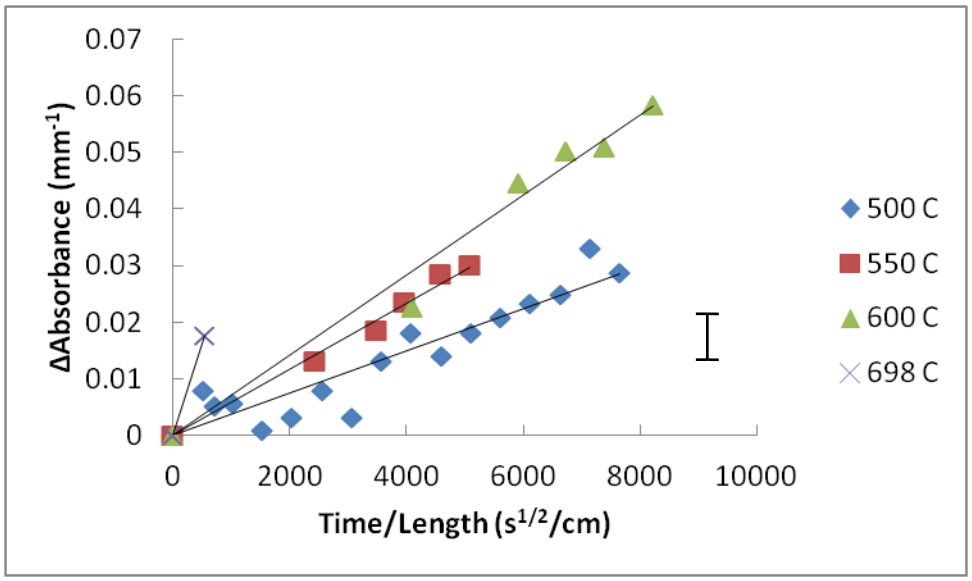

Figure 27. Plot of the change in absorbance of the 3500-3600 cm^{-1} band against the reduction time and the length of the sample for 20 Na_2O – 10 In_2O_3 – 70 SiO_2 (mol%) glasses at various temperatures.

The glasses containing 10 mol% In_2O_3 and different concentrations of Na_2O are comparable, and a representative tarnishing plot of the change in absorbance of the 3550 cm^{-1} hydroxyl band can be found in Figure 28. All of the data points exhibited good linear regression fits with minor scatter. The glass containing 30 mol% Na_2O has the greatest slope of the three compositions compared. The glass containing 15 mol% Na_2O has the next highest slope. The 15 mol% and 20 mol% glasses fit slopes are very similar with respect to error.

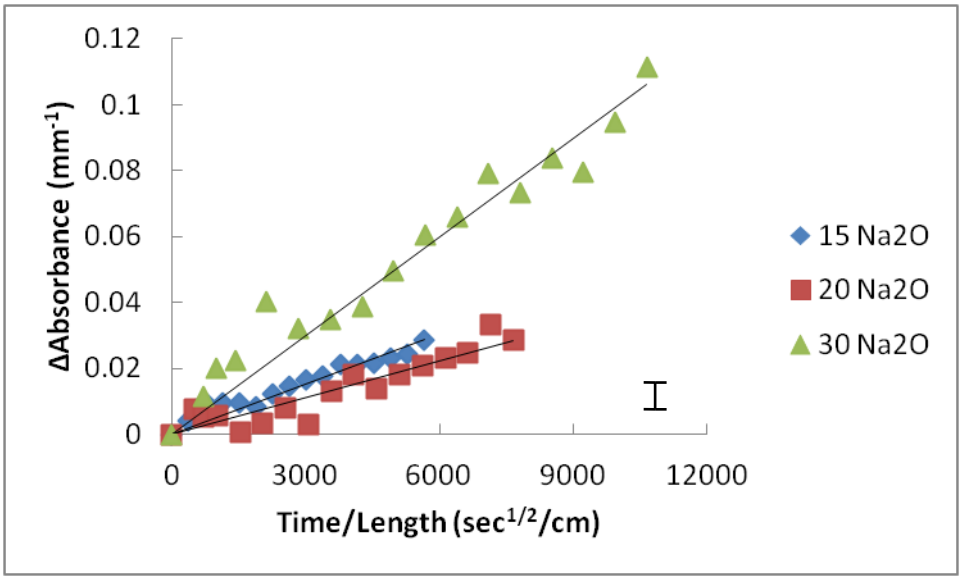

Figure 28. Plot of the change in absorbance of the 3500-3600 cm^{-1} band against the reduction time and the length of the sample for various concentrations of Na_2O and 10 mol% In_2O_3 containing glasses at 500°C.

Table VII. Collection of the Best Fit Linear Regression of the Change in Absorbance of the 3500-3600 Cm^{-1} Band Plotted Against the Reduction Time, Concentration of In_2O_3, and the Length of the Sample for Various Concentrations of Na_2O And In_2O_3 Containing Glasses at Various Temperatures With R^2 Values in Parenthesis

		Slope of Hydroxyl Formation Fit			
Composition		500°C	550°C	600°C	Tg°C
15 Na_2O	2 In_2O_3	1.32E-6 (0.49)	3.31E-6 (0.96)	2.76E-6 (0.93)	6.74E-6 (0.87)
15 Na_2O	5 In_2O_3	5.35E-6 (0.95)	8.07E-6 (0.97)	9.37E-6 (0.98)	2.21E-5 (0.82)
15 Na_2O	7 In_2O_3	1.02E-5 (0.49)	7..85E-6 (0.99)	1.03E-5 (0.94)	2.00E-5 (0.79)
15 Na_2O	10 In_2O_3	5.09E-6 (0.90)	4.40E-6 (0.94)	8.79E-6 (0.89)	5.12E-5 (0.95)
20 Na_2O	10 In_2O_3	3.72E-6 (0.87)	5.85E-6 (0.99)	7.07E-6 (0.98)	3.27E-5 (1.00)
30 Na_2O	10 In_2O_3	9.98E-6 (0.94)	9.81E-6 (0.65)	1.81E-5 (0.91)	6.65E-6 (0.08)

UV-Vis absorption spectra were also collected for this series of glasses during reduction. All of the glasses darkened to some degree during the reduction process to a light gray or sometimes whitish color. The absorption spectra rarely exhibited consistent trends, especially for the treatments done at 500°C. The 15 Na_2O – 10 In_2O_3 – 75 SiO_2 (mol%) glass (along with others) exhibited a shoulder developing near the UV-edge and a general increase in the background (Figure 29). The sample had a consistent gray appearance after reduction. The glass containing 2 mol% In_2O_3 did not exhibit a gray color as did the other glasses, and the glass with 30 mol% Na_2O turned whitish during reduction. Some of the samples exhibited a very inconsistent background increase or decrease during reduction and an example of this can be found in Figure 30. Initially a shoulder develops and the background increases with treatment time. Over time the background appears to reach a maximum and then decreases back to the baseline, and the shoulder appears to recede. Some of the samples exhibit the shoulder growth but variable

background increases and decreases, and others exhibit variable shoulder growth combined with variable background increases and decreases. The only consistent trend found for all of the UV-Vis data was a general increase in the UV-edge of the glasses with treatment time.

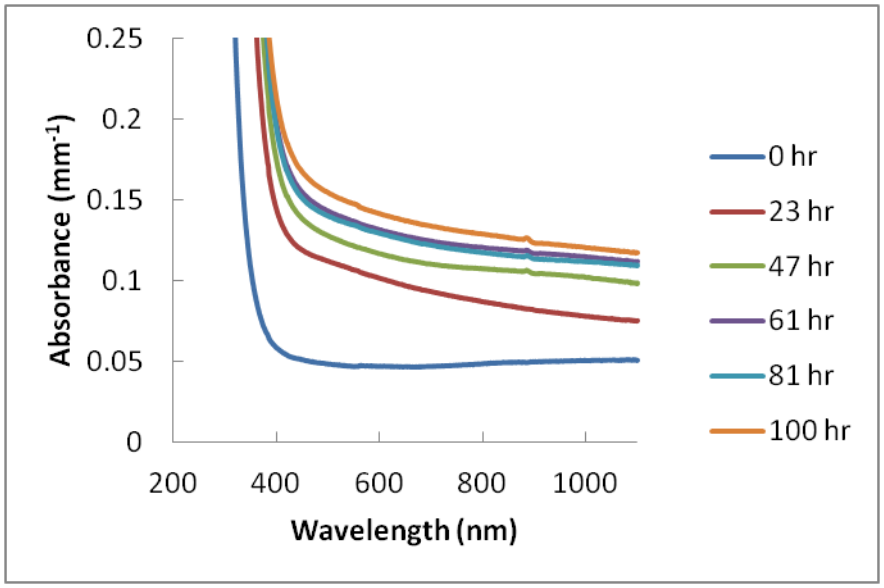

Figure 29. Representative plot of the visible absorbance changes during reduction for the sample containing 10 mol% In_2O_3 and 15 mol% Na_2O.

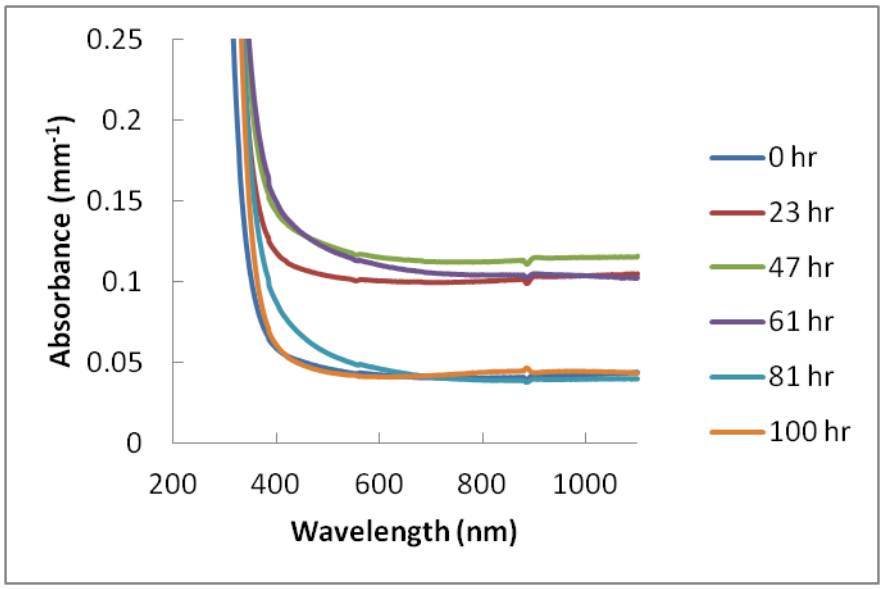

Figure 30. Representative plot of the visible absorbance changes during reduction for the sample containing 10 mol% In_2O_3 and 20 mol% Na_2O.

4.4 Discussion

4.4.1 Reaction

It is important to understand how indium affects the glass structure in question. For the glasses used in this portion of the work, indium exists in these sodium silicate glasses as a 3+ ion (In_20_3) due to the pp_{O2} that is inherent with any ambient melt.[63,88-92] Indium is reported to exist in octahedral coordination, within this glass system, similar to scandium and yttrium in sodium silicates[85]. This is opposite to what one might think as indium is in the same column as aluminum and gallium, which can both exist in tetrahedral coordination in this glass system. An indium-oxygen octahedra would have a net negative charge and thus must be associated with sodium ions to compensate, similar to aluminum-oxygen tetrahedra.

Based on calculations using thermodynamic databases, it has been reported that metallic indium is reducible in hydrogen.[93,94] These calculations are for the reduction of the oxide based on concentrations of hydrogen, water, the oxide and the metal in question. All of these concentrations are more difficult to calculate or realize when considering a glass. It can be said for the glasses used in this study, that indium was reduced from 500°C up to 770°C. It is reported that the concentration of alkali in a glass may also have an effect on any reduction-oxidation (redox) reactions so it must be clearly stated that indium is only reducing in these glass compositions.[63] Based on the apparent ease of reduction, it is probably the case that indium will reduce in most glasses, but without more data that is not a certainty.

For indium to successfully reduce to metal, hydrogen molecules must diffuse to an octahedrally coordinated indium ion and react, thereby donating electrons to the indium ions. The proposed reaction for this case is:

$$InO_{\frac{3}{2}} + \frac{3}{2}H_2 \rightarrow In^0 + 3(Si - OH) \qquad (25)$$

This reaction implies that three hydroxyl groups should form for every indium ion in the glass. The octahedral site of indium, after reduction, should contain three hydrogen atoms each bonded to an oxygen anion. This would balance the charge on the octahedral

site. It is possible that the sodium ions would also react with the octahedra and rearrange the structure, but without more data this cannot be confirmed or denied at this point. A list of the hypothetical concentrations of hydroxyl based on the ideal composition of the glass after reduction and indium ions before is shown in Table VIII.

Table VIII. Calculated Concentrations of Indium Ions in the Various Glasses and the Respective Hydroxyl Sites Generated by Complete Reduction

Base Glass	**Concentration of Indium Ions (mol/L)**	**Concentration of OH (mol/L)**
15 Na_2O - 2 In_2O_3 - 83 SiO_2	1.56	4.67
15 Na_2O - 5 In_2O_3 - 80 SiO_2	3.89	11.68
15 Na_2O - 7 In_2O_3 - 78 SiO_2	5.42	16.26
15 Na_2O - 10 In_2O_3 - 75 SiO_2	7.68	23.05
20 Na_2O - 10 In_2O_3 - 70 SiO_2	7.82	23.46
30 Na_2O - 10 In_2O_3 - 60 SiO_2	7.93	23.79

If all the indium is removed from the glass network, a very different base glass composition would remain. The initial and final compositions are listed in Table IX. These new compositions will be developing at the surface and progressing into the bulk of the base glasses during to the reaction. These altered compositions all lie within the immiscibility dome for binary soda silicate glasses except for the 30 soda (mol%) glass.[95-98] The typical immiscibility dome reported for sodium silicates lies between very low concentrations of soda (i.e. 2-3 mol%) up to 22-23 mol% soda. So, as the indium is being reduced from the structure, the structure is minimizing energy by nucleation and growth of separate glassy phases. This concept is possibly confirmed by the light and dark phases denoted in the BSE SEM micrographs of the glass surfaces.

Table IX. Base Glass Compositions and Composition After Indium Reduction with T_g Values Retrieved from SciGlass

Base Glass	Reduced Glass	T_g (°C)
15 Na_2O - 2 In_2O_3 - 83 SiO_2	15.3 Na_2O - 84.7 SiO_2	485
15 Na_2O - 5 In_2O_3 - 80 SiO_2	15.8 Na_2O - 84.2 SiO_2	485
15 Na_2O - 7 In_2O_3 - 78 SiO_2	16.1 Na_2O - 83.9 SiO_2	485
15 Na_2O - 10 In_2O_3 - 75 SiO_2	16.7 Na_2O - 83.3 SiO_2	486
20 Na_2O - 10 In_2O_3 - 70 SiO_2	22.2 Na_2O - 77.8 SiO_2	481
30 Na_2O - 10 In_2O_3 - 60 SiO_2	33.3 Na_2O - 66.7 SiO_2	453

The light and dark phases located at the glass surface of the imaged samples appeared to have a large concentration difference with respect to indium clusters. There were dark pits noticed where indium possibly once existed. These pits were exposed to the surface and typically large cracks were also associated with these darker regions. A possible explanation for this is phase separation. The surface is clearly a vastly different composition than the bulk indium containing glass, and therefore should have a considerable difference in thermal expansion. If the surface layer also consists of a glassy matrix and droplets of a secondary phase, these too should exhibit differences in thermal expansion. This sample and reduced layer are similar in some respects to a glaze-body type system (or infinite slab with a layer of a different TEC on one side). This allows for a very simplified calculation of the thermal stresses that may exist between the formed soda-silicate reduced layer and the underlying indium containing glass. To the author's knowledge, no thermal expansion data exists for these indium containing soda silicates. The basic equation used to model stress in a glaze is:[52,99]

$$\sigma_{Surface} = E\,(T_o - T')\left(\alpha_{Surface} - \alpha_{Glass}\right)(1 - 3j + 6j^2) \qquad (26)$$

where T_o is the set temperature (or the temperature where stresses are null), T' is the actual temperature, E is the Young's Modulus of the materials the calculation is being used for, and j is the ratio of the thickness of the surface layer to the thickness of the base glass. There are a couple of assumptions that must be mentioned. The value for E is assumed to be the same for both the glass and the substrate material which is false. This term should only affect the magnitude of the calculation and therefore a relative value

was used.[16] Further, the equation also requires that the glass is only bonded on one side and is infinitely long. The estimated values for this calculation used are shown in Table X. The TEC value for the pure sodium silicate was derived from the expression:[9]

$$\alpha \left(\frac{ppm}{K}\right) = 0.55 + x(0.48) \quad (27)$$

where x is the mol% soda in the binary soda silicate in question. This is valid between 300-400°C. Since there is no known TEC data for sodium indium silicates of this composition, three values were used in the calculation to show that the greater the difference between the TEC values the more compressive stress generated (Table XI).

Table X. Estimated and Measured Properties for Thermal Expansion Mismatch Stresses

	Tg (°C)	**TEC (ppm/K)**	**E (GPa)**
16.7 Na_2O - 83.3 SiO_2	485	8.8	80
15 Na_2O - 10 In_2O_3 - 75SiO_2	720	?	80

Table XI. Estimated Values of TEC for the Sodium Indium Silicate Series and Computed Compressive Stresses Associated With Each

~TEC (ppm/K)	**Stress (Mpa)**
6	102.41
5	138.98
4	175.56

A high compressive stress is calculated for the soda silicate surface layer. This itself is not unreasonable as compressive stresses are typically desirable to minimize crazing, which is a result of tensile stresses. This alone does not explain the anomalous cracking, or crazing, depicted in the micrographs of the surfaces. If the two phases imaged are considered, it is reasonable to assume the phases should exhibit different TEC values as they are compositionally different. As these samples were cooled very quickly from at least 500°C, there should be stresses due to thermal expansion mismatch, and this could even result in thermal shock. If all of the stresses are added up, there could be localized regions of tension, which could also cause the crazing seen in the micrographs.

It is also possible that the particles are interacting with the glassy matrix generating local stresses at the interface. This would explain the odd double peaks seen in the GIXRD results for the glass treated at 720°C. This appears to be an increase in the interatomic spacing in the indium crystals which could be caused by an interaction of the indium particle with the glassy matrix surrounding it. Upon cooling, the indium metal solidifies (~156°C), and the metallic particles should contract more quickly than the surrounding glassy matrix with subsequent decreases in temperature. If there is any interaction between the particle and the glassy matrix this could generate tensile stresses within the particle as well as within the surrounding glassy matrix. This too, could contribute to cracking or crazing, but the degree of cracking is quite large in comparison to the particle sizes measured. This crazing could be forceful enough to expel any indium particles exposed to the surface of the glass and would explain the pits. The author must note that the indium particles were exposed to the surface as simply brushing against the surface of the glass would remove particles and care had to be taken to avoid this as it could influence the spectroscopic results.

Comparing the spectra of the indium containing glasses to the alumina containing glasses shows obvious similarities and differences. The alumina containing glass shows a decrease in a band, located close to the IR-edge, with increasing alumina. This is supposed to be explained by the sodium ions being associated with negatively charged alumina tetrahedral to balance charge. This will keep the sodium ions from contributing to non-bridging oxygens in the glass structure. As this lower wavenumber band is attributed to "hydrogen bonded" hydroxyl, it fits with the structural model that is typically associated with glasses of this composition.[9,75-77,100] It is assumed to be similar for the sodium indium silicate series except for the indium forming negatively charged octahedra instead of tetrahedral. Indium is also much heavier which should lead to a general band shift in comparison to any aluminum containing reduced mass. The indium spectra have a much larger band located closer to ~3000 cm^{-1} that is not as clearly distinguishable in the aluminum containing glasses spectra. This is also believed to be due to the octahedral environment associated with indium in this glass system.

The heat treatment in hydrogen induces a great deal of structural change in the glasses. Three bands were identified at roughly 3550, 3000, and 2300 cm^{-1}. It is

generally accepted that the 3550 cm^{-1} band in sodium silicate glasses is due to "free" hydroxyl and the bands at 3000 and 2300 cm^{-1} are caused by "hydrogen bonded" hydroxyl[9,75-77,100]. These water bands in the IR indicate stronger hydrogen bonding for the lower wavenumber bands, and all bands are reported to increase with non-bridging oxygen content. The intensity ratios of the bands in the base glasses all increased after reduction at 500°C. This implies that the amount of "free" hydroxyl is increasing relative to the "hydrogen bonded" hydroxyl. The hydrogen bonding is reportedly between a hydroxyl group and a nearby non-bridging oxygen. In consideration of the proposed reaction model, this phenomenon doesn't make sense. Six oxygens are left behind after reduction of an indium ion. This means that three hydrogen protons would ideally bond to three of the existing oxygen anions, and the remaining oxygen anions most likely bond to nearby modifiers (Na^+). This should imply that there would be more "hydrogen bonded" hydroxyl than "free" hydroxyl. "Hydrogen bonded" hydroxyl bands are present in all of the reduced glasses. It should be noted that the difference spectra always appear to mimic that of the base glass. One would imagine that if indium additions increase the intensity ratio of the (I_{3550}/I_{3000}) bands, the removal of indium should promote a decrease in the intensity ratio. It is possible that longer reduction times would be required to see this expected behavior.

The only sample that exhibited a decrease in the intensity ratio implying an increase in the concentration of "hydrogen bonded" hydroxyl to "free" hydroxyl was the 30 Na_2O–10 In_2O_3–60 SiO_2 (mol%) glass. The main difference between this glass and the others is the amount of sodium which puts this glass composition outside of the immiscibility dome. There would be a fraction of soda that would break apart the silicate network producing a large amount of non-bridging oxygens. The rest of the soda would associate with the indium octahedra. This decreases the viscosity of the glass, and therefore the glass transition temperature. After reduction, the glass composition also has a high concentration of non-bridging oxygens associated with hydroxyl, which explains the very low T_g's reported. This was the first of many indications that a second mechanism besides hydroxylation may be contributing to the changes in the IR spectra which will be discussed more later. As reduction temperatures were increased the spectra

had considerable contributions from background that make intensity ratio data meaningless after the sloped corrections that were employed.

As there are some odd changes noticed in the IR spectra, a second mechanism is believed to be contributing to changes in the IR spectra. It is well established that water exists in glass naturally as a function of the pp_{H2O} in atmosphere during the melting process. This implies that an equilibrium between pp_{H2O} and the concentration of hydroxyl in a glass exists.[78,101-107] During these reduction reactions, the glass is exposed to essentially pure molecular hydrogen gas. This means that any hydroxyl being formed in the glass has a considerable driving force to react with nearby hydroxyls forming molecular water, and then reacting and diffusing out of the glass into the hydrogen atmosphere. A hydrogen atmosphere is effectively a vacuum with respect to molecular water. This phenomena is briefly mentioned in the literature as a possible explanation for lower than expected permeabilities calculated based on reaction kinetic measurements.[32] A proposed "backwards" reaction to the earlier proposed reduction reaction is:

$$2(Si-OH) \rightarrow Si-O-Si+H_2O \tag{28}$$

If this reaction is valid, it is quite possible that two of the three hydroxyls in the oxygen octahedra left over from the reduction of indium can potentially reduce and react and diffuse out of the glass into the hydrogen atmosphere. Since Si-O-Si bonds are somewhat more stable than two Si-OH bonds in the glass network, it is plausible that in a hydrogen atmosphere two Si-OH groups will recombine forming molecular water and Si-O-Si. With no water in the atmosphere, there is no concentration gradient driving the effective diffusion of the water to some equilibrium concentration in the glass, and the molecular water should diffuse out of the glass into the atmosphere. This changing of the structure post reduction could help to explain the intensity ratio changes that were noted. It is also possible that the hydroxyl is forming faster than the dehydroxylation is occurring. This would indicate, especially at lower temperatures and times, that the "free" hydroxyl band is increasing more rapidly than the "hydrogen bonded" hydroxyl band.

Dehydroxylation is problematic for a number of reasons. If water is diffusing out of the glass during reduction, this changes the surrounding atmosphere that the glass is being exposed to. Since water, hydrogen gas, and oxygen gas all exist at various temperatures in equilibrium concentrations with each other, dictated by thermodynamics,

if the hydrogen atmosphere comes into contact with water, it will begin to form some equilibrium concentration of oxygen. Oxygen gas may also diffuse into the glass network and react with the ions and can shift the overall reduction potential of the dissolved hydrogen potentially reforming oxides of indium. The diffusion of oxygen is much slower than that of hydrogen in glasses, so this process would be much less readily visible, but it could still pose a problem.

The way these samples were treated and the size of the samples with respect to the atmosphere indicates that any pressures of water or oxygen would be minute in comparison to the hydrogen atmosphere used for reduction treatments, especially when considering that most of the samples were taken out periodically and then the apparatus was refilled with pure hydrogen and treated for longer periods.

The tarnishing model was initially discussed by Crank to explain moving boundary reactions.[28] The tarnishing model is often described as:

$$\frac{(C-C_i)}{(C_f-C_i)} = (8KPt/L^2C_x)^{1/2} \quad (29)$$

where C is the concentration of hydroxyl at a given time, C_i is the initial concentration of hydroxyl, C_f is the final concentration of hydroxyl, K is the permeability of hydrogen in the glass, P is the partial pressure of hydrogen, t is the treatment time, L is the sample thickness, and C_x is the concentration of reaction sites. The term at the left of the equal sign is essentially a value from zero to one, where one would signify a completed reaction. This model has successfully been applied to hydrogen reaction experiments to describe various reaction kinetics.[7,12,22,29-32,34,35,108]

The band located at ~3550 cm^{-1} is attributed to "free" hydroxyl and any increases in this band are directly related to the reduction of indium ions. This band was the only one used in this study due to the sloped background correction employed to remove scattering increases caused by the formation of metal clusters. None of the reactions were found to reach completion, and no known extinction coefficients were found to relate the bands in IR to concentrations of hydroxyl. This means that the various compositions are unable to be directly compared without more data. All of the data from a single starting composition is organized and compared to the different temperatures of treatment. Since the only term that ideally will be affected by the temperature is

permeability, this is a direct method of measuring the affect that temperature has on the permeability of hydrogen in these glasses. The C_x term can be affected by temperature but it is assumed to remain constant here.[22]

The glasses all exhibit odd behavior with respect to the tarnishing model. It is believed that this is due to the difficulty of the background correction as well as the reverse reaction of dehydroxylation discussed earlier. Most of the data did exhibit a linear relationship between the changes in absorbance and the square root of time of treatment. This is proof that most of the data collected can be described by a linear moving boundary reaction. The data points taken from spectra collected for samples treated at and above 600°C, in all cases, had the most difficult backgrounds to correct and this is makes discussion difficult. The changing composition at the surface also must affect the data as the spectra for the base glass without indium has a very significant proportion of water existing in the band near the IR-edge. Without the ability to account for this band at the higher treatment temperatures it is difficult to provide a quantitative discussion. The IR spectra should approach that of a glass without indium due to the reduction. This dramatic change in the glass at the surface will affect the diffusion and solubility of hydrogen as well, thereby altering the concentration of dissolved hydrogen which, in turn, could affect the redox behavior of indium.

The measured change in absorbance did not exhibit an obvious trend with treatment temperature, as predicted by the tarnishing model, for a majority of the glasses. This could be in part due to the spectra beginning to revert back to that of a soda-silicate glass due to the reduction of indium. At higher temperatures, more indium is removed from the structure, and it is plausible that the 3500 cm^{-1} band is decreasing in intensity because of this fact. This may also be explained by the fact that hydroxyl concentrations have been shown to saturate when melted in high pressures of water. The water will tend to dissolve as a molecule instead of a reacted hydroxyl group after these concentrations have been reached indicating some sort of equilibrium inherent to the glass.[109-113] These saturation concentrations are typically reported to be between 3.2 – 4.5E+21 OH groups/cm^3 and are typically achieved through melting in conditions containing thousands of atmospheres of water vapor and allowing sufficient time for equilibrium to be reached. In the glasses used in this study, the calculated hydroxyl calculations for all

the glasses, except for the 2 mol% In_2O_3 glass, are well above the hydroxyl for saturation in typical geologic glasses. It is unlikely that more hydroxyl could be stable in these glasses. It is also noted that Q_3 groups are less reactive with water than Q_4 groups and water will always prefer to react with Q_4 silica. If the reduction reaction is forming the concentrations of hydroxyl calculated, there will be a propensity for the hydroxyl to recombine and diffuse out of the structure. With that in mind, the IR absorbance data is incredibly difficult to analyze in terms of the tarnishing model as it is most assuredly lower in intensity than it should be.

This saturation concentration is a byproduct of water formed by melting in high pressures of water vapor and it is possible that these hydroxyl sites are different than the hydroxyl sites formed by reduction. It has been stated in literature that some of the hydroxyl formed by reduction is more difficult to remove than hydroxyl formed by melting in water vapor, i.e. some hydroxyl formed by reduction is more stable than hydroxyl formed by equilibrating a melt in water vapor.[12] Some of the water formed by reduction in these glasses appears to leave the structure with relative ease. This is why saturation concentrations are being considered here. If the water forming is more thermodynamically unstable due to the high concentrations which drive the reaction towards the development of molecular water, it is reasonable to assume that the hydroxyl concentrations should be more variable due to this reaction. Molecular water is capable of reacting and diffusing out of the glass which, as mentioned previously, can also complicate the reactions in this study. Without more concrete data on the saturation concentrations and for the diffusion of water in these glasses, it is difficult to say more. This reverse reaction clearly complicates application of the tarnishing model to this glass sytem, as well as the dramatic composition change.

4.4.2 Nucleation and Growth

The SEM data exhibits the existence of larger metallic particles deeper below the surface of the glass. This has been noted in literature and a possible explanation has to do with the concentration of dissolved indium ions in the glass.[30,114] If one considers the surface of a glass, and the distance which indium atoms must diffuse to grow a cluster, it is conceivable that the clusters that develop at or near the surface have half as much

indium to contribute to the diffusion limited growth. Distinct layers of particles were reported in literature that move periodically into the bulk of the glass and were not seen here. A possible reason is that the surface viscosity of the reduced glasses is so low that the particles were not contained as much as they may have been had all treatments occurred below the soda silicates T_g. It is also apparent that the viscosity of the glass has a large impact on the size and shape of the clusters. A more viscous glass structure potentially limits the growth of the clusters due to strain, and a less viscous structure allows for much larger particles to develop. If the viscosity is low enough the particles do appear to take on shapes based on the metallic structure. In typical nucleation and growth discussions, the viscosity of the glass is often related to diffusion coefficients through the Stokes-Einstein relationship.[42,49]

The glass treated above the T_g of the indium containing glass crystallized noticeably. This is normal since typical nucleation and growth temperatures exist above T_g. This system also offers reduced indium atoms and clusters as potential nucleation sites, which could explain the low indium peak intensity in the GIXRD data due to crystals of different compositions forming around indium or absorbing indium to grow.

Since indium melts around 156°C, the clusters are forming as liquid droplets within a glassy matrix, in some respects quite similar to phase separation. The indium clusters either push aside the silicate network, form around the silicate network, or some sort of transport mechanism is involved with the diffusion of ions away from the cluster to allow it to grow. It is also well established that hydroxyl can greatly affect the properties in a glass such as T_g.[101] This implies that the glass structure where indium has been reduced could have a locally lower T_g than the rest of the glass and this could mean the structure may deform more readily to accommodate a growing droplet than one would normally expect. There were instances where clusters appeared to contain pieces of glass and that may indicate that the particles form around the silica network. There is one image of a number of small particles coalescing to form a much larger particle. This potentially could surround the silicate network containing it in indium metal. Regardless the UV-Vis data collected indicates that the particles are forming after very short treatment times and the number volume and sizes are most likely contributing to the spectra collected. It was also determined that the UV-Vis data can be interpreted by

considering the agglomeration of many smaller particles to make larger particles. This would potentially reduce the UV-edge changes associated with a Plasmon resonance absorption of very small particles and potentially could reduce the scattering as the number volume of particles is changing drastically.[115] This combination of smaller particles into larger clusters is believed to occur due to the much lower viscosity of the surface layer allowing clusters to aggregate and form larger clusters.

It is interesting to consider why the indium atoms agglomerate. It is typically considered to minimize thermodynamic energy as long as there is enough energy to surpass the activation energy for the atoms to diffuse together. In consideration of the thermodynamic energy term, there are a number of potential driving forces for energy minimization. An atom has a very high surface area, so clustering may occur to minimize the ratio of surface area to volume of the particles. Discreet atoms would exhibit discrete energy levels, and it may be more thermodynamically favorable as a cluster would exhibit much fewer energy levels due to the development of an electronic band structure. Atoms also have three degrees of freedom, and it may be more favorable from a thermodynamic standpoint if the system does not have a large concentration of particles with three degrees of freedom. This could lead to agglomeration as atoms in a cluster would have fewer degrees of freedom due to bonding.

5. THE REDUCTION OF 2+ IONS IN SODA LIME SILICA GLASSES

5.1 Introduction

The reduction of SLS glasses is nothing new. Many different polyvalent ions have been reduced over time in this series of glasses. The possibility of reaction and diffusion controlled temperature regimes in hydrogen reduction reactions explicitly for cobalt containing glasses has recently been proposed. Miller and Shelby noted that the permeabilities calculated for hydrogen based on the reduction data for cobalt were lower than what would be expected for the glass system. In fact they mention that the permeabilities appear to get further from expected with lower temperatures. This is interesting, and raises a considerable question as to how valid the tarnishing model is between different 2+ ions in SLS glass. The tarnishing model explicitly requires that the reaction rate should be fast with respect to the diffusion of hydrogen to a reaction site. If this is not true then the degree with which the data obeys the tarnishing model will be less than desired. It would be of interest to the scientific community to see if there is a reaction controlled process in these glasses, and if so, can the tarnishing model be corrected to account for this reactivity.[7,22,28]

5.2 Results

The glasses used for this portion of work are all based on a baseline composition of 16 Na_2O–9 CaO–1 RO–74 SiO_2 (mol%) glass where R is Co, Ni, Pb, or Cu. The glasses were all treated in 0.92 atm of hydrogen at 500°C, 550°C, and at 600°C. The tarnishing model predicts a parabolic relationship between the reaction of ionic metal dissolved in the glasses being discussed and time, as well as permeability of hydrogen, pressure of hydrogen, the concentration of ionic metal present in the glass, and the thickness of the sample. None of the glasses treated in this study reached the completion of the reaction, but the glasses all contain such similar concentrations of 2^+ ions that they are directly comparable as completion should be at roughly the same concentration of

hydroxyl formation for each glass. By using glasses of roughly the same composition, other variables of the reaction are removed from the study such as permeability. This allows for a more direct analysis of the reaction rate of the dissolved metals with respect to the temperature of treatment. Spectra for all of the glasses studied were typical of SLS glasses, but there was some variation in band intensities due to the presence of NIR bands in the spectra for nickel and cobalt containing glasses. The spectra for the base SLS glass, lead, and copper containing glasses were very similar. Base refers to the base glass 16 Na_2O–10 CaO–74 SiO_2 (mol%). The presence of these NIR bands was the motivation for a valid background technique and led to the development of the procedures mentioned in the Appendix (A-1). The background changes for this set of results were quite considerable so any discussion must avoid anything but the 3500 cm^{-1} band as it is the least distorted by the background correction. A typical series of difference spectra collected throughout a reduction experiment can be found in Figure 32. In all spectra collected three bands were identified after reduction and they were typically located at approximately 3500 cm^{-1}, 2800 cm^{-1}, and 2300 cm^{-1}. The band at 3500 cm^{-1} increases with treatment time in hydrogen. Some of the glasses tested showed an initial decrease in the band intensities with the onset of reduction. Difference spectra were calculated to examine these changes in closer detail; an example of the difference spectra collected can be found in Figure 33. These difference spectra exhibit two clear broad bands in the same locations as the base spectra located at approximately 3500 cm^{-1} and 2800 cm^{-1}. The third band found in the difference spectra of the glasses containing metal ions after reduction is not as clearly present, but most likely is hidden by the changes in the edge. The band at 2800 cm^{-1} appears to decrease at a faster rate than the band located at 3500 cm^{-1}. A general decrease in the spectra was seen with treatment time.

An example of the changes in the 3500 cm^{-1} band for this series of glasses with treatment in hydrogen at 500°C before correction can be found in Figure 34. It is clear that any expected linear trend between the changes in absorbance of the band the square root of time per length of the sample is vague at best. This is an example of the need for a valid background correction technique for this glass series in particular. After using the procedure mentioned in A-1, the tarnishing plot exhibits a strong linear relationship between the increases in the 3500 cm^{-1} band and the square root of time per length of

sample (Figure 35). The 3500 cm^{-1} band increases the fastest for the copper containing glass, followed by lead, and next the fits for nickel and cobalt lie on top of each other. The linear fits for nickel and cobalt were poor and it appears as if the nickel set of data exhibits a curved rather than a linear relationship. The cobalt glass does appear to exhibit an immediate increase in the absorbance, but after this initial increase the absorbance of the cobalt containing glass does not appear to change. The slopes for these linear fits and others are shown in Table XII.

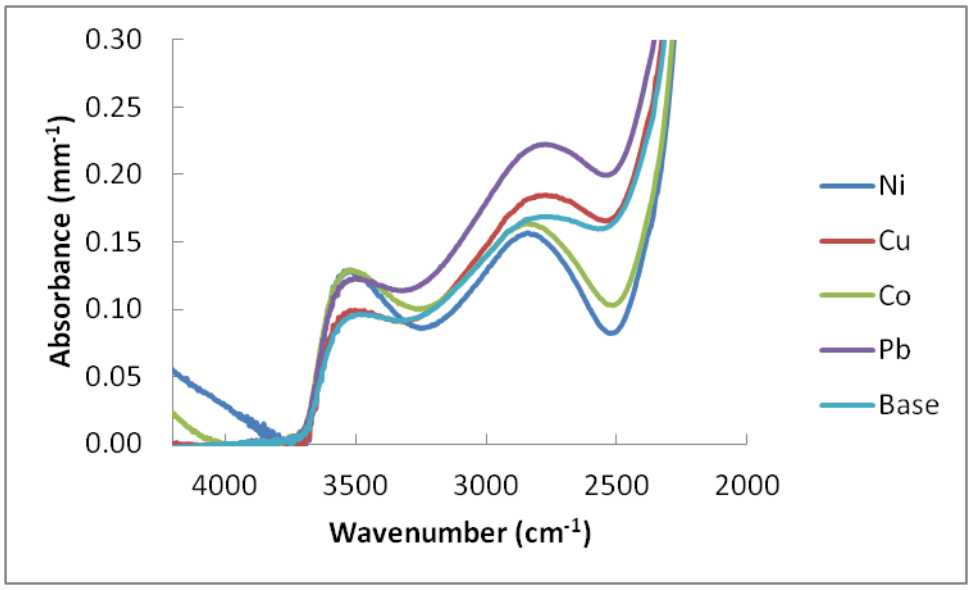

Figure 31. Representative IR spectra for glasses of composition 16 Na_2O – 9 CaO – 1 RO – SiO_2 (mol%) where R is Co, Ni, Cu, or Pb.

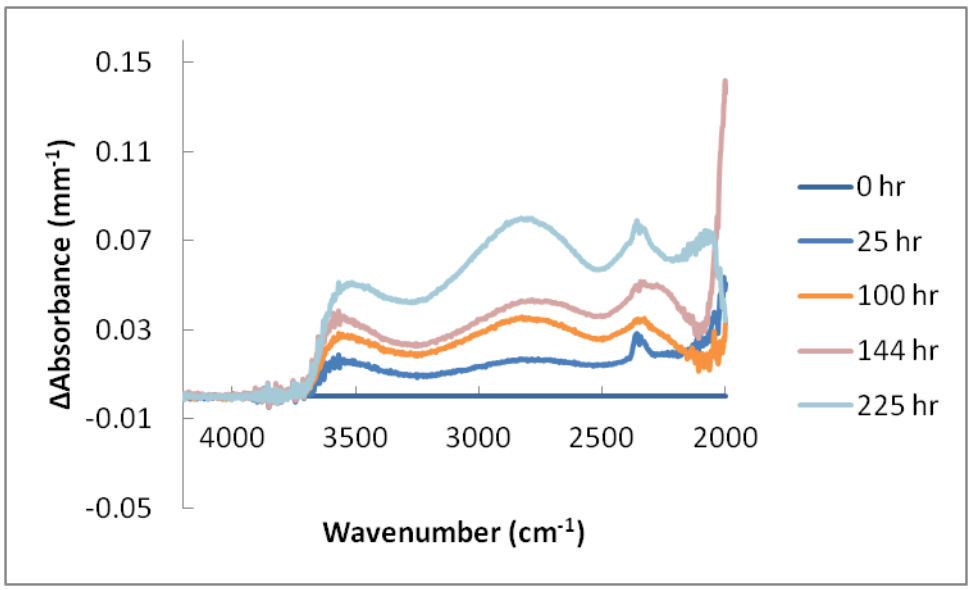

Figure 32. Representative difference spectra for SLS glass containing lead treated at 500°C for various times.

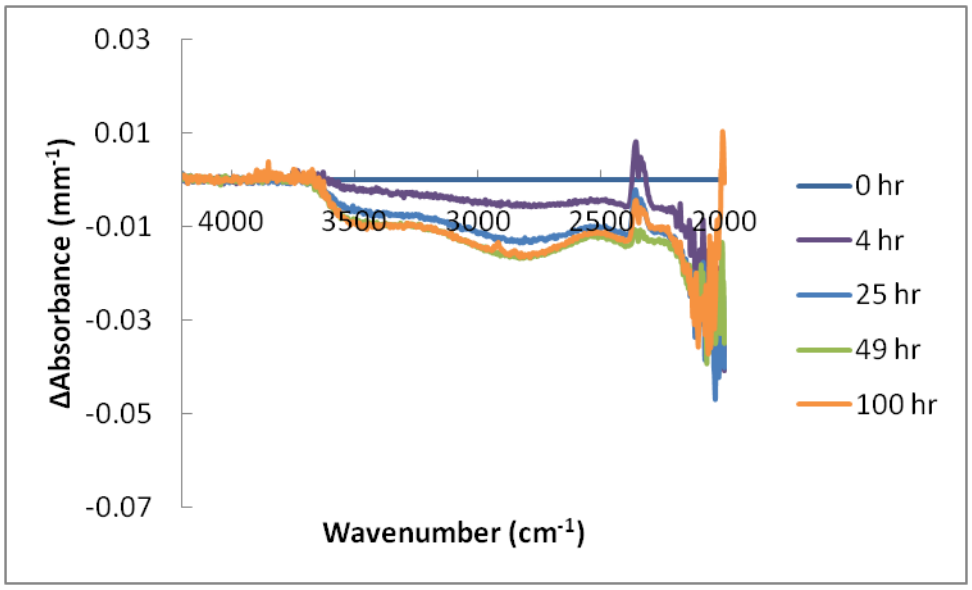

Figure 33. Representative difference spectra for the base SLS glass treated at 550°C in a hydrogen atmosphere.

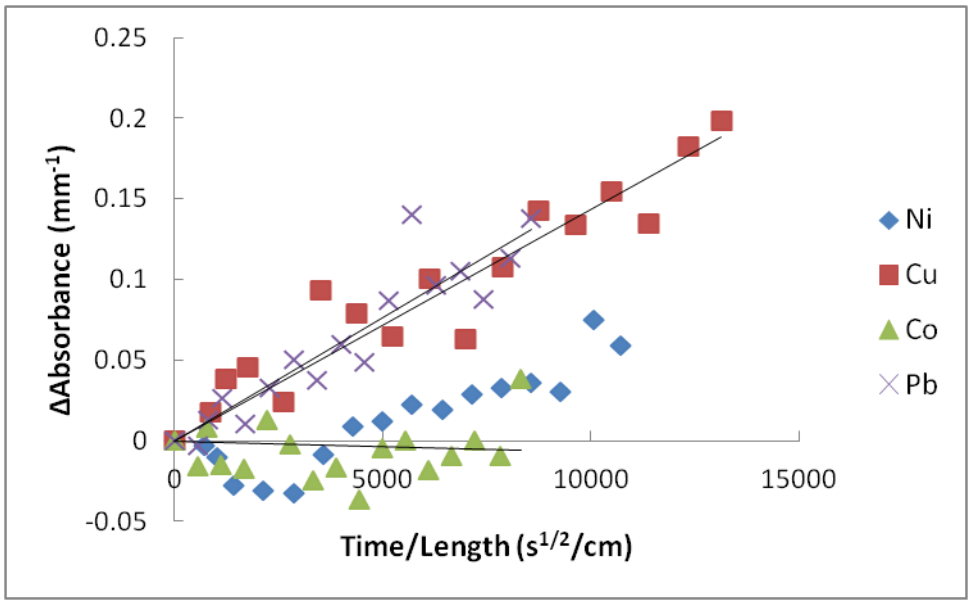

Figure 34. Plot of the change in absorbance of the 3500 cm^{-1} band against the reduction time and the length of the sample for SLS glasses containing various 2^{+} metal ions at 500°C for IR spectra before sloped background correction.

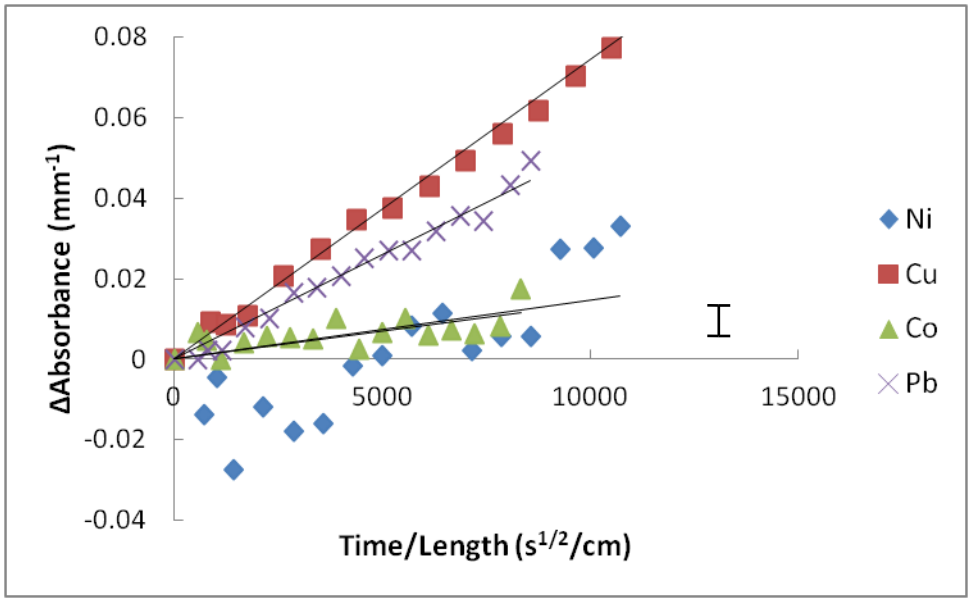

Figure 35. Plot of the change in absorbance of the 3500 cm^{-1} band against the reduction time and the length of the sample for SLS glasses containing various 2^{+} metal ions at 500°C for IR spectra after sloped background correction.

The glasses containing the various metal ions were then treated at 550°C for various times and the relationship between the changes in absorbance and the treatment

time and length and sample thickness are plotted in Figure 36. It must be noted that at these temperatures the spectra for the copper containing glasses exhibited unusual backgrounds that make the sloped correction questionable (Figure 37). The backgrounds began to appear similar to known interference patterns which obscure the 3500 cm^{-1} band drastically. This implies that the copper data in the plot is questionable. The trend is the same as noted for the treatment at 500°C, i.e. copper is reducing faster than lead which is reducing faster than nickel which is reducing faster than cobalt. It is clear that the lead and nickel containing glasses are reducing at approximately the same rates. The nickel and cobalt containing glasses exhibit a curved relationship with time and sample length at this treatment temperature. Again the slopes for the linear regression fits are shown in Table XII.

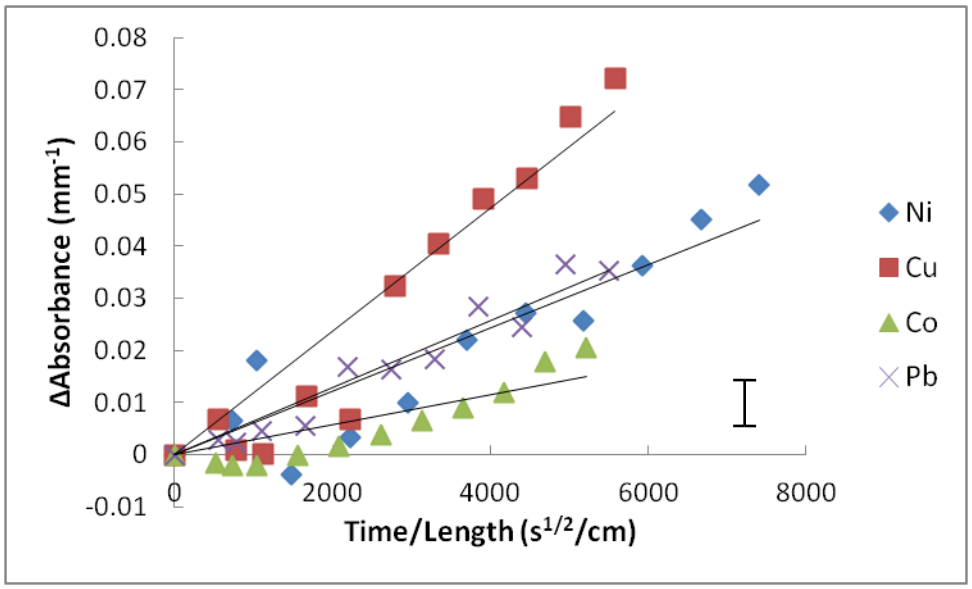

Figure 36. Plot of the change in absorbance of the 3500 cm^{-1} band against the reduction time and the length of the sample for SLS glasses containing various 2^{+} metal ions at 550°C for IR spectra.

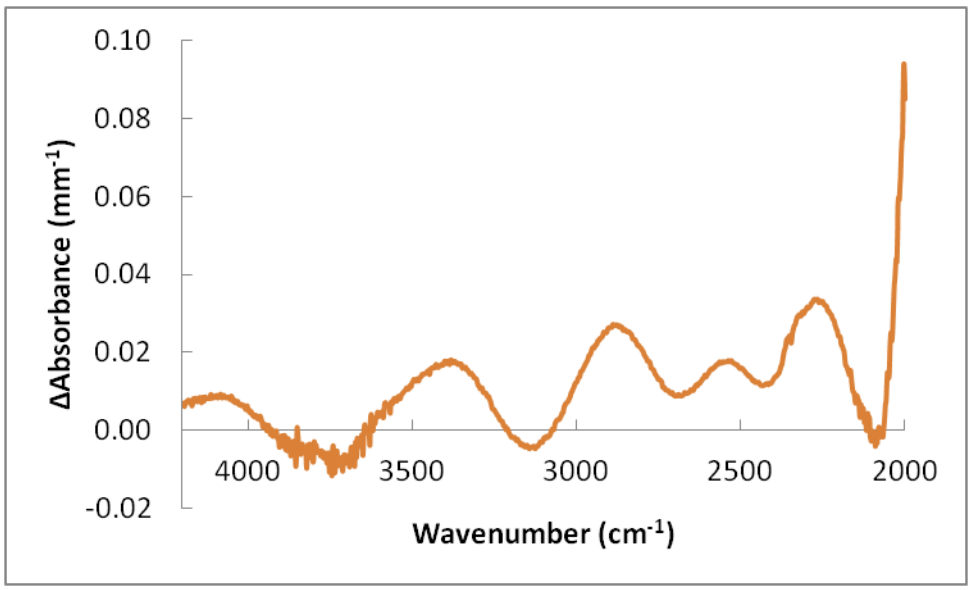

Figure 37. Representative difference spectra for copper containing glass treated at 550°C for 16 hours in hydrogen.

The glasses containing the various metal ions were then treated at 600°C for various times and the relationship between the changes in absorbance and the treatment time and length and sample thickness are plotted in Figure 38. The copper data again exhibits an unusual background and the sloped correction technique employed does not seem reasonable. The glasses containing the remaining three metal ions exhibited strong linear relationships between the change in absorbance with treatment time and sample length. The glasses containing lead ions reduce faster than the glasses containing nickel which reduces faster than the glass containing cobalt. That said, the relative absorbance changes for all three metal ions are very similar and the slopes of the linear regression fits are the most similar in comparison to the data sets from the other treatment temperatures. This data from this treatment temperature did not exhibit the curved relationships noticed at 500 and 550°C. In all glasses an increase in the change in absorbance of the 3500 cm^{-1} band was observed with increasing treatment temperature.

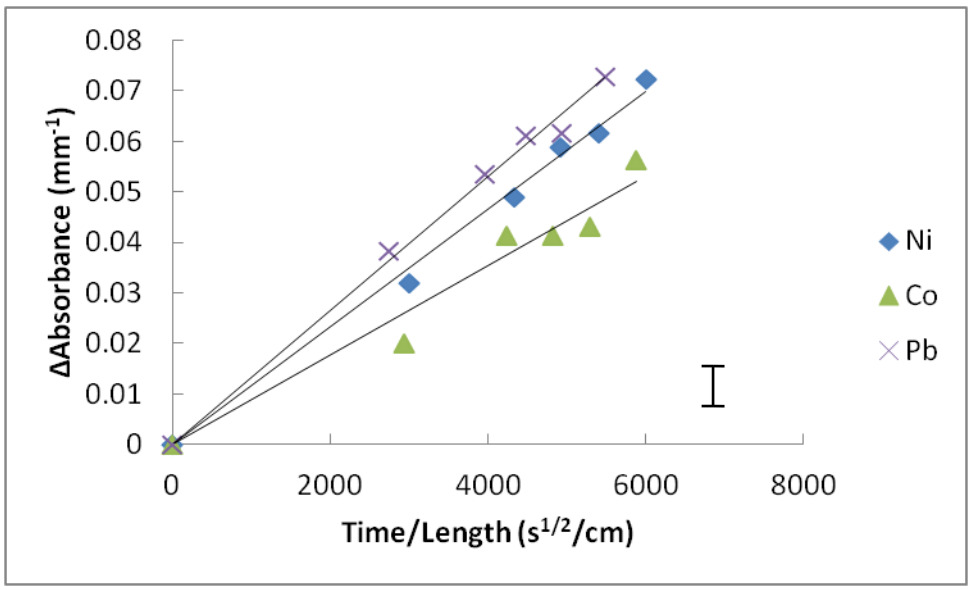

Figure 38. Plot of the change in absorbance of the 3500 cm^{-1} band against the reduction time and the length of the sample for SLS glasses containing various 2^{+} metal ions at 600°C for IR spectra.

The curved relationships between the absorbance changes of the 3500 cm^{-1} band when plotted against the square root of time and sample thickness for the nickel and cobalt containing glasses is clearly a function of treatment temperature (Figure 39 and Figure 40). The linear data is fit with a best fit linear regression, while any curvature is merely drawn on to indicate the general trend. The nickel containing SLS glass absorbance data shows the most prominent curvature for the treatment at 500°C. The initial absorbance data drops well below the baseline before it begins to increase. The curvature is still apparent at 550°C although the data does not appear to drop much below baseline, and the data points appear to exhibit a linear relationship at 600°C. The cobalt containing SLS glass absorbance data has a weak linear trend at 500°C. There is an initial increase and very little increase in the absorbance of the 3500 cm^{-1} band following that. At 550°C the absorbance data exhibits a very prominent curved relationship with the square root of time and sample thickness very similar to the nickel containing glass treated at 500°C. This curvature appears to be very minimal if nonexistent in the absorbance data treated at 600°C.

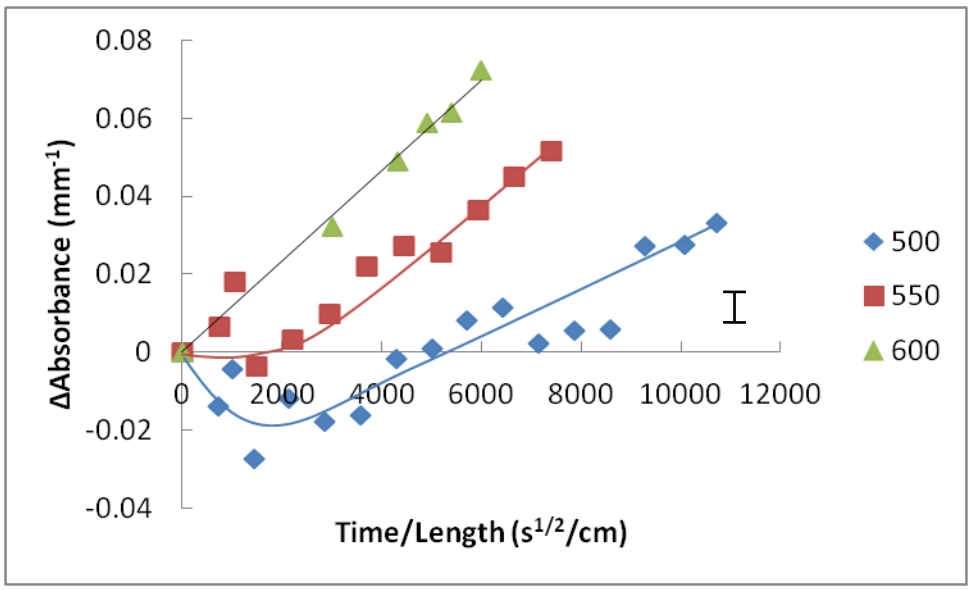

Figure 39. Plot of the change in absorbance of the 3500 cm^{-1} band against the reduction time and the length of the sample for SLS glasses containing nickel ions for various temperatures.

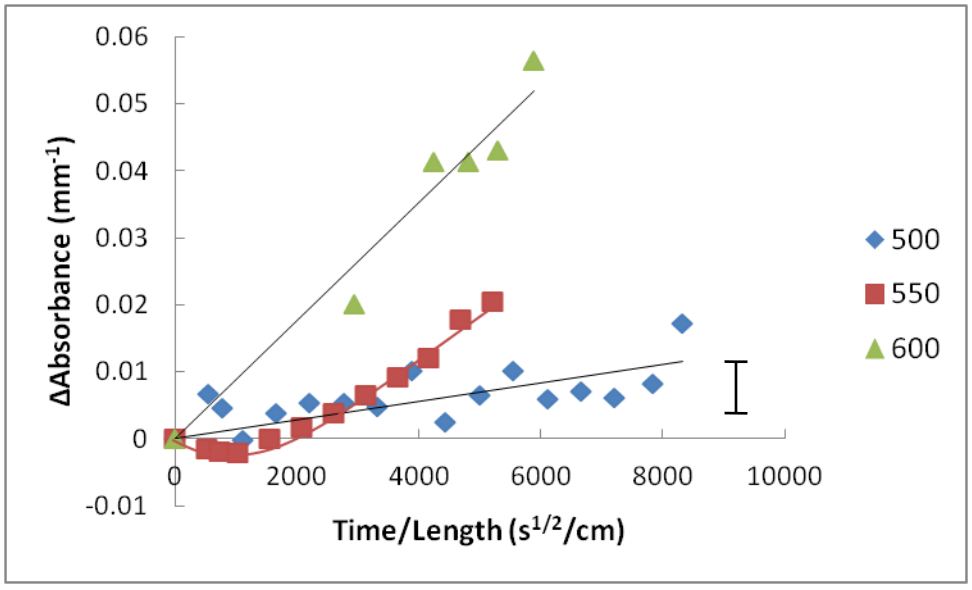

Figure 40. Plot of the change in absorbance of the 3500 cm^{-1} band against the reduction time and the length of the sample for SLS glasses containing cobalt ions for various temperatures.

The linear regression fit data is shown in Table XII. It is clear that the nickel and cobalt containing glasses do not have strong linear fits until treatment at 600°C, but the fit

does appear to get stronger with increased temperature. The lead containing glasses exhibit strong linear fits for all treatment temperatures. The copper containing glasses exhibit strong linear fits at low temperatures and the fit gets worse as temperature increases due to the background issues mentioned earlier. It is clear that the slopes of the fits increase with increasing treatment temperature, and they appear to become more similar with increasing temperature (this applies to all data except the copper containing glass data). The nickel containing glass also has a very similar slope to the lead containing glass at 550°C even with a small degree of curvature.

Table XII. Collection of Best Fit Linear Regression Slopes to the Difference Spectra Tarnishing Model Relationships With R^2 Values in Parenthesis

	Temperature (°C)		
dopant	500	550	600
CoO	1.39E-6 (0.36)	2.89E-6 (0.76)	8.84E-6 (0.96)
NiO	1.46E-6 (0.29)	6.07E-6 (0.84)	1.17E-5 (0.99)
PbO	5.19E-6 (0.98)	6.44E-6 (0.94)	1.33E-5 (0.99)
CuO	7.47E-6 (0.99)	1.18E-5 (0.90)	3.73E-5 (0.83)

The data for the absorbance changes for the nickel containing glass during reduction at 600°C exhibited a strong linear fit after the typical sloped correction. This data was consistent enough to attempt the Rayleigh correction also mentioned in the Appendix (A-1) in order to have two bands at proper intensities. After correction the data was converted to ppm hydroxyl through use of the Scholze two band approximation (Figure 41):[76-78]

$$C_{OH} = \frac{17000}{x*d}\left(\frac{A_{3500}}{\varepsilon_{3500}} + 4/3\,\frac{A_{3500}}{\varepsilon_{3500}}\right) \quad (30)$$

where C_{OH} is the concentration of hydroxyl in ppm, x is the sample thickness (cm), d is the glass density in (g/cm^3), A is the intensity of the absorbance of the band in question, and ε is the related extinction coefficient.[74-81] The used extinction coefficients were assumed to be ~0.53 (ε_{H2O}).[74] This relationship along with the reported extinction coefficients (ε_{H2O}) being ε_{3500}=70 l/mol*cm and ε_{2800}=150 l/mol*cm allowed the amount of hydroxyl being generated in the glass to be determined.[22,75] By assuming that all of

the nickel present in the base glass could be reduced and that two hydroxyls would accompany the reduction process, a calculated value of C_f was determined. This new value of C_f allows for an extrapolation of the slope of the tarnishing model data to determine the square root of treatment time per sample thickness at reaction completion. This value is typically experimentally determined. This data was used to estimate the permeability of the glass being reduced and the calculated value was 2.76E8 (molecules/atm*cm*s).

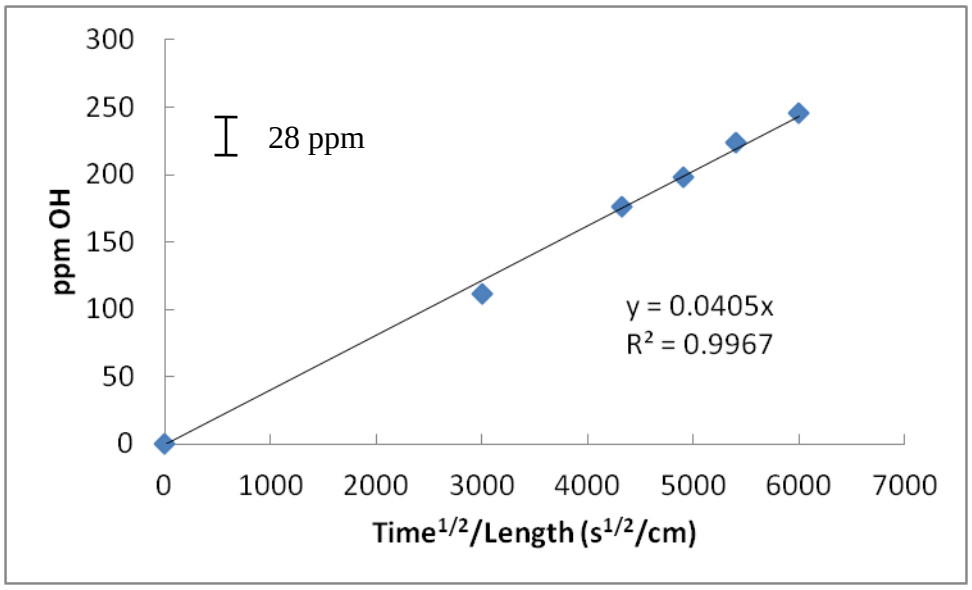

Figure 41. The change in absorbance of the nickel containing glass throughout reduction at 600°C converted to ppm OH and plotted against the square root of time and sample thickness.

UV-Vis data were collected throughout this series of reduction experiments. Nearly all samples exhibited some degree of color change throughout the reduction. Three out of the four samples were colored in the visible region prior to reduction due to ligand field absorptions of the transition metal dopants in the ionic state (Figure 42). The nickel containing SLS glass clearly exhibits a visible absorption envelope consisting of three bands and a much broader band with a maximum absorbance somewhere outside of the data collected in this study. The three bands in the visible envelope are located at ~450, ~560, and ~630 nm. There is another broad band in the higher wavelength region of the spectra. The copper containing SLS glass clearly exhibits a visible absorption

located at ~780 nm. The UV-edge is also slightly shifted to higher wavelengths than any of the other glasses measured. The cobalt containing SLS glass exhibits a visible absorption envelope. This envelope typically consists of three bands similar to nickel containing SLS glasses, but the data went off scale too quickly to resolve these features. The lead containing glass has no related absorptions in the visible region of the spectrum. All of the glasses exhibited a minor absorption near 380 nm and a broad minor absorption near 1000 nm.

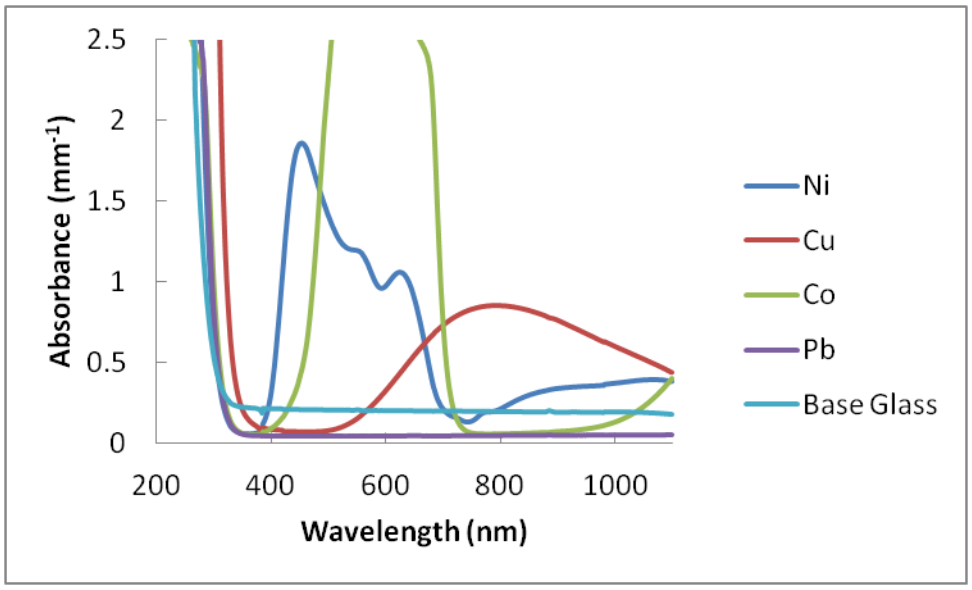

Figure 42. Representative plot of absorbance for all glasses used before reduction.

UV-Vis spectra were collected for all of the samples at various times throughout the reduction experiments. All of the samples containing metal ions exhibited a visible color change after reduction. The nickel containing SLS glass is initially a brown/black color and after reduction it appears black (Figure 43). Difference spectra were calculated in order to more clearly show the changes in optical absorption caused by reduction. The clearest trends found were the increase in absorbance with increased treatment time and temperature. The spectra all increased most rapidly near the UV-edge followed by an absorption tail that extended throughout the visible region. The difference spectra were then converted to absorption coefficients. Attenuated Mie scattering calculations[17] were performed to model the plasma resonance absorption coefficient of small metallic

particles of nickel dispersed in a dielectric matrix and compare to the measured data. The absorption coefficient of small (<40 nm) metallic particles dispersed in a dielectric matrix is given by:[17]

$$\gamma = NV \frac{\left(36\pi n k {n_o}^3\right)}{\lambda\left(\left(n^2 - k^2 + 2{n_o}^2\right) + 4n^2k^2\right)} \tag{31}$$

where N is the number of particles per unit volume, V is the volume of the particles, n_o is the refractive index of the glass, and n and k are optical constants of the metal.

The attenuated Mie absorption calculation relates very closely to the measured spectra and explains the increase in all the spectra taken for the baseline near the UV-edge. There is some difficulty in modeling these difference spectra due to decreases in the aforementioned bands in the visible after reduction. The glasses treated at 500°C clearly have much lower absorption coefficients than those treated at 550°C (Figure 44 and Figure 45). The glasses treated at 500°C also exhibit a more uniform decrease of the three bands constituting the visible envelope for nickel ligand field absorptions, although the band located at ~450 nm decreases the most with respect to the modeled Mie absorption. The glasses treated at 550°C exhibit a more prominent decrease of the band located at ~450 nm than of the other two bands in the envelope. The band decreases approximately three times more quickly than the band located at ~630 nm.

The copper containing SLS glass is initially a light blue color and after reduction it appears dark red (Figure 46). It is clear that a sharp absorption band develops around 560 nm and there is a large general change in the spectra around this band during the treatment. The absorbance increases with treatment temperature and time so that much of the data collected was off scale soon after treatment. This stack of spectra is once again not very informative, so difference spectra were calculated in order to show the changes more clearly. The difference spectra were converted to absorption coefficients and then an attenuated Mie scattering calculation was performed to model the plasma resonance absorption coefficient of small metallic particles of copper dispersed in a dielectric matrix and compare to the measured data. This process will be covered in more detail in the discussion. The attenuated Mie absorption calculation relates very closely to the measured spectra and explains the increase in all the spectra taken for the baseline near

the UV-edge. The calculated data does not match up well far above or below the ~560 nm band in the difference spectra, but in general is very similar.

The cobalt containing SLS glass is initially a dark blue color and after reduction it changes to a gray shade (Figure 48). The greatest degree of change in the spectra occurs near the UV-edge as a general increase. The increase in absorbance appears to have a tail that covers the entire visible region of the spectra. Due to a majority of the bands in the visible being off scale, Mie calculations were not performed to compare to this data. The glass again exhibits a greater degree of change with temperature and with treatment time.

The lead containing SLS glass is initially clear and after reduction becomes dark black. The absorbance change occurs most rapidly near the UV-edge and again appears to have a tail throughout the visible region of the spectra. A band starts to resolve out of the changing spectra again located near the UV-edge. The spectra do change more quickly with temperature and longer treatment times. Again, the absorptions went off scale after short treatment times.

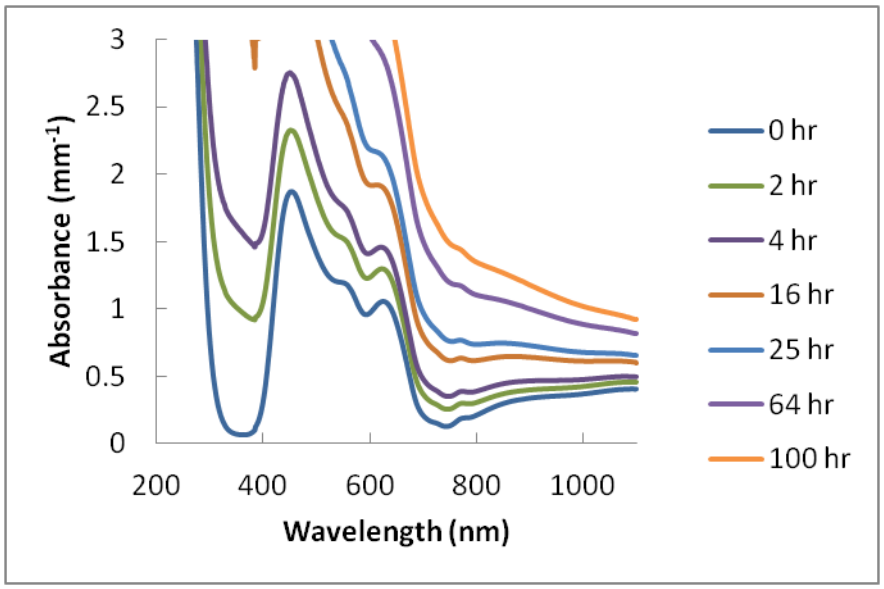

Figure 43. Representative UV-Vis spectra of nickel containing glass after various reduction times in hydrogen at 550°C.

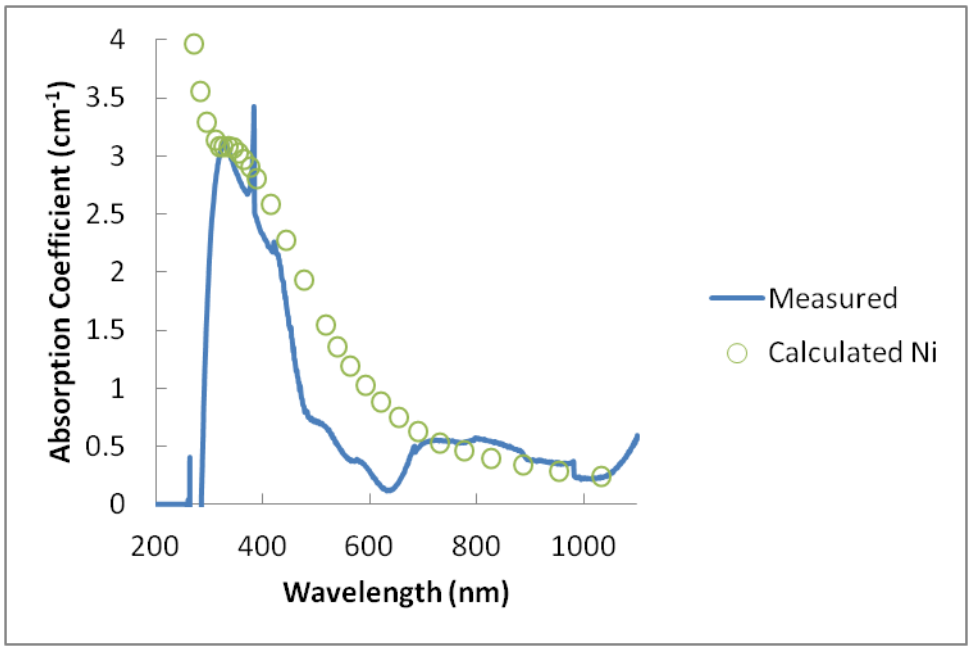

Figure 44. Attenuated Mie absorption calculation compared to difference spectra for nickel containing glass treated at 500°C for four hours.

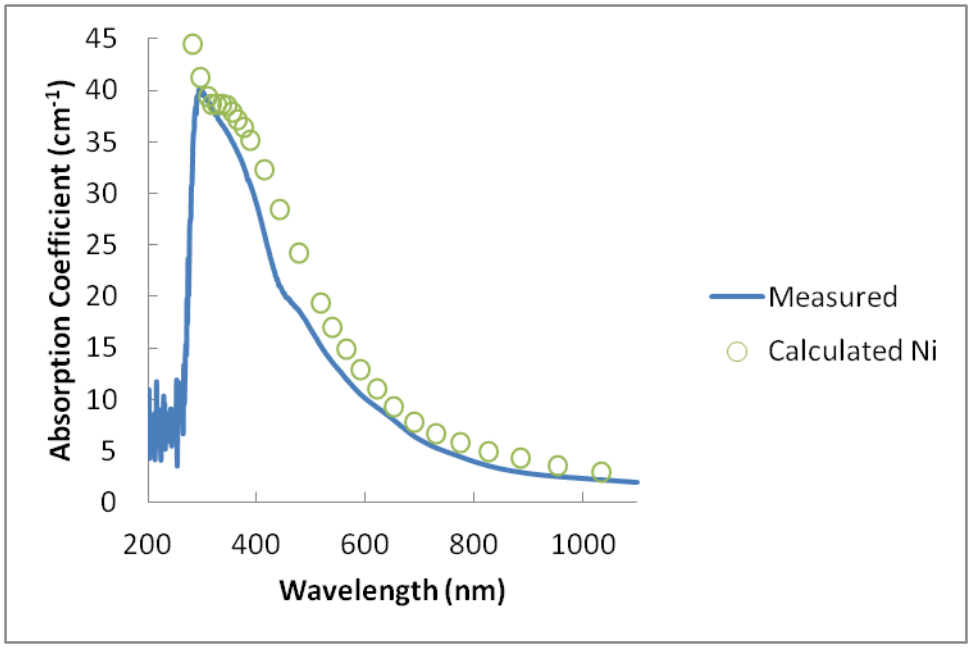

Figure 45. Attenuated Mie absorption calculation compared to difference spectra for nickel containing glass treated at 550°C for four hours.

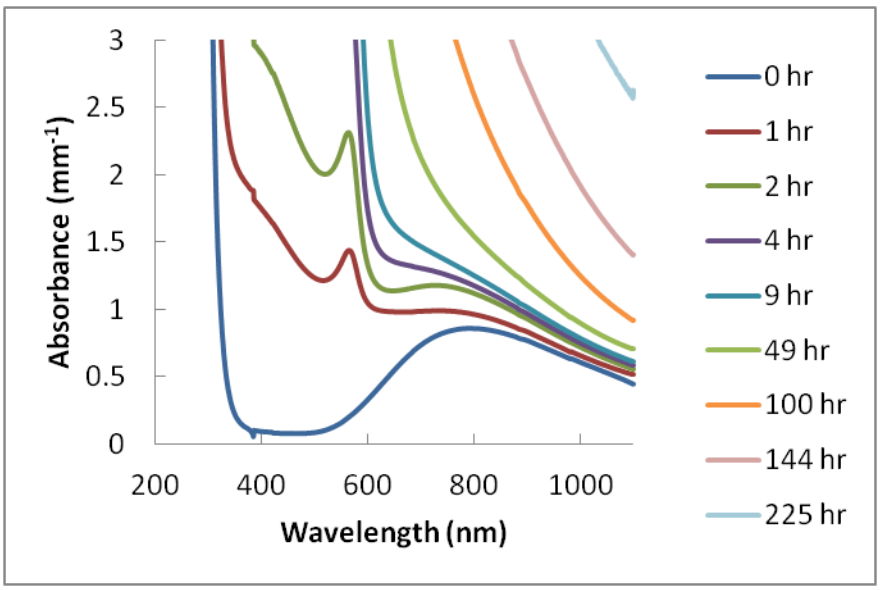

Figure 46. Representative UV-Vis spectra of copper containing glass after various reduction times in hydrogen at 500°C.

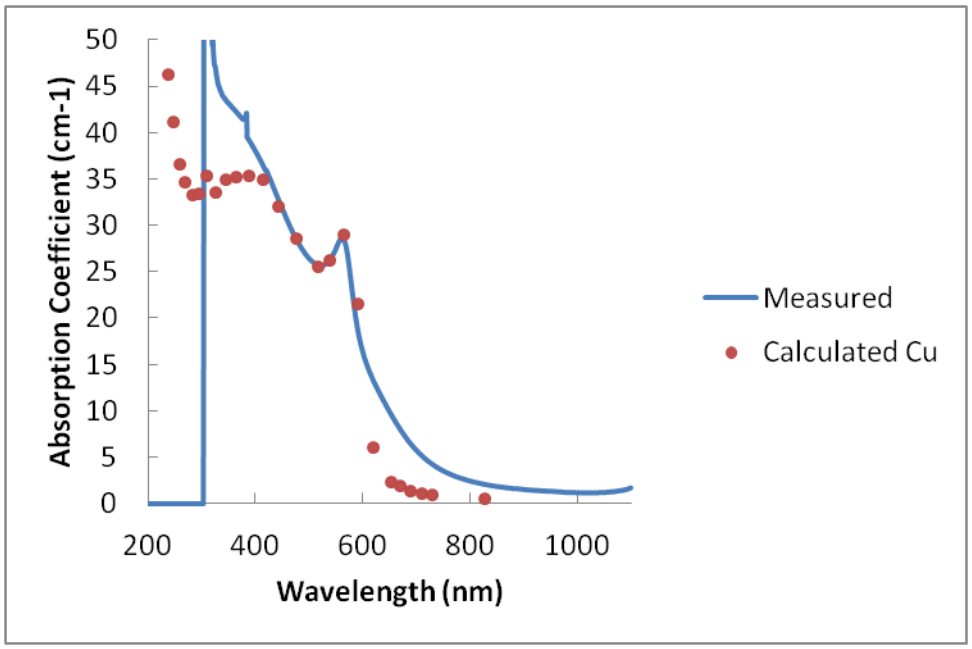

Figure 47. Attenuated Mie absorption calculation compared to difference spectra for copper containing glass treated at 500°C for one hour.

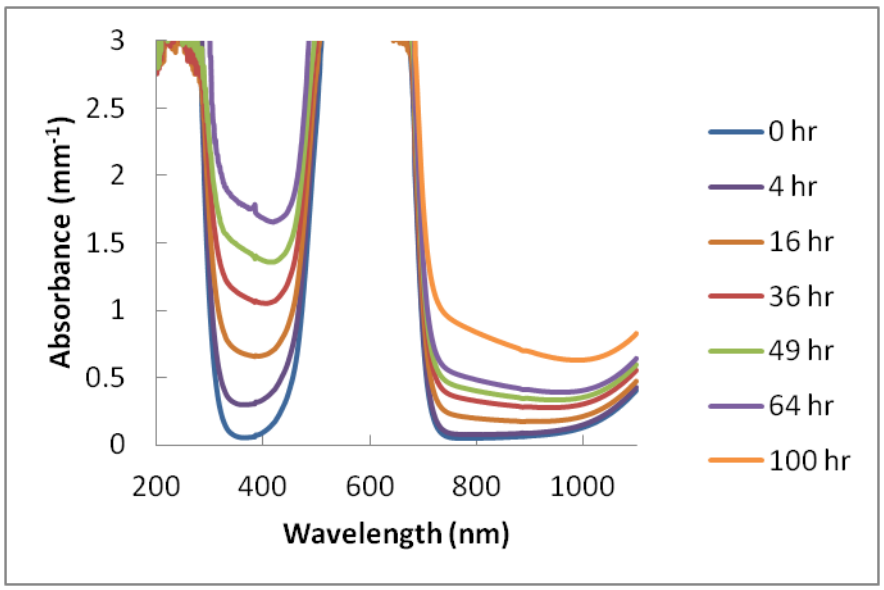

Figure 48. Representative UV-Vis spectra of cobalt containing glass after various reduction times in hydrogen at 550°C.

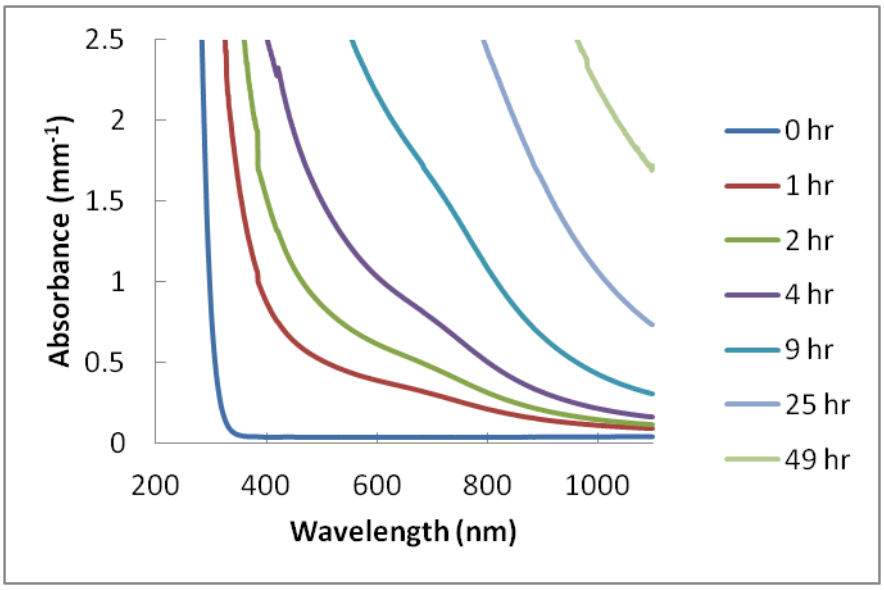

Figure 49. Representative UV-Vis spectra of lead containing glass after various reduction times in hydrogen at 550°C.

The presence of metallic clusters of nickel, copper, cobalt, and lead in the respective glasses was confirmed using GIXRD. The presence of nickel and cobalt crystals was confirmed through the identification of the (111) diffraction peak which is

the only peak present in the patterns collected for the reduced nickel or cobalt containing glasses (Figure 50). It is the only peak that is distinguishable from background for all treatment temperatures. The peak is very weak even for the 600°C treatment which produced the largest peaks for all the samples tested with respect to background, and the nickel peak was slightly more resolved than the cobalt peak. The reduced glasses containing copper and lead both exhibited much stronger peaks at every treatment temperature. The respective series of GIXRD patterns can be found in Figure 50. The reduced copper containing glass exhibited two distinguishable peaks identified to be from the (111) and (200) planes. The reduced lead containing glass exhibited four distinguishable peaks at the end of the 500 and 550°C treatments, and 5 peaks at the end of the 600°C treatment. It must be noted that any pattern for 500°C treatment is after 225 hours of treatment while 550 and 600°C were only after 100 hours of treatment. The copper and lead containing glass GIXRD data were well resolved enough to attempt to calculate particle sizes based on the broadening of the peaks. The instrumental broadening was subtracted for reference material SRM 676. It should also be noted that although the calculation will state particle size it also could relate to a grain size within the particles. The particle size of copper particles dispersed in the glass matrix increases with treatment temperature (Table XIII). The difference between 550°C and 600°C sample particle sizes indicates that the size of the particles increased only slightly. The particle size of the lead particles dispersed in the glass matrix also increases with treatment temperature. The lead particle size increases with treatment temperature. The particle size of lead is smaller at 500°C than for copper, and greater than for copper at both of the higher treatment temperatures.

The broadening should primarily be due to particle size changes as the shape of these particles is assumed spherical. This further implies that any shifting of the peaks would be due to uniform strain throughout a particle embedded in a glassy matrix. There was an identifiable, although minor, peak shift for all the distinguishable peaks measured. This shift was identified thoroughly for the lead containing glass as the peaks had the best signal to noise ratio. There is an increase in the "d" spacing for the (111) plane on the order of 0.005 Å. This increase is greater for the glasses treated at higher temperatures than for the glasses treated at 500°C.

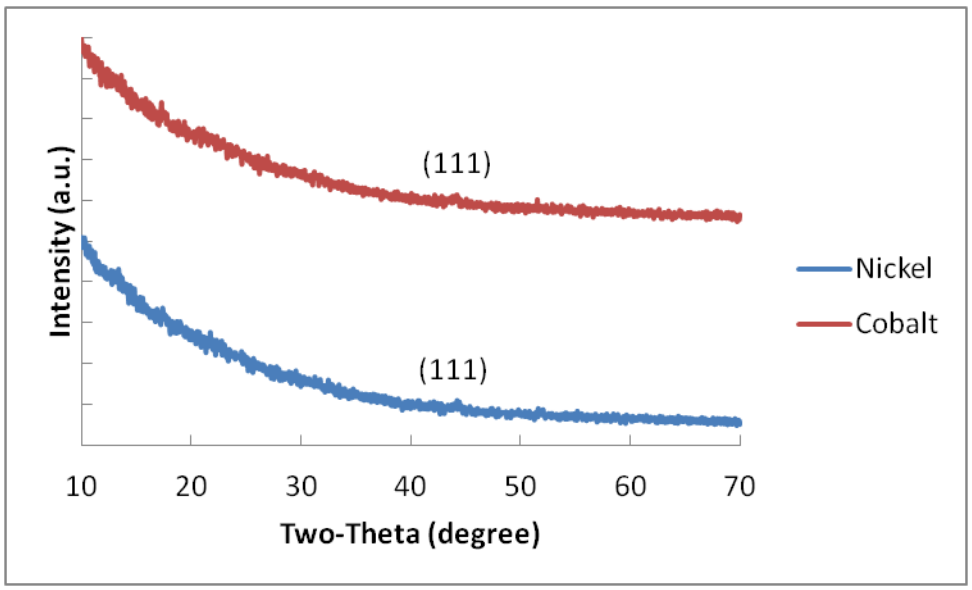

Figure 50. Representative GIXRD pattern for glasses containing nickel and cobalt after treatment for 100 hours in hydrogen at 600°C.

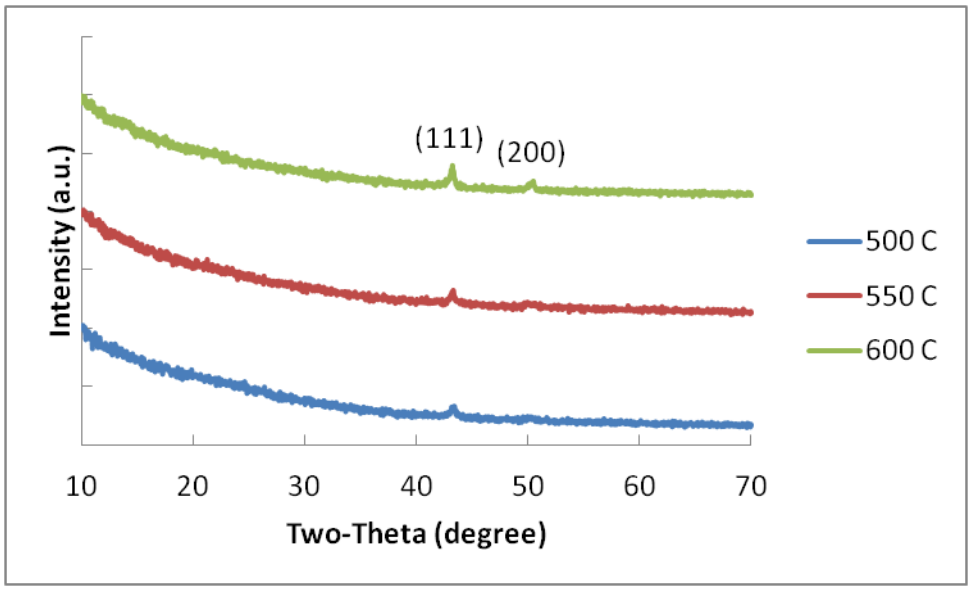

Figure 51. Representative GIXRD pattern for glasses containing copper after treatment for various temperatures in hydrogen.

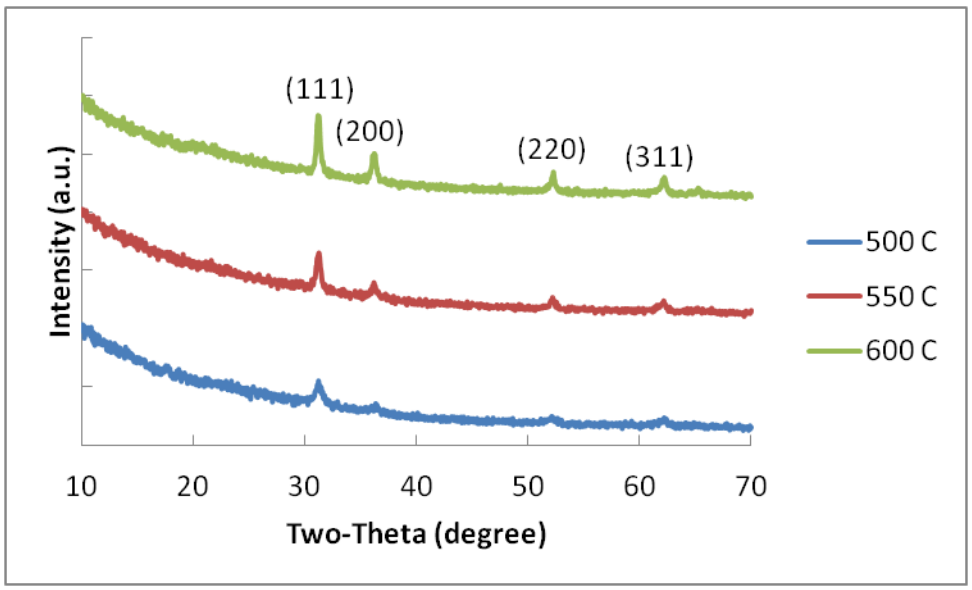

Figure 52. Representative GIXRD pattern for glasses containing lead after treatment for various temperatures in hydrogen.

Table XIII. Calculated Particle Size Data Based on GIXRD Peak Broadening Calculations

		500°C	550°C	600°C
Lead	**Particle Size (nm)**	10.3	19.3	24.3
	Standard Deviation	0.6	0.6	1.2
Copper	**Particle Size (nm)**	13.7	18.0	18.7
	Standard Deviation	3.1	1.0	1.5

Table XIV. Calculated "d" Spacing Data for the (111) Plane in Lead Particles from GIXRD Data

	500°C	550°C	600°C
(111) d spacing (Å)	2.859	2.862	2.861
Standard Deviation	0.003	0.001	0.001
Reference "d" Spacing (Å)	2.856	2.856	2.856

5.3 Discussion

5.3.1 Reaction

The tarnishing model was initially discussed by Crank to explain moving boundary reactions.[28] The tarnishing model is often described as:

$$\frac{(C-C_i)}{(C_f-C_i)} = (8KPt/L^2C_x)^{1/2} \quad (32)$$

where C is the concentration of hydroxyl at a given time, C_i is the initial concentration of hydroxyl, C_f is the final concentration of hydroxyl, K is the permeability of hydrogen in the glass, P is the partial pressure of hydrogen, t is the treatment time, L is the sample thickness, and C_x is the concentration of reaction sites. The term at the left of the equal sign reaches between a value from zero to one, where one would signify a completed reaction. This model has successfully been applied to hydrogen reaction experiments in literature to describe various reaction kinetics.[7,12,22,29-32,34,35,108]

This set of glasses was chosen to eliminate a large number of variables in the tarnishing model. These glasses ideally contain the same amount of reaction sites and the same permeabilities. This means that for a given tarnishing model plot, the slopes of any of the existing 2^+ ions should lie on top of one another. This was not found for any experimental data. It must be noted that copper exists as Cu^{2+} and Cu^{1+} and lead exists as Pb^{2+} and Pb^{4+} in these glasses. It is believed that the majority of ions start out in the 2^+ state in these glass systems based on the oxygen rich atmosphere during melting.[9,11,15,63] A proposed reaction for this system is:

$$RO + H_2 \rightarrow R^0 + 2(Si-OH) \quad (33)$$

The data is not following all of the trends predicted by the tarnishing model alone. It is clear that the absorbance change is typically linear with respect to the square root of treatment time, and for this data is a relative indicator of the amount of the reaction completed. The glasses reduce at rates in the order Cu>Pb>Ni>Co for all temperatures. This implies that there is some sort of reaction controlled aspect to the reduction of these ions from SLS glasses. This order of reduction appears to follow suit with the Gibb's free energies of oxide formation as reported in literature (Table XV).[52,63,92] The higher, or less negative, the value in the table, the less stable thermodynamically the oxide,

implying that the thermodynamic drive to form an oxide increases in the order $Cu^{1+}<Cu^{2+}<Pb^{2+}<Ni^{2+}<Co^{2+}<H_2$. It is apparent from these calculations that hydrogen thermodynamically will bond with oxygen which will lower the system's free energy by the largest amount. Therefore hydrogen should donate electrons to these metals as they are less stable oxides. This reduction process is typically discussed in terms of concentrations, and concentrations of anything dissolved in a glass should be different than unity due to interatomic interactions changing the effective concentrations. As similar trends were seen in the reduction data collected and the published data for oxides, these energies are clearly relatable. It even follows that the similarity in values for the nickel, cobalt and water indicate that the hydrogen has the most difficulty removing the oxygens from a nickel or cobalt ion and that indeed was seen in the data at 500°C.

The concentration of molecular hydrogen, molecular water, oxygen, and the metal in question are paramount to the equilibrium of these oxide formation calculations. When anything is dissolved in a glass, the effective concentration is known to change, and this new effective concentration is often referred to as the activity. This makes it difficult to directly apply these energies realistically to a glass system. Furthermore, the reducible species is molecular hydrogen, and the concentration of molecular hydrogen in a volume of glass is linearly related to the solubility of hydrogen in the glass and the ppH_2 outside the glass otherwise known as Henry's Law.[22] Unfortunately, molecular hydrogen too should have an effective concentration due to intermolecular forces in the glass so a concentration alone may not be enough to successfully model these reactions.

These reactions also occur very slowly, and for any real thermodynamic calculations to be viable, equilibrium must be achieved. At the time scales of this study, it is unlikely that equilibrium is ever met. The reduction in a hydrogen atmosphere is creating a new metastable state that is attempting to approach equilibrium in hydrogen. This means that once the glass is removed, it is again in a highly metastable state kinetically unable to change. Glass is by nature considered metastable due to the viscosity temperature relationship it exhibits. Any analysis must carefully consider all the variables being presented.

Table XV. Gibb's Free Energy of Oxide Formation Calculated for Various Reduction Temperatures

	Gibb's Free Energy of Oxide Formation (kcals)					
Temperature (°C)	**NiO**	**CuO**	**Cu_2O**	**CoO**	**PbO**	**H_2O**
500	-80.48	-52.89	-28.64	-85.67	-66.86	-97.91
550	-78.13	-51.25	-26.25	-83.98	-64.29	-96.64
600	-75.77	-49.62	-23.87	-82.29	-61.72	-95.35

There are a few assumptions that are associated with the use of the tarnishing model. The concentration of hydrogen at the interface between the moving boundary of reduced glass and the base glass is assumed to be zero. This implies that the rate of reaction is so fast that the moving boundary is controlled entirely by the diffusion of the gas. The reduced layer is assumed to contain a steady-state gradient of molecular hydrogen to the unreacted glass. This implies that the surface of the sample is completely saturated with molecular hydrogen. Some of the tarnishing plots exhibited a clearly non-linear relationship with the square root of time. These possibilities have been discussed thoroughly in literature.[116,117] The model depicts a sharp boundary and this can broaden due to the depicted reaction not being much greater than the reverse reaction. This would imply, for this system that if nickel re-oxidizing in the glass occurs fast enough, the tarnishing boundary formed by the reduction of nickel can broaden. This is a case where the tarnishing model is not valid, but it is unlikely that this is the cause of the curved data shown in some of the tarnishing plots containing nickel and cobalt. Another example is where there is a slow surface reaction which would also make the tarnishing model invalid. This is possible in the data collected here. Nickel and cobalt both reduced much more slowly than copper and lead, and they both exhibited a non-linear relationship with the tarnishing model. This concept of reaction rates for the reduction of cobalt and nickel has been noted in literature.[6,7] A final condition to consider is one where the dissolved concentration of hydrogen is not much smaller than the concentration of reducible species in the glass. This moving boundary is still going to move with the square root of time, but there is a proportionality factor that must be applied to keep the concentration gradient linear throughout the reacted region.

It is clear that the slow measured reactions for nickel and cobalt probably contribute to the curved relationship between the increase in absorbance of the "free" hydroxyl band and the square root of time. The initial portions of the curves are most likely a result of dehydroxylation occurring more rapidly than the reduction reaction. At some time the reduction reaction begins to dominate and the slope is again positive. The nickel and cobalt data appear to become linear at higher temperatures indicating that the reaction rates approach an appropriately rapid rate for the tarnishing model to be used. It is also clear that the data appear to increase at more similar rates at elevated temperatures for nickel, cobalt, and lead. This agrees with literature that as temperature increases there is a transition at some point to a diffusion controlled boundary growth instead of the reaction controlled growth seen at lower temperatures.[7] This makes sense as the permeability should be the same for all of the samples and the permeability is directly related to the slope of the data in the plots. This led to an attempt to calculate the hydrogen permeability of the SLS glass based on the formation of hydroxyl for the nickel containing glass treated at 600°C. The calculated hydrogen permeability based on the hydroxyl rate of formation is ~30x below an experimentally determined permeability (~8.12E9 molecules/atm*cm*s).[22,23] The measured permeability would require a slope greater than 5 times what was measured for the relationship between ppm OH to the square root of time per sample thickness. This implies that the measured rate of hydroxyl formation in these glasses with reduction is occurring far below what would be predicted by the tarnishing model. Johnston and Chelko[32] report that a glass being fully reduced contains ~1/3 the hydroxyl expected based on calculation. It is reasonable to assume that there is again hydroxyl recombining by the mechanism:

$$2(Si-OH) \rightarrow Si-O-Si+H_2O \quad (34)$$

This proposed recombination of hydroxyl groups to form molecular water is possible and would explain the discrepancy between the calculated permeability and that expected based on composition alone. Since these ions are ideally all 2^+ in these glasses, it is likely that two hydroxyl groups are forming to liberate each ion from the glass structure. This conceptually would put two hydroxyl groups within the vicinity of one another, which could lead to a dehydroxylation type reaction. It should also be noted that the base glass was treated as well and indicated a very irregular but measureable decrease

in hydroxyl which indicates that hydroxyl from the melt is recombining and potentially diffusing out of the glass. This decrease was also noted in the nickel and cobalt containing glasses as the reaction was very slow at low temperatures for these glasses. It is also possible that the reaction rate is still slowing the formation of hydroxyl which could also be lowering the calculated permeability.

5.3.2 Nucleation/Growth

Subsequent nucleation and growth of metallic particles can occur after the initial reduction reaction takes place. These processes are somewhat indistinguishable with the data in this study. It is believed that the reduction produces atoms which agglomerate and then grow metallic clusters. The Anderson-Stuart model[118] indicates that this is a reasonable assumption for nickel, copper and cobalt as the activation energy for diffusion is lower for the atoms than the respective ions (Table XVI). There is one anomaly, and that is the activation energy for diffusion of lead. The reported atomic radius is ~1.75 Å[119] for atomic lead and the ion is reportedly smaller. Lead is well known to be highly polarizable and this could potentially aid in the diffusion through the structure.

Table XVI. Atomic and Ionic Sizes of Relevant Elements and Activation Energies for Diffusion Based on the Anderson-Stuart Model

	Activation Energy(kcal/mol)			
	Atomic		**2^+ Ion**	
	Size (nm)	**E_A (kcal/mol)**	**Size (nm)**	**E_A (kcal/mol)**
Ni	1.25	13.5	0.69	36
Cu	1.28	15	0.87	36
Co	1.25	13.5	0.72	35.5
Pb	1.75	40	1.2	32

The peak broadening in GIXRD was attributed to particle size and not to strain. These particles are assumed to all be spherical and therefore any strain would be uniform which should not impact the broadness of the peaks, rather the locations. This assumption allows for a Scherrer estimation of particle size based on peak broadening.[82]

The GIXRD data indicates that the copper particles are larger than that for lead at 500°C and smaller than lead particles for the other two treatment temperatures. This is difficult to discuss as the concentration of atoms to diffuse to growth sites is changing until all the reducible atoms have been liberated. It is also the case that the reaction rate is faster for the copper containing glass. Copper atoms do have a lower activation energy for diffusion implying that less energy is required to move an atom from one site in the glass to another. Since GIXRD is sampling the surface layer of the glass it is reasonable to think that the depths being sampled are completely reacted for at least the 600°C samples, and still the lead containing glass exhibits particle sizes that are greater than for copper. As with the previous section, it must be stated that this is not necessarily a measurement of particle size as these particles are probably polycrystalline in nature, but more of a grain size within the particles. Also, the lead containing glass exhibited stronger peaks, due to the electronic density of lead, making the peak fitting much more reliable. The copper UV-Vis data was shown to exhibit interference patterns while the lead glass was not. It is still unclear as to whether the interference patterns were a result of light scattering off of high densities of particles or the formation of layers. It must be noted that lead is forming as liquid droplets while copper is not. This could have something to do with the size of the particles or grains within the particles as the lead is solidifying upon cooling.

The growth at short treatment times was easily confirmed through the attenuated Mie calculations. It is reasonable to assume that the particle sizes are less than 30 nm for the first few hours of treatment. The calculated spectra matched the difference UV-Vis spectra very closely for copper containing glasses. The only real mismatch is above 560 nm at the base of the tail. This is most likely due to Cu^{2+}, which has a band centered around 790 nm, being removed from the structure due to the reduction which should lower the intensity of this band, and that is not accounted for in the estimated Mie data. Otherwise there is great agreement. The nickel containing glass also is reproduced well, but some interesting differences were noted. The difference spectra exhibits a decrease in the envelope that contains three bands located at ~450, ~560, and ~630 nm.[19] The 450 nm band is known to relate to octahedrally coordinated nickel while the other two are related to tetrahedrally coordinated nickel. The octahedrally coordinated nickel band is

roughly 3x greater in intensity for these glasses than the tetrahedrally coordinated nickel bands.[15] The decreases were checked for any difference in ratio but within uncertainty they decreased at a ratio of 3:1 for the octahedral band to the tetrahedral band intensities. Initial data shows some difference in this ratio but due to the possibility of surface related coordination issues, this is not discussed.

A peak shift was noted in much of the GIXRD data collected which is related to interatomic spacing changes in the particles upon cooling. These estimations were done only for the lead glasses as the peaks for this system were the most intense and therefore background subtraction was the most reliable. The lead data indicates that there is an increase, especially for the two temperatures above 500°C. This is believable as lead has a much greater thermal expansion coefficient than a SLS glass.[52] This means that upon cooling, lead will contract more than the surrounding glass matrix encapsulating it. The only way an interatomic increase should exist is if there is some interaction between the matrix glass and the particles. This seems to be evidence suggesting this as a possibility. Lead is forming as a droplet, and solidifies at approximately 327°C. It is believed that the stress from this thermal expansion mismatch would initiate at this temperature and increase down to room temperature. The mismatch is so large that stress and strain are to be expected, and lead is known to be a relatively soft metal.

6. THE FORMATION OF NI-CU ALLOYS IN GLASSES THROUGH HYDROGEN REDUCTION

6.1 Introduction

The possibility of giving bulk glass properties that are not typically ascribed to glasses is an exciting new reality. Alloys have been formed in glasses for some time, but most of them require ion implantation techniques to exceed saturation limits and thus allow nucleation and growth. Even the ancient glassware, the Lycurgus Cup, is reported to contain an alloy of gold and silver giving it unique optical properties. Using hydrogen allows for the reduction of a wide array of metals which can subsequently form alloys with ranges of properties.

The author has found evidence of three reported studies involving alloy formation due to hydrogen reduction in glasses, all of which occurred at Alfred University. Miller and Shelby[6] studied the formation of nickel and cobalt alloys in borosilicate glasses and were able to confirm their presence through a variety of analytical techniques. Carpenter and Shelby[4] and Kolehmainen and Shelby[5] formed nickel and cobalt alloys in SLS glasses. These authors even detected a composition change during different measurement techniques which they ascribed to a diffusion related composition change of the clusters. The real question here is what else can form an alloy in a glass via hydrogen reduction. There are many elements to choose from based on basic thermodynamic data. Nickel and cobalt seem to react at very similar rates with hydrogen which could imply that for alloy formation to occur in a glass, the separate ions must have a similar thermodynamic state.[4-6]

To better understand whether reaction rate governs alloy formation or not, copper and nickel containing glasses were chosen for this work. Copper reduces the fastest in the glasses measured to date, and nickel reduces much more slowly. If they can form an alloy, this would indicate that reaction rate is not necessarily a governing factor for alloy formation. Nickel and copper also form an alloy at standard temperature and pressure based on related phase diagrams. And lastly, nickel copper alloys have found use as

catalysts in the steam reformation industry, which could give rise to a new and exciting application for a very traditional SLS glass.[120]

6.2 Results

The glasses used for this portion of work are all based on various compositions of 16 Na_2O–9 CaO–1 RO–74 SiO_2 (mol%) glass where R is Ni, Cu, or some mixture of the two. The glasses were all treated in 0.92 atm of hydrogen at 500°C, 550°C, and at 600°C. The tarnishing model predicts a parabolic relationship between the reaction of ionic metal dissolved in the glasses being discussed and time, permeability of hydrogen, pressure of hydrogen, and the concentration of ionic metal present in the glass. None of the glasses treated in this study reached the completion of the reaction. IR spectra were collected for the various samples used throughout the reduction to monitor the rate of reaction. The spectra are very similar to those collected in the previous section and therefore will not be shown here. For the samples treated at 500°C, a linear relationship between the change in absorbance and the square root of time per sample thickness can be seen for the sample containing 1 Cu and 0.1 Ni/0.9 Cu (mol%) (Figure 53). The samples containing more nickel have a curved relationship as shown in the previous section. The linear data is fit with a best fit linear regression while any curvature is merely drawn on to indicate the general trend. The 1 Ni (mol%) containing sample has the slowest change in absorbance noted for this temperature. The 1 Cu and 0.1 Ni/0.9 Cu (mol%) containing samples have the quickest changes in absorbance recorded at this temperature and were about the same with consideration of error. The 0.5 Ni/0.5 Cu and 0.9 Ni/0.1 Cu (mol%) containing samples did not follow the general trend exhibited by the rest of the samples. They both exhibited curvature, but the sample containing 0.9 Ni/0.1 Cu (mol%) appears to reduce more quickly than the sample containing 0.5 Ni/0.5 Cu (mol%). This sample did exhibit a great deal of scatter. The general trend ideally would be the reaction rate increases with increased percentage of copper in the glass as copper reduces so much more quickly than nickel, especially at this temperature.

For the samples treated at 550°C, a clear linear relationship between the change in absorbance and the square root of time per sample thickness can be seen for the samples

containing 1 Cu, 0.1 Ni/0.9 Cu, and 0.5 Ni/0.5 Cu (mol%) (Figure 54). These data points all lie within the error of the measurement and there is no readily distinguishable difference between them. The change in absorbance for the 1 Ni and 0.9 Ni/0.1 Cu (mol%) containing glasses treated at this temperature exhibit a more curved relationship which was drawn over the data points to show the shape more clearly. The two lines are too close within the error of the measurement and the apparent scatter for the data points of the 0.9 Ni/0.1 Cu (mol%) containing sample to make any more concrete statements. In general, the glasses containing more copper are linear with respect to the square root of treatment time and increase in absorbance more quickly than glasses containing more nickel.

For the samples treated at 600°C, a linear relationship between the change in absorbance and the square root of time per sample thickness can be seen for all the samples measured (Figure 55). Again data for the copper containing sample is not reported due to questions with the background correction used being appropriate for that case.

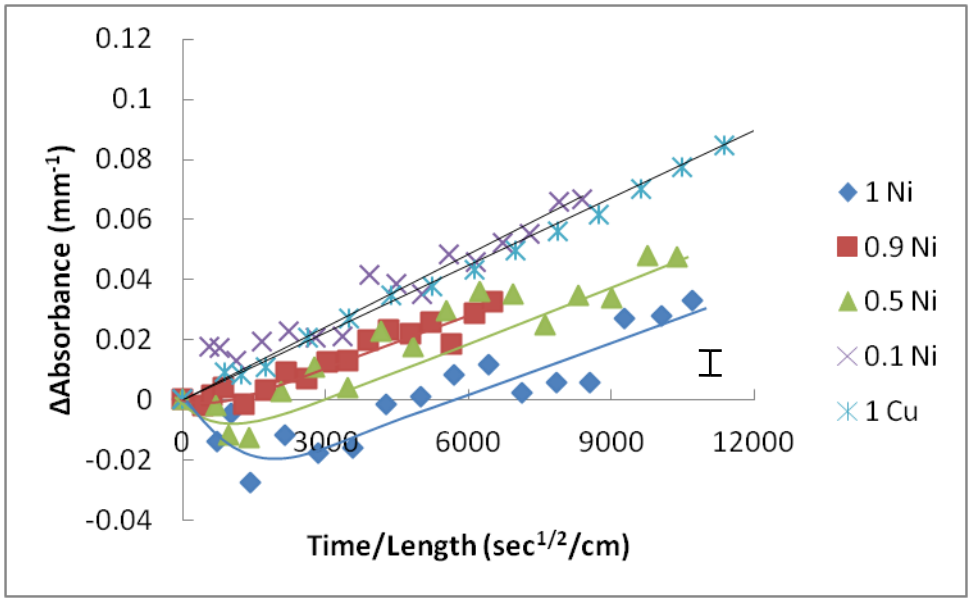

Figure 53. Plot of the change in absorbance of the 3500 cm^{-1} band against the reduction time and the length of the sample for SLS glasses containing nickel, copper, and mixtures of the two at 500°C.

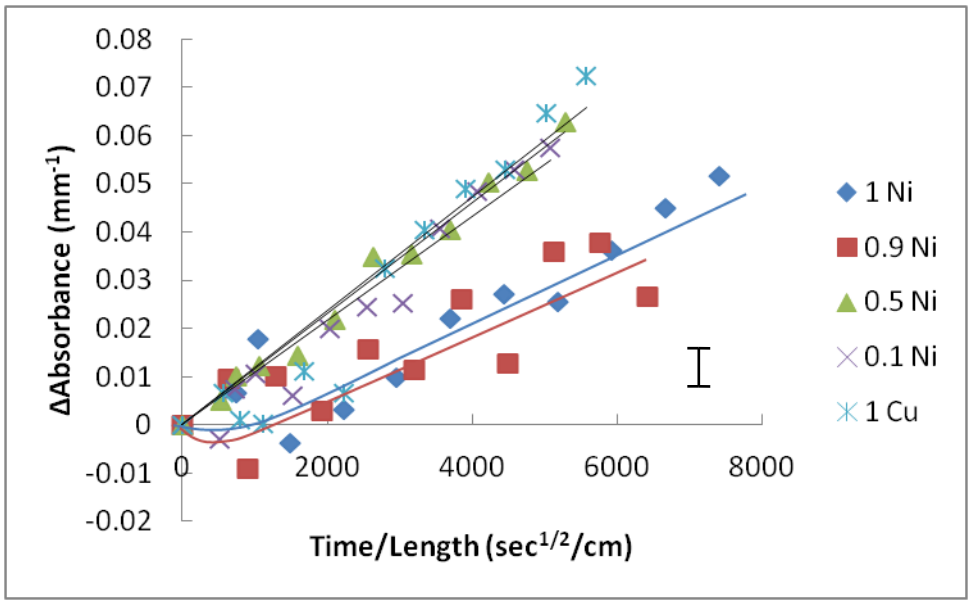

Figure 54. Plot of the change in absorbance of the 3500 cm^{-1} band against the reduction time and the length of the sample for SLS glasses containing nickel, copper, and mixtures of the two at 550°C.

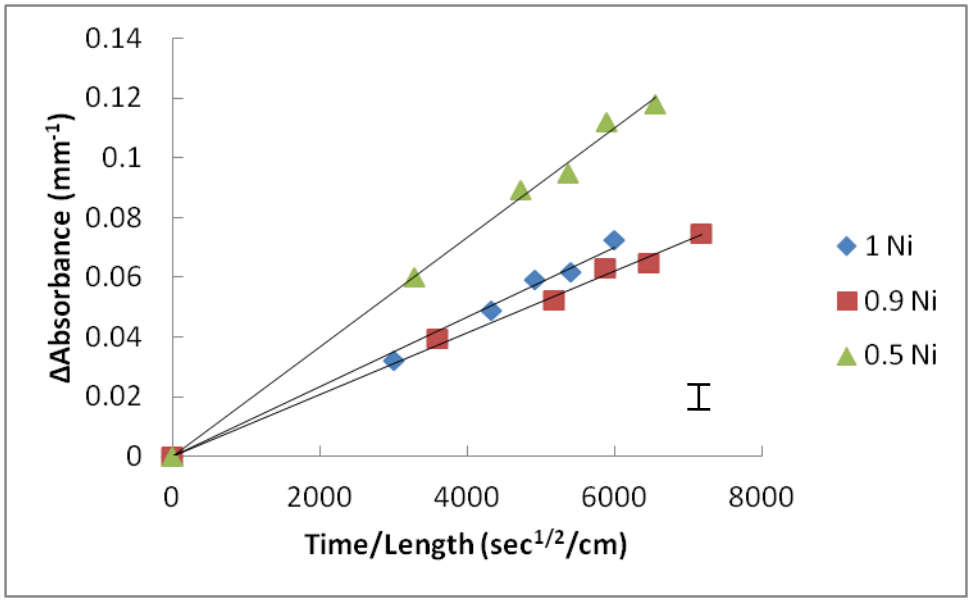

Figure 55. Plot of the change in absorbance of the 3500 cm^{-1} band against the reduction time and the length of the sample for SLS glasses containing nickel, copper, and mixtures of the two at 600°C.

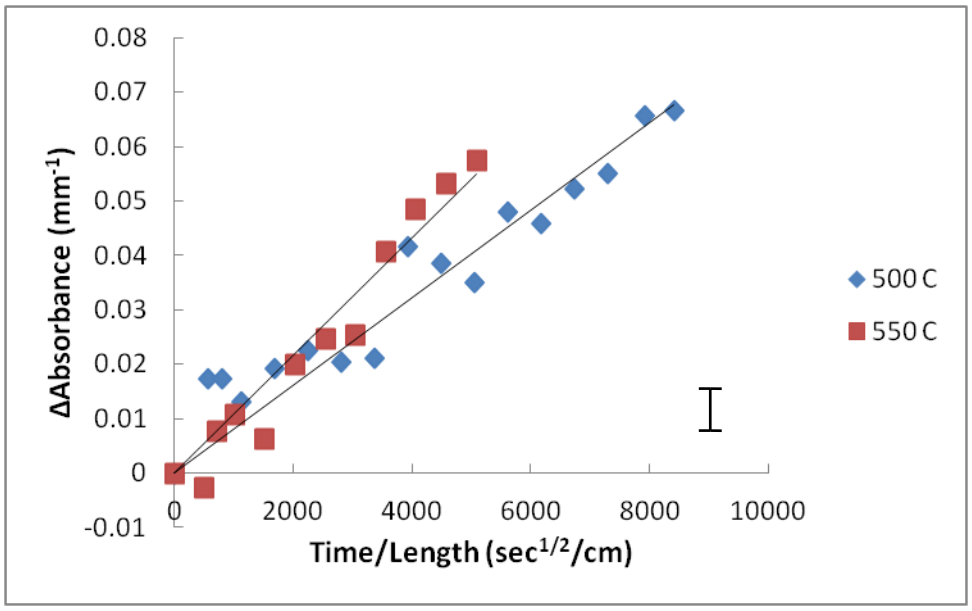

Figure 56. Plot of the change in absorbance of the 3500 cm^{-1} band against the reduction time and the length of the sample for SLS glasses containing 0.9 Ni/0.1 Cu (mol%) treated at various temperatures.

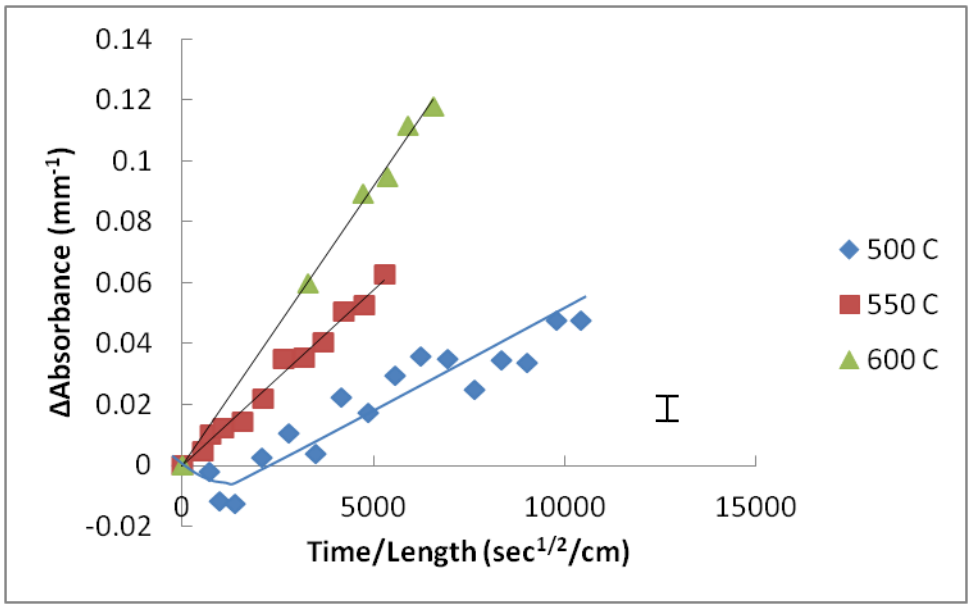

Figure 57. Plot of the change in absorbance of the 3500 cm^{-1} band against the reduction time and the length of the sample for SLS glasses containing 0.5 Ni/0.5 Cu (mol%) treated at various temperatures.

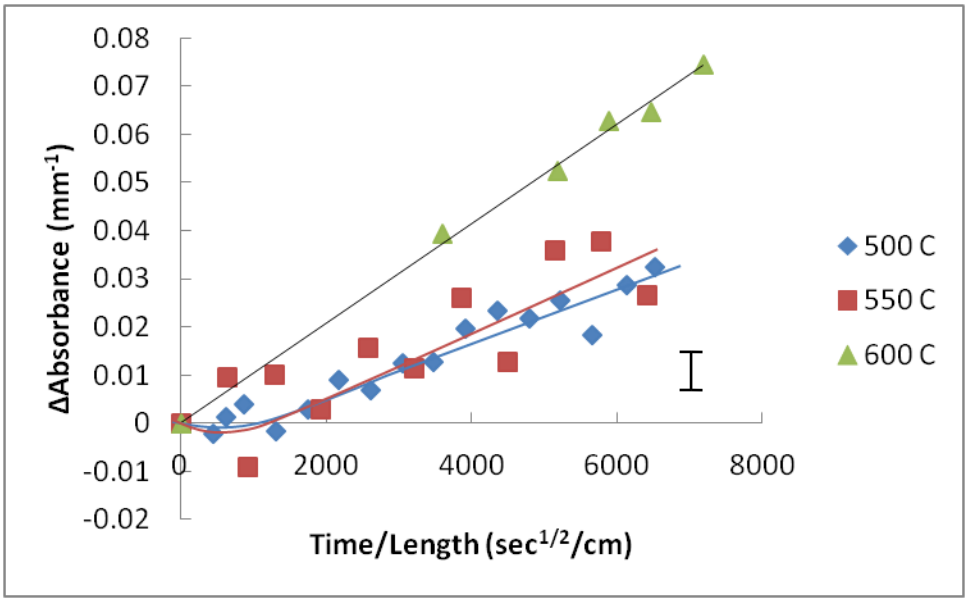

Figure 58. Plot of the change in absorbance of the 3500 cm^{-1} band against the reduction time and the length of the sample for SLS glasses containing 0.1 Ni/0.9 Cu (mol%) treated at various temperatures.

UV-Vis data were collected throughout this series of reduction experiments. Nearly all samples exhibited some degree of color change throughout the reduction. Three out of the four samples were colored in the visible region prior to reduction due to ligand field absorptions (Figure 59). The nickel containing SLS glass clearly exhibits a visible absorption envelope consisting of three bands and a much broader band with a maximum absorbance somewhere outside of the data collected in this study. The three bands in the visible envelope are located at ~450, ~560, and ~630 nm. There is another broad band in the higher wavelength region of the spectra. The copper containing SLS glass clearly exhibits a visible absorption located at ~780 nm. The UV-edge is also slightly shifted to higher wavelengths more than for any of the other glasses measured. The mixtures of nickel and copper in the SLS glasses all exhibit combinations of bands present in the base spectra for nickel and copper SLS glasses. The glasses with mixtures have decreased intensities for the bands with respect to the changes in concentration of nickel and copper in comparison to the base glasses.

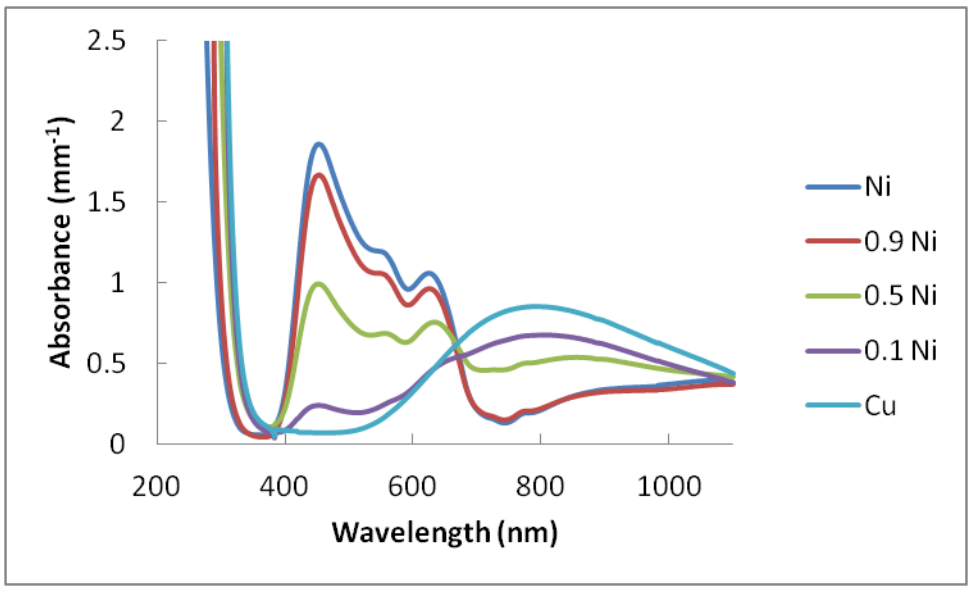

Figure 59. Representative plot of absorbance for all glasses used before reduction.

UV-Vis spectra were collected for all of the samples at various times throughout the reduction experiments. All of the samples containing metal ions exhibited a visible color change after reduction. The nickel containing SLS glass is initially a brown/black color and after reduction it appears black. The copper containing SLS glass is initially a light blue color and after reduction it appears dark red. The glasses containing mixtures of the two all took on shades of red and brown. The redder glasses had more copper, and the browner glasses had more nickel. The glass containing 0.9 Ni/ 0.1 Cu (mol%) had a red tint but was primarily brown. The darkening of the sample increased with temperature and treatment time, and an example plot of the affect of treatment time on the spectra can be found in Figure 60. Just as with the pure nickel containing SLS glass reported in the previous section, this spectrum shows the most prominent increase near the UV-edge and a tail that extends through the entire visible region. The difference spectra were converted to absorption coefficients and then an attenuated Mie scattering calculation was performed to model the plasma resonance absorption coefficient of small metallic particles of copper and nickel dispersed in a dielectric matrix and compare to the measured data. The contributions from nickel and copper particles were summed together to attempt to recreate the measured spectra (Figure 61). This process will be covered in more detail in the discussion. The attenuated Mie absorption calculation

relates somewhat closely to the measured spectra. Just as was noticed in the spectra for pure nickel, there were some decreases in the visible band envelope which makes the fitting difficult. The calculated data does appear to indicate that the spectra are comprised of primarily nickel clusters. The calculated data does not match up well at the lower wavelength regions of the spectra. In general the spectra were reproducible, but not to the degree some of the pure metal spectra were reproduced by calculation in the previous section.

The glass containing 0.5 Ni/ 0.5 Cu (mol%) turned reddish after reduction. The darkening of the sample was accelerated with temperature and treatment time, and an example plot of the affect of treatment time on the spectra can be found in Figure 62. Just as with the pure nickel containing SLS glass reported in the previous section, this spectrum shows the most prominent increase near the UV-edge and a tail that extends through the entire visible region. The difference spectra were converted to absorption coefficients and then an attenuated Mie scattering calculation was performed to model the plasma resonance absorption coefficient of small metallic particles of copper and nickel dispersed in a dielectric matrix and compare to the measured data. The contributions from nickel and copper particles were summed together to attempt to recreate the measured spectra (Figure 63). Mie scattering calculations were performed to model the plasma resonance absorption coefficient of small metallic particles of nickel dispersed in a dielectric matrix and compare to the measured data. The absorption coefficient of small (<40 nm) metallic particles dispersed in a dielectric matrix is given by:[17]

$$\gamma = NV \frac{\left(36\pi n k {n_o}^3\right)}{\lambda\left(\left(n^2 - k^2 + 2{n_o}^2\right) + 4n^2k^2\right)} \qquad (35)$$

where N is the number of particles per unit volume, V is the volume of the particles, n_o is the refractive index of the glass, and n and k are optical constants of the metal.

The attenuated Mie absorption calculation relates very closely to the measured spectra. Just as was noticed in the spectra for pure copper, there is a band forming near ~560 nm. It again appears that the contributions of nickel particles are potentially greater than those noted for copper particles indicating higher concentrations of nickel particles in this sample at these early reduction times. The calculated data does not match up

incredibly well at the lowest wavelength regions of the spectra collected. The spectra are very reproducible with calculation for the glasses containing 0.5 Ni/ 0.5 Cu (mol%).

The glass containing 0.1 Ni/ 0.9 Cu (mol%) turned a very dark red after reduction. The darkening of the sample was accelerated with temperature and treatment time, and an example plot of the affect of treatment time on the spectra can be found in Figure 64. Just as with the pure copper containing SLS glass reported in the previous section, this spectra shows the most prominent increase at ~560 nm and a tail that extends through the rest of visible region. The difference spectra were converted to absorption coefficients and then an attenuated Mie scattering calculation was performed to model the plasma resonance absorption coefficient of small metallic particles of copper and nickel dispersed in a dielectric matrix and compare to the measured data. The contributions from nickel and copper particles were summed together to attempt to recreate the measured spectra (Figure 65). This process will be covered in more detail in the discussion. The attenuated Mie absorption calculation relates very closely to the measured spectra. Just as was noticed in the spectra for pure copper, there is a very prominent band forming near ~560 nm. For these samples it appears that the contributions of the copper particles are potentially greater than those noted for the nickel particles indicating higher concentrations of copper particles in this sample at these early reduction times. The calculated data matches up well even at the lowest wavelength regions of the spectra collected. The spectra are very reproducible with calculation for the glasses containing 0.1 Ni/ 0.9 Cu (mol%).

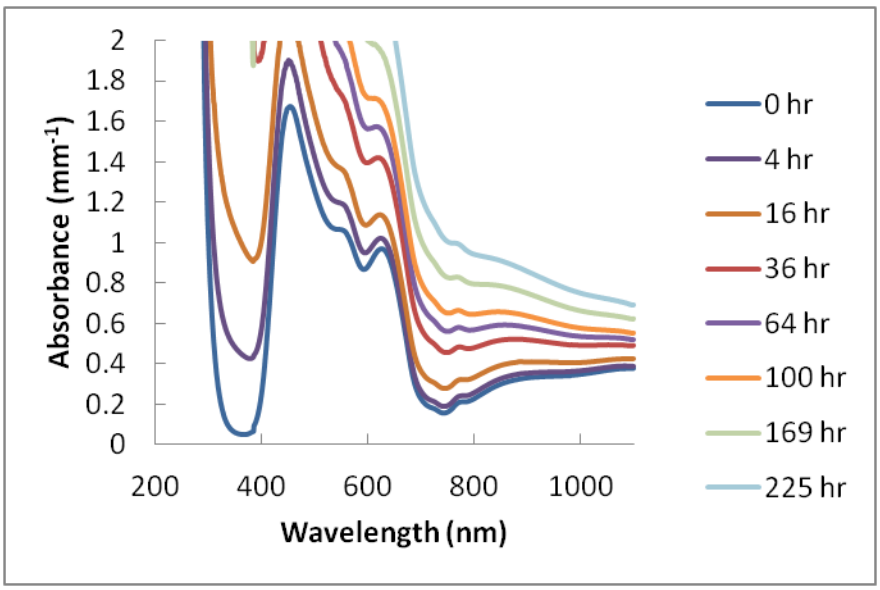

Figure 60. Representative UV-Vis spectra of glass containing 0.9 Ni/ 0.1 Cu (mol%) after various reduction times in hydrogen at 500°C.

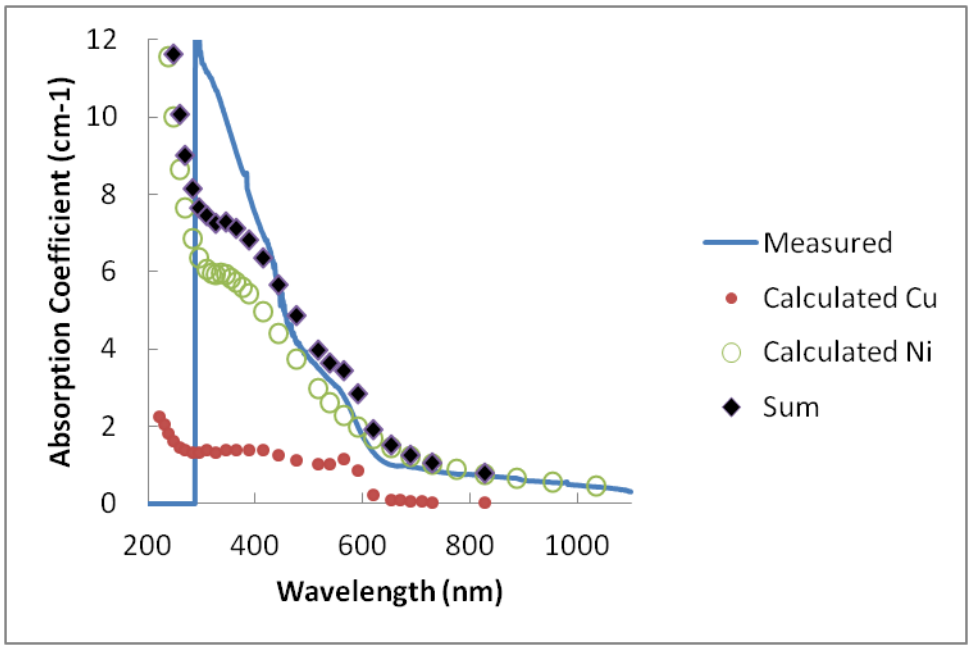

Figure 61. Attenuated Mie absorption calculation compared to difference spectra for glass containing 0.9 Ni/0.1 Cu (mol%) treated at 500°C for four hours.

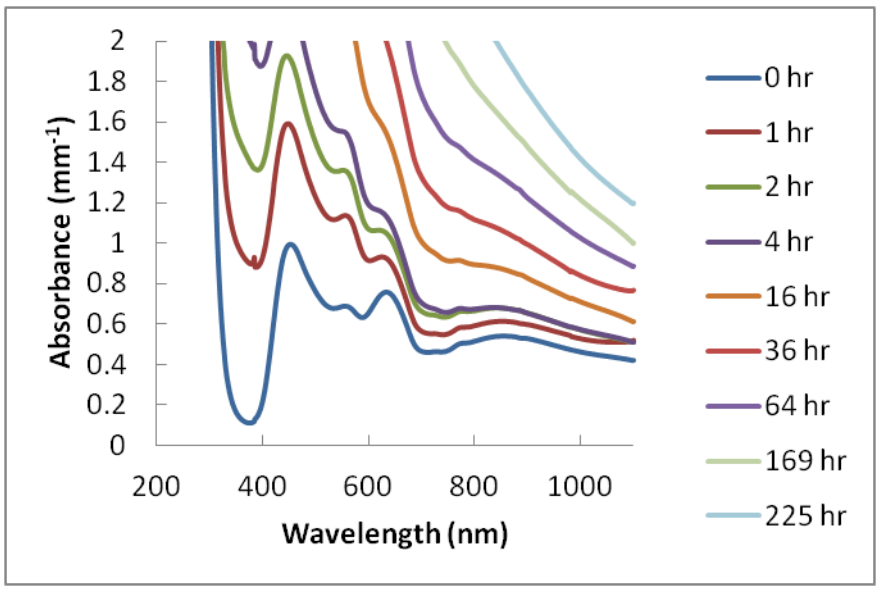

Figure 62. Representative UV-Vis spectra of glass containing 0.5 Ni/ 0.5 Cu (mol%) after various reduction times in hydrogen at 500°C.

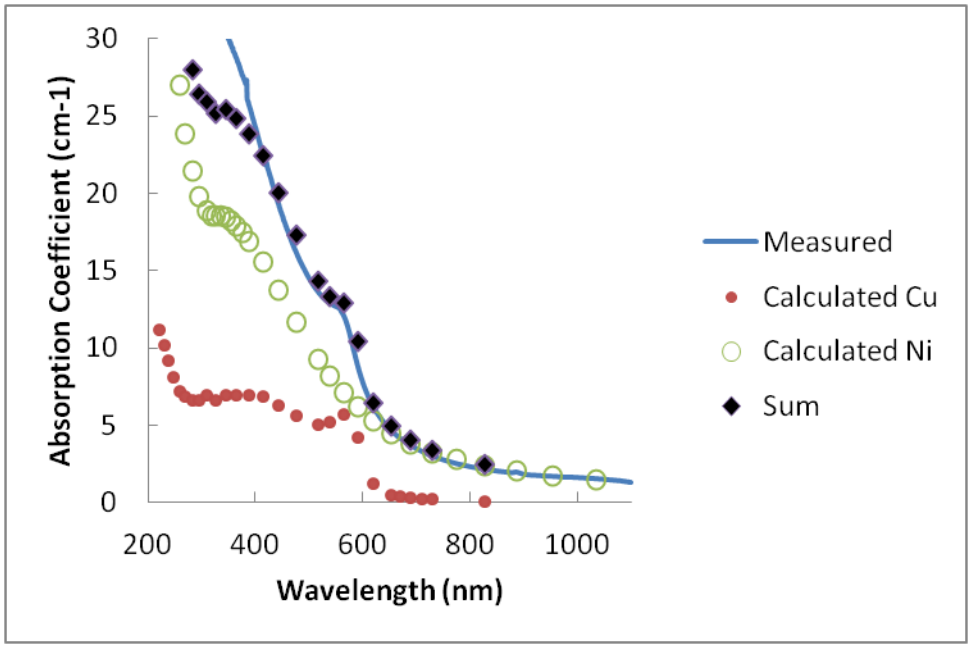

Figure 63. Attenuated Mie absorption calculation compared to difference spectra for glass containing 0.5 Ni/0.5 Cu (mol%) treated at 500°C for four hours.

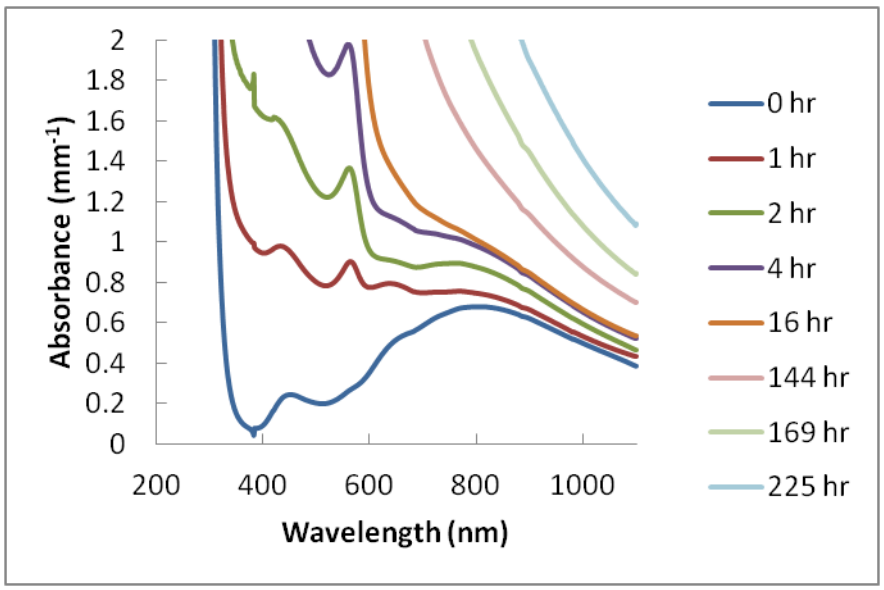

Figure 64. Representative UV-Vis spectra of glass containing 0.1 Ni/ 0.9 Cu (mol%) after various reduction times in hydrogen at 500°C.

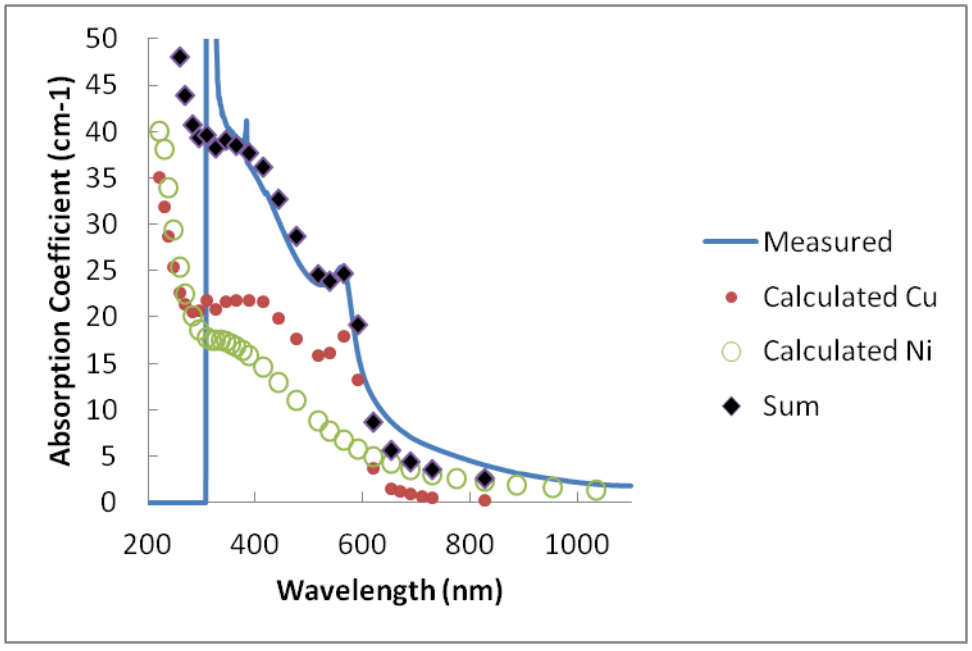

Figure 65. Attenuated Mie absorption calculation compared to difference spectra for glass containing 0.1 Ni/0.9 Cu (mol%) treated at 500°C for two hours.

The presence of metallic clusters of nickel, copper, and potential alloys in the respective glasses was confirmed using GIXRD. The presence of nickel and copper crystals was confirmed through the identification of the (111) diffraction peak which is the most intense in the pattern for both. To determine the possible existence of an alloy in the glasses containing nickel and copper, the interatomic spacings ("d" spacings) were calculated using GIXRD peak fitting software. A decrease in the interatomic spacings was recorded with increasing amounts of nickel in the glasses (Figure 66 and Table XVII). The red symbols in Figure 66 are taken from reported XRD data for known alloys of nickel and copper and pure nickel and copper metals to create a typical Vegard's Law composition plot. The measured interatomic spacings at the different temperature of treatment are plotted with respect to the initial glass composition. The interatomic spacings for pure copper and the 0.1 Ni/ 0.9 Cu (mol%) containing glasses appear to be higher than reported in literature. This phenomena is described in the previous section as a potential strain due to thermal expansion mismatch, and it further complicates any attempts to quantify the data. Trends still exist in relation to temperature and initial glass composition. The composition of all measured particles appears to increase in nickel content with an increase in the nickel content of the base glass except for the samples containing 0.1 Ni/ 0.9 Cu (mol%) for all temperatures of treatment. It also appears that the particles are all at higher copper concentrations than predicted by the base glass composition. The 0.9 Ni/ 0.1 Cu containing glass treated at 500°C appears to contain alloyed particles with the highest nickel content, followed by the glass treated at 550°C, and then the glass treated at 600°C. The intensity of the (111) peak became increasingly smaller with higher concentrations of nickel in the base glass and this did increase the error related to the fitting procedure. The standard deviation decreased with increasing treatment temperature for this composition and this too is related to the size of the peak to fit. The calculated alloy composition is more skewed towards copper and thus less nickel for the 0.5 Ni/ 0.5 Cu containing glass at lower temperatures. Particle sizes for the alloyed clusters were calculated based on the broadening of the GIXRD peaks (Table XVIII). All of the estimated particle sizes increase with increasing treatment temperature except for the sample containing 0.5 Ni/ 0.5 Cu and treated at 550 and 600°C. They are

very close in consideration of the standard deviation. The particles appear to increase in size when the base glass contains higher concentrations of copper.

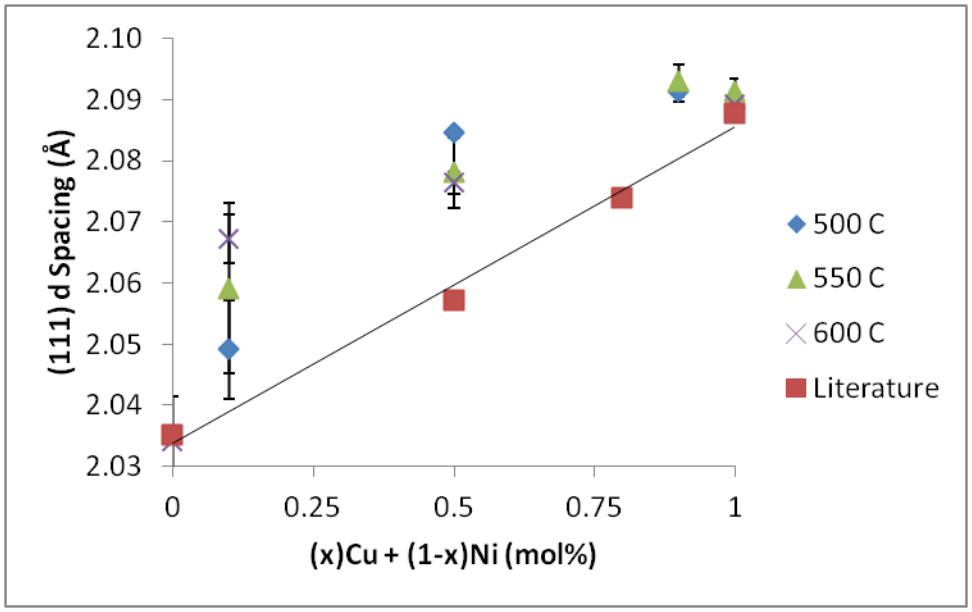

Figure 66. Calculated interatomic spacings for GIXRD peak fitting to the (111) peaks.

Table XVII. GIXRD Calculated Interatomic Spacings From Peak Fit Data for (111) Peaks in all Glasses Tested

	1% Cu	0.9% Cu 0.1% Ni	0.5% Cu 0.5% Ni	0.1% Cu 0.9% Ni	1% Ni
500°C					
(111) d spacing (Å)	2.089	2.091	2.085	2.049	-
Standard Deviation	0.001	0.002	0.000	0.008	-
550°C					
(111) d spacing (Å)	2.091	2.093	2.078	2.059	-
Standard Deviation	0.002	0.003	0.006	0.014	-
600°C					
(111) d spacing (Å)	2.089	-	2.076	2.067	2.034
Standard Deviation	0.001	-	0.002	0.004	0.007
Reported d spacing (Å)	2.088	-	2.057	-	2.035

Table XVIII. GIXRD Calculated Particle Sizes From Peak Broadening Data for (111) Peaks in all Glasses Tested

	1% Cu	0.9% Cu 0.1% Ni	0.5% Cu 0.5% Ni	0.1% Cu 0.9% Ni	1% Ni
500°C					
Particle Size (nm)	13.7	9.3	5.3	5.3	-
Standard Deviation	3.1	1.5	0.6	1.2	-
550°C					
Particle Size (nm)	18.0	15.0	10.0	8.7	-
Standard Deviation	1.0	1.0	1.0	0.6	-
600°C					
Particle Size (nm)	18.7	-	8.7	12.3	16.0
Standard Deviation	1.5	-	0.6	4.2	6.0

6.3 Discussion

The tarnishing model was initially discussed by Crank to explain moving boundary reactions.[28] The tarnishing model is often described as:

$$\frac{(C - C_i)}{(C_f - C_i)} = (8KPt/L^2C_x)^{1/2}$$

where C is the concentration of hydroxyl at a given time, C_i is the initial concentration of hydroxyl, C_f is the final concentration of hydroxyl, K is the permeability of hydrogen in the glass, P is the partial pressure of hydrogen, t is the treatment time, L is the sample thickness, and C_x is the concentration of reaction sites. The term at the left of the equal sign is essentially a value from zero to one, where one would signify a completed reaction. This model has successfully been applied to hydrogen reaction experiments in literature to describe various reaction kinetics.[7,12,22,29-32,34,35,108]

This set of glasses was specifically chosen to eliminate a large number of variables in the tarnishing model. These glasses ideally contain the same amount of reaction sites and the same permeabilities. This means that for a given tarnishing model plot, the slopes of any of the existing 2^+ ions, or ratios of the two ions used, should lie on top of one another. This was not found for any experimental data. It must be noted that

copper exists as Cu^{2+} and Cu^{1+} in these glasses. It is believed that the majority of ions start out in the 2^+ state in these glass systems based on the oxygen rich atmosphere during melting.[9,11,15,63]

The data does exhibit some of the same features described in the previous section. The pure nickel containing glass absorbance changes exhibit a curved relationship with the square root of time and this is believed to be due to the slow reaction rate of nickel spreading the diffusion boundary. This was seen to be more prominent in the glasses containing 0.5 mol% nickel and higher at 500°C, for 0.9 mol% nickel and higher at 550°C, and was no longer seen at 600°C. This again indicates the reaction rate becoming rapid enough that the tarnishing model is again valid, which implies a diffusion limited sharp boundary is again present. In general the glasses with high concentrations of copper always exhibited similar increases in absorbance, or similar reaction rates, and glasses with high concentrations of nickel always exhibited slower reaction rates. Again this could be due to the discussion from the previous section in consideration of the Gibb's free energy of oxide formation.

Equilibrium in a glass containing one reducible oxide is typically based on glass composition, melting conditions, batching composition, and the furnace atmosphere.[65] When a glass contains more than one reducible species, equilibrium is considered to be much more complex. Tables have been developed to relate thermodynamic free energies of reduction-oxidation reactions for a species to other species present in the same glass.[88,89] The species in question here have not been found tabulated together. A similar study done found that nickel and cobalt added together exhibit an increased reaction rate,[6] but this data was not found for nickel and copper added together in these glasses.

The UV-Vis data was again compared to an attenuated mie absorption theory for small particles dispersed in a dielectric matrix. This should be valid at the shorter treatment times. The absorption coefficients are reproducible to a high degree of accuracy for the two glasses containing more copper than nickel. The absorption coefficient data for the 0.9 Ni/0.1 Cu (mol%) sample was close to the calculated points, but the calculation does seem to be lacking. These calculations are assuming that there are discrete particles of nickel and copper present in the matrix and the sum of their absorptions are contributing to the spectra measured. This implies that the measured

spectra for high copper containing mixtures indicate the presence of discreet particles of nickel and copper. The measured spectra for high nickel containing mixtures indicates that there may be a third type of particle which ideally would be due to an alloy of nickel and copper. Optical data was not found for the alloy system so it could not be modeled in the same fashion, but due to the inability to reproduce the measured spectra with the accuracy of the other two mixtures, this seems to be a reasonable possibility. The measured spectra for 0.1 Ni/0.9 Cu (mol%) appears to have a greater absorption coefficient due to nanoparticles of copper, and this modeled absorption coefficient decreases with decreasing copper content in the base glass. This trend was also found for the modeled nickel absorption coefficients.

The most important evidence of an alloy being formed was based on GIXRD data after long treatment times. Vegard's Law establishes that there is a linear relationship between interatomic spacings between the two pure metals in an alloy.[52] This was found in literature for existing Ni-Cu alloys and plotted. The samples treated in hydrogen all exhibited a primary (111) diffraction peak and this was fit to determine the peak location. Again, any strain is assumed to be uniform as these are spherical particles, which will also contribute to a shift. This complicates these findings, but as the data indicates, the shift due to any strain is small in comparison to the shift measured, and in the opposite direction. The measured data is related to the starting composition and clearly this does not relate to the actual composition. Due to the complications of uniform strain, no exact compositions will be stated here, but the general trend indicates that the more nickel in the starting glass before treatment, the greater the composition of nickel in the final alloy. It seems that the alloying is possibly occurring by a diffusion mechanism, and this is further supported by the UV-Vis modeling. It is possible that initially the particles are forming separately, or even plating on top of one another, due to the reaction rate aspect of the reduction (Figure 67). This plating has been reported in literature for a different type of sample preparation.[8] Either way, this would explain the UV-Vis data and this GIXRD data. The reaction rate would indicate that nickel is reducing after copper, and this would mean that nickel is either forming separate particles or plating onto copper particles effectively minimizing absorptions due to the copper particles. The copper particles would be forming first, and at greater depths than the nickel particles due to the

reaction rate being so slow for nickel, and this means that pure copper particles would still exist. This would explain the UV-Vis modeling at early treatment times. Nickel has been reported to diffuse into copper, although the calculated diffusion coefficient is very low at these temperatures ($D \sim 10^{-12}$ cm^2/s).[121] It is still reasonable to say that this diffusion is the limiting factor to the development of these alloys and the concentration gradient is influenced by the reaction rate of the reduction and diffusivities of the atoms reduced in the glass to the growing clusters.

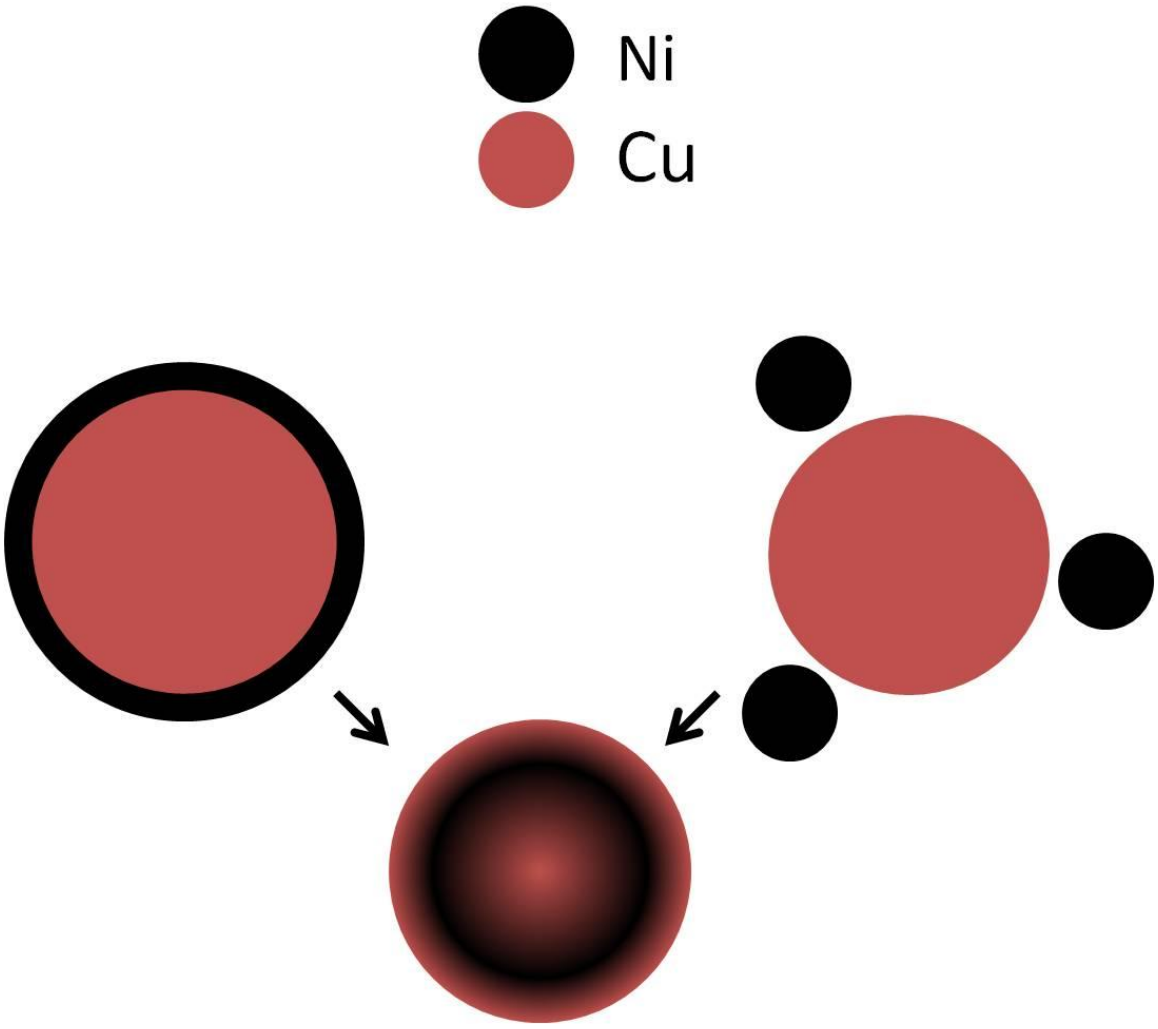

Figure 67. Possible growth mechanisms for glassed doped with two metals.

7. CONCLUSIONS

All of this work can be successfully discussed in terms of reaction of reducible species with hydrogen, and subsequent nucleation and growth of metallic clusters. The initial reaction of dissolved hydrogen with the reactive sites in the glass is clearly related to the permeability of hydrogen, i.e. the solubility and the diffusivity of hydrogen in the glasses in question. To determine the percentage of reaction, the concentration of hydroxyl formed in the glasses was measured using IR spectroscopy. The tarnishing model predicts a linear relationship between the percentage of the reaction that has occurred and the square root of time. This was exhibited for most of the glasses studied. There are clearly cases where the reaction rate is so slow at the temperatures and concentrations of dissolved hydrogen present, that a curved relationship develops. These cases are almost explicitly limited to glasses containing nickel and cobalt. Any non linearity for the rest of the glasses measured is so minimal that it could not be detected, or it is believed to be an artifact of the background. Even though no curvature is measured for copper or lead reduction in the SLS glasses, they still exhibit different rates of hydroxyl formation. This would imply that the permeabilities of these glasses are different, but this is most likely not the case. It is more evident that hydrogen reaction in glasses is controlled by the reaction rate. The difference in the rate of formation of hydroxyl does appear to decrease with increased temperature, and this would indicate that the reaction is going fast enough that the glass is beginning to exhibit a diffusion of hydrogen to reaction sites controlled moving boundary as predicted by the tarnishing model. All of these ions reduce, especially at lower temperatures in the same order as would be expected based on a simplistic view of oxide formation energy.

While it is good that increased temperature allows more accurate application of the tarnishing model in terms of reaction rate, this also allows for recombination of hydroxyl to form molecular water, and for the molecular water to react and diffuse out of the glass into the vacuum of the applied hydrogen atmosphere. There is evidence in literature[12] indicating that this is a much slower process, kinetically, than the reaction

itself. If it is a kinetic process in a glass then it is reasonable to assume that it is somewhat limited by viscosity. Therefore, a less viscous glass should be easier to remove hydroxyl from than a more viscous glass. This is difficult for the measurements done in this study as higher temperatures remove reaction rate issues, but higher temperatures also increase the probability of water to diffuse and react out of the glass. The hydroxyl concentrations based on initial compositions were calculated for the indium silicates and it was realized that the amount of hydroxyl being formed was most likely well above any known saturation limits for hydroxyl in glasses. This indicates a thermodynamic propensity for the formation of molecular water besides just the concentration gradient. The indium silicate glasses also exhibited the most variable hydroxyl formation data of any of the glasses studied and it is proposed that this is a direct result of the saturation limits being potentially surpassed.

The work with the indium containing glasses brings light to the possibilities of glasses with very different surface chemistries. Indium, being the durable component of the sodium-indium-silicates, makes a very stable glass system. When it is reduced, and thereby removed from the structural sites it resides in, the glass reverts to a phase separated sodium silicate composition. This composition is very reactive with atmosphere making a gel layer quickly, and corroding. This phenomenon could potentially be exploited to make a functional surface containing particles, such as catalysts. The surface will weather, if engineered properly, continuously exposing new catalytic surfaces. The glass underneath the reacted layers would still be very durable and contain indium in the ionic 3^+ state.

The work with the alloyed compositions of nickel and copper really redefines the situations necessary to form an alloy using hydrogen reduction in glasses. The reaction rate of the reduction process does not matter as long as the reduced atoms have sufficiently high diffusion coefficients at the temperatures of the treatment to allow the composition of the alloyed particle to approach some sort of equilibrium. This equilibrium may take a long time to reach, as it clearly did not reach equilibrium in this data, but the compositions of the particles should be similar to the base compositions. Any alloy should be possible to form in a glass via hydrogen reduction if it would form

an alloy at standard temperature and pressure, if the diffusion of the atoms is high enough in the metal, and if the components are reducible.

The growth of the particles also appears to bring light to some new concepts. The particles clearly increase with size and concentration with temperature for the SLS glasses. It is believed that the indium containing glasses, having a very fluid sodium silicate surface layer allowed the formation of much larger particles than would be present in a more viscous material. The indium glasses also exhibited some crystallization of cristobalite and a sodium indium silicate phase which lowered the concentration of metal particles detected above the glass transition range. It is believed that the clusters are growing via an atomic diffusion mechanism to a nucleation site as noted by the activation energy calculations for the atoms and ions involved in these glasses. When the viscosity is low enough, it was noted that it appears that small clusters tend to aggregate together. This fits well with nucleation and growth theory in terms of the activation energy for viscous flow being clearly important.

It was also determined that the particles exhibit some interesting lattice spacing changes from what would be expected. This is explained as a result of an interaction between the particle and the glass matrix containing the particle. Upon cooling the particles being metal, and having much higher thermal expansions than the glass containing them, should contract much more than the glass phase. This contraction, if the particle is bound, should result in a uniform strain of the lattice as noted in the GIXRD data collected.

8. FUTURE WORK

Much work needs to be done with cluster formation in glasses. It is clear that a study must be formulated to monitor the amount of water that diffuses out of a reduced glass system at various temperatures. It would also be important to determine the hydroxyl solubility equilibrium for the glasses used to determine how much hydroxyl should exist after the dehydroxylation. Many more alloys should be explored as the possibilities seem to be much greater than were initially thought. This interaction region between the particle and glass should also be investigated to determine what kind of bonding is at the surface and how that affects the particles for any kind of commercial possibilities. The tarnishing model should really be corrected with temperature to alleviate the issues with reaction rate for the various ions in question, and more likely this would be a study of the activities of the various ions and components for these reductions to occur. It would be interesting to study the growth of the particles and determine if the activation energy for diffusion to the particle itself mimics any interdiffusion values for the glass system.

REFERENCES

1. R.H. Brill, "The Chemistry of the Lycurgus Cup," pp. 223.1-33.13 in *Comptes Redus: VIIe Congrès International du Verre.* Bruxelles, 1965.

2. K. Nassau, *The Physics and Chemistry of Color, The Fifteen Causes of Color,* 2nd ed. pp. 231-46, John Wiley & Sons, New York, 2001.

3. A. Ruivo, C. Gomes, A. Lima, M.L. Botelho, R. Melo, A. Belchior, and A.P.d. Matos, "Gold Nanoparticles in Ancient and Contemporary Ruby Glass," *J. Cultural Heritage,* **9** e134-e7 (2008).

4. J.R. Carpenter, "Ferromagnetic Colloids of Alloyed Nickel and Cobalt n Soda Lime Silicate Glass"; Bachelor of Science Thesis. Alfred University, Alfred, NY, 2008.

5. A.S. Kolehmainen, "Alloying and Phase-Separation Effects on the Formation oof Magnetic Nanocrystals in Nickel/Cobalt Oxide Doped Silicate Glasses"; Master of Science Thesis. Alfred University, Alfred, NY, 2011.

6. M.E. Miller, "Formation of Transition-Metal Crystallites in Glass"; Master of Science Thesis. Alfred University, Alfred, NY, 2005.

7. M.E. Miller and J.E. Shelby, "Formation of Cobalt Nanocrystals in a Borosilicate Glass," *Phys. Chem. Glasses: Eur. J. Glass Sci. Technol. B,* **51** [2] 100-6 (2010).

8. F. Raziewski and J.E. Shelby, "Multilayer Colloid Formtion in Soda Lime Silica Glass," *J. Non. Cryst. Sol.,* **352** [6-7] 528-33 (2006).

9. J.E. Shelby, *Introduction to Glass Science and Technology*. pp. 69-82, Royal Society of Chemistry, Cambridge, 1997.

10. M.R. Tuzzolo and J.E. Shelby, "Hydrogen-Induced Formation of colloids of Arsenic, Antimony, and Bismuth in Oxide Glasses," *J. Non. Cryst. Sol.,* **143** 181-90 (1992).

11. A.K. Varshneya, *Fundamentals of Inorganic Glasses*. Academic Press, San Diego, CA, 182-215, 1994.

12. E.M. Sturdevant and J.E. Shelby, "Hydroxyl Formation by Reaction of Molecular hydrogen with Germania-Doped Vitreous Silica," *Phys. Chem. Glasses: Eur. J. Glass Sci. Technol. B,* **49** [2] 73-80 (2008).

13. A.L. Youchak, "Hydrogen Interactions with Alkali Aluminogermanate Glasses"; Master of Science Thesis. Alfred University, Alfred, NY, 2007.

14. U. Kolberg, "Coloured Glasses," pp. 364-7 in *The Properties of Optical Glass.* Edited by H. Bach and N. Neuroth. Springer, New York, 1995.

15. C.R. Bamford, *Colour Generation and Control in Glass: Glass Science and Technology 2*. pp. 34-50, Elsevier, Amsterdam, 1977.

16. R.H. Doremus, *Glass Science*, 2nd ed. pp. 90-115, John Wiley & Sons, New York, 1994.

17. H. Rawson, *Properties and Applications of Glass: Glass Science and Technology 3*. pp. 216-21, Elsevier, Amsterdam, 1980.

18. W.A. Weyl, "Coloured Glasses: IV, The Colours Produced by Metals," *J. Soc. Glass Technol.,* **29** 289-389 (1945).

19. W.A. Weyl, *Coloured Glasses*. pp. 333-419, Society of Glass Technology, Sheffield, 1967.

20. A.E. Badger, W.A. Weyl, and H. Rudow, "Effect of Heat Treatment on Color of Gold Ruby Glass," *Glass Ind.,* **20** 407-14 (1939).

21. J. Lafait, S. Berthier, C. Andraud, V. Reillon, and J. Boulenguez, "Physical Colors in Cultural Heritage: Surface Plasmons in Glass," *C. R. Physique,* **10** 649-59 (2009).

22. J.E. Shelby, *Handbook of Gas Diffusion in Solids and Melts*. pp. 8-26, ASM International, Materials Park, OH, 1996.

23. F.J. Norton, "Permeation of Gases Through Solids," *J. Appl. Phys.*, **28** [1] 34-9 (1957).

24. R.W. Lee, "Diffusion of Hydrogen in Natural and Synthetic Fused Quartz," *J. Chem. Phys.*, **38** [2] 448-55 (1963).

25. R.W. Lee, R.C. Frank, and D.E. Swets, "Diffusion of Hydrogen and Deuterium in Fused Quartz," *J. Chem. Phys.*, **36** [4] 1062-71 (1962).

26. J.E. Shelby, "Molecular Diffusion and Solubility of Hydrogen Isotopes in Vitreous Silica," *J. Appl. Phys.*, **48** [8] 3387-94 (1977).

27. W.G. Perkins and D.R. Begeal, "Diffusion and Permeation of He, Ne, Ar, Kr, and D2 through Silicon Oxide Thin Films," *J. Chem. Phys.*, **54** [4] 1683-94 (1971).

28. J. Crank, *The Mathematics of Diffusion*. pp. 117-46, Clarendon Press, Oxford, 1975.

29. J.L. Barton and M. Morain, "Hydrogen Diffusion in Silicate Glasses," *J. Non. Cryst. Sol.,* **3** 115 (1970).

30. C. Estournes, N. Cornu, and J.L. Guille, "Reduction of Copper in Soda-Lime-Silica Glass by Hydrogen," *J. Non. Cryst. Sol.,* **170** [3] 287-94 (1994).

31. C. Estournes, T. Lutz, and J.L. Guille, "Reduction of Nickel in Soda-Lime Silicate Glass by hydrogen," *J. Non. Cryst. Sol.,* **197** 192-6 (1996).

32. W.D. Johnston and A.J. Chelko, "Reduction of Ions in Glass by Hydrogen," *J. Am. Ceram. Soc.,* **53** [6] 295-301 (1970).

33. J.T. Kohli, B.M. Wright, J.M. Jewell, and J.E. Shelby, "Hydrogen-Induced Coloration of Glasses Containing Arsenic," *Phys. Chem. Glasses,* **31** [4] 133-7 (1990).

34. J.E. Shelby, "Reaction of Hydrogen with Hydroxyl-Free Vitreous Silica," *J. Appl. Phys.,* **51** [5] 2589-93 (1980).

35. J.E. Shelby and J. J. Vitko, "The Reduction of Iron in Soda-Lime-Silicate Glasses by Reaction with Hydrogen," *J. Non. Cryst. Sol.,* **53** [1,2] 155-63 (1982).

36. S.D. Stookey, "Glass Ceramics," U.S. Pat. 2,920,971, 1960.

37. J.J. Hammel, "Nucleation in Glass - A Review," pp. 1-9 in *Advances in Nucleation and Crystallization in Glasses.* Edited by L. L. Hench and S. W. Freiman. The American Ceramic Society, Columbus, OH, 1971.

38. R.H. Doremus, *Rates of Phase Transformations*. pp. 63-91, Academic Press, San Diego, 1985.

39. V.M. Fokin, E.D. Zanotto, N.S. Yuritsyn, and J.W.P. Schmelzer, "Homogeneous Crystal Nucleation in Silicate Glasses: A 40 Year Perspective," *J. Non. Cryst. Sol.,* **352** 2681-714 (2006).

40. L. Granasy and P.F. James, "Nucleation in Oxide Glasses: Comparison of Theory and Experiment," *Proc. R. Soc. Lond. A,* **454** 1745-66 (1998).

41. W. Holand, V. Rheinberger, and M. Schweiger, "Control of Nucleation in Glass Ceramics," *Phil. Trans. R. Soc. Lond. A,* **361** 575-89 (2003).

42. P.F. James, "Nucleation in Glass Forming Systems - A Review," pp. 1-65 in *Nucleation and Crystallization in Glasses.* Edited by J. H. Simmons, D. R. Uhlmann, and G. H. Beall. The American Ceramic Society, Columbus, OH, 1982.

43. J.W.P. Schmelzer, V.M. Fokin, A.S. Abyzov, E.D. Zanotto, and I. Gutzow, "How Do Crystals Form mand Grow in Liquids: Ostwald's Rule of Stages and Beyond," *Int. Jour. Appl. Glass Sci.,* **1** [1] 16-26 (2012).

44. E.D. Zanotto and V.M. Fokin, "Recent Studies of Internal and Surface Nucleation in Silicate Glasses," *Phil. Trans. R. Soc. Lond. A,* **361** 591-613 (2003).

45. P.F. James, "Volume Nucleation in Silicate Glasses," pp. 35-89 in *Glasses and Glass-Ceramics.* Edited by M. H. Lewis. Chapman and Hall, London, 1989.

46. D. Turnbull and J.C. Fisher, "Rate of Nucleation in Condensed Systems," *J. Chem. Phys.,* **17** [1] 71-3 (1949).

47. C.J.R. Gonzalez-Oliver and P.F. James, "Crystal Nucleation and Growth in Soda-Lime-Silica Glasses," *Glass Technol.,* **20** [6] 204 (1979).

48. C.J.R. Gonzalez-Oliver, P.S. Johnson, and P.F. James, "Influence of Water Content on the Rates of Crystal Nucleation and Growth in Lithia-Silica and Soda-Lime-Silica Glasses," *J. Mater. Sci.,* **14** [5] 1159-69 (1979).

49. P.F. James, "Kinetics of Crystal Nucleation in Lithium Silicate Glasses," *Phys. Chem. Glasses,* **15** [4] 95-105 (1974).

50. D. Kashciev, "Solution of the Non-Steady State Problem in Nucleation Kinetics," *Surface Science,* **14** 209-20 (1969).

51. K.F. Kelton, "Crystal Nucleation in Liquids and Glasses," *Solid State Physics,* **45** 75-177 (1991).

52. W.D. Kingery, H.K. Bowen, and D.R. Uhlmann, *Introduction to Ceramics, Second Ed.* pp. 350-395, John Wiley & Sons, New York, 1976.

53. S.P. Mukherjee and P.S. Rogers, "Nucleation and Crystal Growth in Silicate Glasses Containing Fluorides," *Phys. Chem. Glasses,* **8** [3] 81-7 (1967).

54. G. Tammann, "Glass Formation and Devitrification," *Z. Elektrochemie,* **10** 532-8 (1904).

55. E.D. Zanotto, "Isothermal and Adiabatic Nucleation in Glass," *J. Non. Cryst. Solids,* **89** 361-70 (1987).

56. J.W. Christian, *The Theory of Transformations in Metals and Alloys*. pp. 175-205, Pergamon, London, 1965.

57. R.J. Charles, "Phase Separation in Borosilicate Glasses," *J. Am. Ceram. Soc.*, **47** [11] 559-63 (1964).

58. R.J. Charles, "Metastable Liquid Immiscibility in Alkali Metal Oxide-Silica Systems," *J. Am. Ceram. Soc.*, **49** [2] 55-62 (1966).

59. D.R. Uhlmann, "Crystal Growth in Glass-Forming Systems - A Review," pp. 91-115 in *Advances in Nucleation and Crystallization in Glasses.* Edited by L. L. Hench and S. W. Freiman. The American Ceramic Society, Columbus, OH, 1971.

60. D.R. Uhlmann, "Crystal Growth in Glass Forming Systems: A Ten Year Perspective," pp. 80-124 in *Nucleation and Crystallization in Glasses.* Edited by J. H. Simmons, D. R. Uhlmann, and G. H. Beall. The American Ceramic Society, Columbus, OH, 1982.

61. D. Turnbull and M.H. Cohen, *Modern Aspects of the Vitreous State*, Vol. 1. pp. 32-45, Edited by J. D. Mackenzie. Butterworths, London, 1960.

62. R.T. DeHoff, *Thermodynamics in Materials Science*. pp. 301-54, McGraw-Hill, New York, 1993.

63. A. Paul, *Chemistry of Glasses*, 2nd ed. pp. 219-45, Chapman and Hall, New York, 1990.

64. H.D. Schreiber, S.J. Kozak, A.L. Fritchman, D.S. Goldman, and H.A. Schaeffer, "Redox Kinetics and Oxygen Diffusion in a Borosilicate Melt," *Phys. Chem. Glasses*, **27** [4] 152-77 (1986).

65. A. Paul and R.W. Douglas, "Mutual interactoin of Different Redox Pairs in Glass," *Phys. Chem. Glasses*, **7** [1] 1-13 (1966).

66. J. G.H. Sigel, "Optical Absorption of Glasses," pp. 4-89 in Vol. 12, *Treatise on Materials Science and Technology, Glass I: Interaction with Electromagnetic Radiation.* Edited by M. Tomozawa and R. H. Doremus. Academic Press, New York, 1977.

67. R.H. Doremus, S. Kao, and R. Garcia, "Optical Absorption of Small Copper Particles and the Optical Properties of Copper," *Applied Optics*, **31** [27] 5773-8 (1992).

68. R.H. Doremus, "Optical Properties of Small Silver Particles," *J. Chem. Phys.*, **42** [1] 414-7 (1965).

69. R.D. Maurer, "Nucleation and Growth in a Photosensitive Glass," *J. Appl. Phys.*, **29** [1-8] (1958).

70. R.H. Doremus, "Optical Properties of Small Gold Particles," *J. Chem. Phys.*, **40** [8] 2389-96 (1964).

71. D.G. Galimov, A.M. Gubaidullina, and A.I. Neich, "Optical Properties of Colloidal Particles of Copper in Glasses," *Fizika i Khimiya Stekla.*, **13** [1] 50-4 (1987).

72. H. Rawson, "The Calculation of Transmission Curves of Glass Stained by Copper and Silver Compounds," *Phys. Chem. Glasses*, **6** [3] 81-4 (1965).

73. H. Nagao, M. Misonou, and H. Kawahara, "Mechanism of Coloration in Copper-Stained Float Glass," *J. Non. Cryst. Sol.*, **120** 199-206 (1990).

74. Y. Abe and D.E. Clark, "Determination of Combined Water in Glasses by Infrared Spectroscopy," *J. Mater. Sci. Letters*, **9** [2] 244-5 (1990).

75. F. Geotti-Bianchini and L.D. Riu, "Infrared Spectroscopic Analysis of Water Incorporated in the Structure of Industrial Soda-Lime-Silica Glasses," *Glastech. Ber. Glass Sci. Technol.*, **68** [7] 228-40 (1995).

76. H. Scholze, "Der Einbau des Wassers in Glasern," *Glastech. Ber.*, **32** [3] 81-8 (1959).

77. H. Scholze, "Der Einbau des Wassers in Glasern," *Glastech. Ber.*, **32** [4] 142-52 (1959).

78. H. Scholze and A. Dietzel, "Infrared Studies of Hydrous Silicates," *Naturwissenchaften*, **42** 342-3 (1955).

79. R.V. Adams, "Infrared Absorption Due to Water in Glasses," *Phys. Chem. Glasses*, **2** [2] 39-49 (1961).

80. T. Bell, G. Hetherington, and K.H. Jack, "Water in Vitreous Silica, Part 2: Some Aspects of Hydrogen-Water-Silica Equilibria," *Phys. Chem. Glasses*, **3** [5] 141-6 (1962).

81. G. Hetherington and K.H. Jack, "Water in Vitreous Silica, Part I. Influence of 'Water' Content on the Properties of Vitreous Silica," *Phys. Chem. Glasses*, **3** [4] 129-33 (1962).

82. B.D. Cullity, *Elements of X-Ray Diffraction*, 2nd ed. pp. 96-103, Addison-Wesley Publishing Company, Reading, Massachusetts, 1956.

83. G.K. Williamson and W.H. Hall, "X-Ray Line Broadening From Filed Aluminum and Wolfram," *Acta Met.,* **1** 22-31 (1953).

84. R. Jenkins and R.L. Snyder, *Introduction to X-Ray Powder Diffractometry*. pp. 89-102, John Wiley & Sons, New York, 1996.

85. J.E. Shelby and J.J. Noonan, "Formation and Properties of Sodium Indium Silicate Glasses," *Phys. Chem. Glasses,* **39** [1] 36-40 (1998).

86. L.R. VanCott, "Hydrogen-Induced Formation of Colloids in Sodium Indium Silicate Glasses"; Bachelor of Science Thesis. Alfred University, Alfred, NY, 2007.

87. K.F.J. Heinrich, "Identification of Inclusions With the Electron Probe Microanalyzer," *ASTM Special Technical Publication,* **393** 39-46 (1965).

88. C. Kuhl, H. Rudow, and W.A. Weyl, "Oxidation and Reduction Equilibria in Colored Glasses," *Sprechsall,* **71** [7] 117-8 (1938).

89. H.J. Tress, "Thermodynamic Approach to Redox Equilibria in Glasses," *Phys. Chem. Glasses,* **1** 196-7 (1960).

90. R.W. Hopkins and W.H. Manring, "Factors Influencing Control of Color in Amber Glasses," *Glass Ind.,* **34** 251-76 (1953).

91. W. Simpson and D.D. Myers, "The Redox Number Concept and its Use by the Glass Technologist," *Glass Technol.,* **19** [4] 82-5 (1978).

92. H.J.T. Ellingham, "Reducibility of Oxides and Sulfides in Metallurgical Processes," *J. Soc. Chem. Ind.,* **63** 125-33 (1944).

93. S. Luidold and H. Antrekowitsch, "Hydrogen as a Reducing Agent: Thermodynamic Possibilities," *J. Mater. Sci.,* **59** [10] 58-62 (2007).

94. S. Luidold and H. Antrekowitsch, "Hydrogen as a Reducing Agent: State-of-the-Art Science and Technology," *J. Mater. Sci.,* **59** [6] 20-6 (2007).

95. V. McGahay and M. Tomozawa, "The Effect of Water on Phase Separation of Sodium Silicate Glasses," *J. Non. Cryst. Sol.,* **167** 127-38 (1994).

96. O.V. Mazurin, G.P. Roskova, and V.P. Kluyev, "Properties of Phase-Separated Soda-Silica Glasses as a Means of Investigation of Their Structure," *Disc. Farad. Soc.,* **50** [191-199] (1970).

97. E.A. Porai-Koshits and V.I. Averjanov, "Primary and Secondary Phase Separation of Sodium Silicate Glasses," *J. Non. Cryst. Sol.,* **1** 29-38 (1968).

98. W. Haller, D.H. Blackburn, and J.H. Simmons, "Miscibility Gaps in Alkali-Silicate Binaries-Data and Thermodynamic Interpretation," *J. Am. Ceram. Soc.,* **57** [3] 120-6 (1974).

99. W.D. Kingery, "Factors Affecting Thermal Stress Resistance of Ceramic Materials," *J. Am. Ceram. Soc.,* **38** [1] 3-15 (1955).

100. J.J. Noonan, J.J. Peek, and J.E. Shelby, "Formation and Properties of Sodium Praseodymium Silicate Glasses," *Phys. Chem. Glasses: Eur. J. Glass Sci. Technol. B,* **48** [2] 1-6 (2007).

101. J.M. Jewell and J.E. Shelby, "Effect of Water Content on the Properties of Sodium Aluminosilicate Glasses," *J. Am. Ceram. Soc.,* **75** [4] 878-83 (1992).

102. L. Nemec, "Refining of Glass Melts," *Glass Technol.,* **15** [6] 153-6 (1974).

103. B.J. Todd, "Outgassing of Glass," *J. Appl. Phys.,* **26** [10] 1238 (1955).

104. Encyclopedia Chemical Technology, *Glass*; pp. 807-80. Edited by D.C. Boyd and D.A. Thompson M. Grayson and D. Eckroth. Wiley, New York, 1980.

105. D.R. Cockram, Z. Haider, and G.J. Roberts, "The Diffusion of "Water" in Soda-Lime-Silica Glasses," *Phys. Chem. Glasses,* **10** 18 (1969).

106. A.J. Moulson and J.P. Roberts, "Water in Silica Glass," *Trans. Brit. Ceram. Soc.,* **57** 1208 (1960).

107. A.J. Moulson and J.P. Roberts, "Entry of Water into Silica Glass," *Nature,* **182** 200-1 (1958).

108. J.E. Shelby, "Reaction of Hydrogen with Optical Defects in Glasses," *J. Am. Ceram. Soc.,* **67** [5] C-93-4 (1984).

109. R.H. Doremus, "Water Speciation in Silicate Glasses and Melts: Langmuir Limited Site Model," *Am. Min.,* **85** [11-12] 1674-80 (2000).

110. F. Holtz, H. Behrens, D.B. Dingwell, and W. Johannes, "H2O Solubility in Haplogranitic Melts: Compositional, Pressure, and Temperature Dependence," *Am. Mineral,* **80** 94-108 (1995).

111. K.S. Pitzer and S.M. Sterner, "Equations of State Valid Continuously from Zero to Extreme Pressures with H2O and CO2 as Examples," *J. Chem. Phys.,* **101** [4] 3111-6 (1994).

112. F. Holtz, J. Roux, H. Behrens, and M. Pichavant, "Water Solubility in Silica and Quartzofeldspathic Melts," *Am. Mineral.*, **85** [5-6] 682-86 (2000).

113. F.A. Ochs and R.A. Lange, "The Partial Molar Volume, Thermal Expansivity, and Compressibility of H2O in NaAlSi3O8 Liquid: New Measurements and an Internally Consistent Model," *Contrib. Mineral. Petrol.*, **129** [2-3] 155-65 (1997).

114. D.L. Edson, "Effects of Halogen Substitutions on the Formation of Copper Colloids by Hydrogen Reduction in Sodium Borate Glasses." Doctor of Science Thesis, Alfred University, Alfred, NY, 2003.

115. J.A. Creighton and D.G. Eadon, "Ultraviolet-Visible Absorption Spectra of the Colloidal Metallic Elements," *J. Chem. Soc., Faraday Trans.*, **87** [24] 3881-91 (1991).

116. R.H. Doremus, *Diffusion of Reactive Species in Solids and Melts*. pp. 24-35, John Wiley & Sons, New York, 2002.

117. F. Booth, "Theory of Surface Diffusion Reactions," *Trans. Faraday Soc.*, **44** 796-801 (1948).

118. O.L. Anderson and D.A. Stuart, "Calculation of Activation Energy of Ionic Conductivity in Silica Glasses by Classical Methods," *J. Am. Ceram. Soc.*, **37** [12] 573-80 (1954).

119. J.C. Slater, "Atomic Radii in Crystals," *Journal of Chem. Phys.*, **15** 3199-204 (1964).

120. I. Alstrup, M.T. Tavares, C.A. Bernardo, O. Sorensen, and J.R. Rostrup-Nielsen, "Carbon Formation on Nickel and Nickel-Copper Alloy Catalysts," *Materials and Corrosion*, **49** 367-72 (1998).

121. C.A. Mackliet, "Diffusion of Iron, Cobalt, and Nickel in Single Crystals of Pure Copper," *Physical Review*, **109** [4] 1964-70 (1958).

APPENDIX

A-1 Background Correction for IR Spectra

Complex backgrounds made data analysis quite difficult for the IR spectra collected throughout this work. Three separate methods were investigated and two were deemed valid for use in this study. Typical IR spectra are corrected based on a simple Y-value shift. This is fine as long as there is no wavelength dependent scattering contributing to the overall spectra. The data collected here exhibited a large degree of wavelength dependent scattering. This led to the development of a sloped background extraction technique based on the initial linear portion of the spectra from 4100-3800 cm^{-1}. It is not valid to apply this technique to the pure spectra being collected due to the presence of near IR bands in nickel and cobalt containing glasses. This led to the use of difference spectra to correct the data. The difference spectra show only the changes that have occurred due to treatment with respect to baseline. This left a very linear portion in the region aforementioned, although with a fair amount of scatter. Regardless, the data was successfully corrected using this sloped technique. It became apparent during this procedure that there is a curvature developing in much of the data. Since small metal clusters are developing in these glasses, a Rayleigh type of scattering may be possible. The difference spectra was then process with a Rayleigh correction based on the λ^{-4} relationship this scattering has with small particles. These two correction techniques are shown on a uncorrected difference spectra plot in Figure 68 . After subtraction of the background it is clear there is a difference between the two (Figure 69). It is clear that the two differ more dramatically at lower wavenumbers, and it is assumed at this point that the Rayleigh correction is more accurate than a typical sloped correction, especially if the lower wavenumber bands must be considered. The percent difference between the two correction techniques is shown in Table XIX. This is only for this system shown. As the degree of curvature of the background increases, so too does the difference of the lower wavenumber regions. This was difficult to quantify but the 3550 cm-1 band was found to not differ more than ~9-10% from the Rayleigh correction. The Rayleigh

correction is also not always valid as some spectra exhibited the typical absorbance wavelength independent shift, and others exhibited a background that is still not understood (Figure 70).

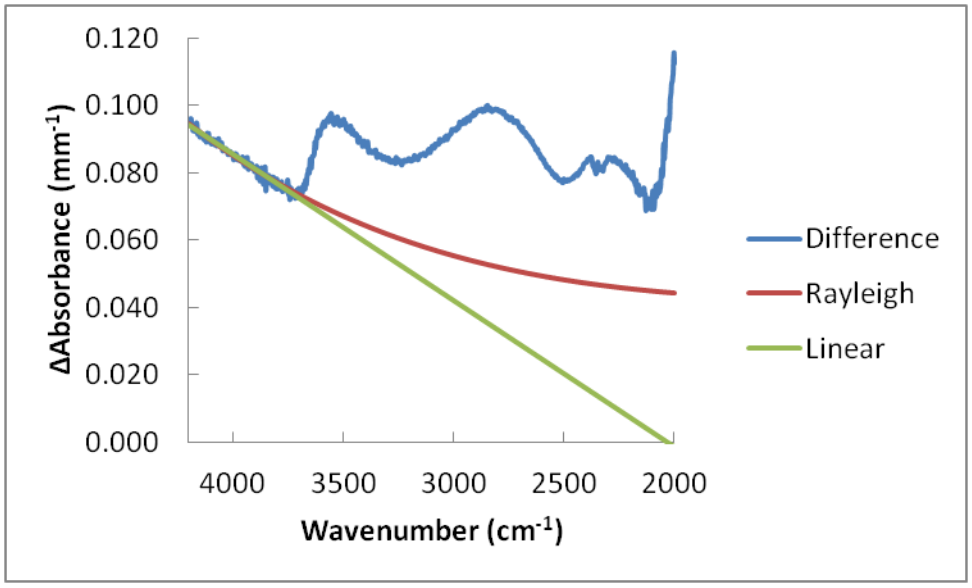

Figure 68. Different correction techniques shown on an uncorrected difference spectra for 1 mol% Ni containing SLS glass treated at 600°C for 25 hours.

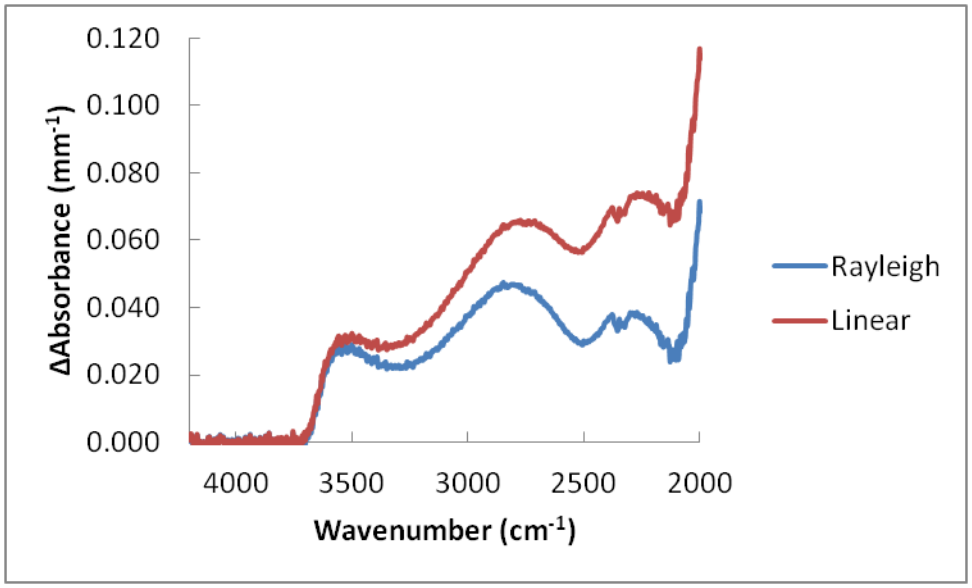

Figure 69. Corrected difference spectra for 1 mol% Ni containing SLS glass treated at 600°C for 25 hours.

Table XIX. Band intensities with the different correction techniques.

Band Position	Rayleigh	Linear	% Difference
3550 cm^{-1}	.029 mm^{-1}	.032 mm^{-1}	9.80%
2790 cm^{-1}	.047 mm^{-1}	.066 mm^{-1}	33.60%
2270 cm^{-1}	.038 mm^{-1}	.074 mm^{-1}	64.3%

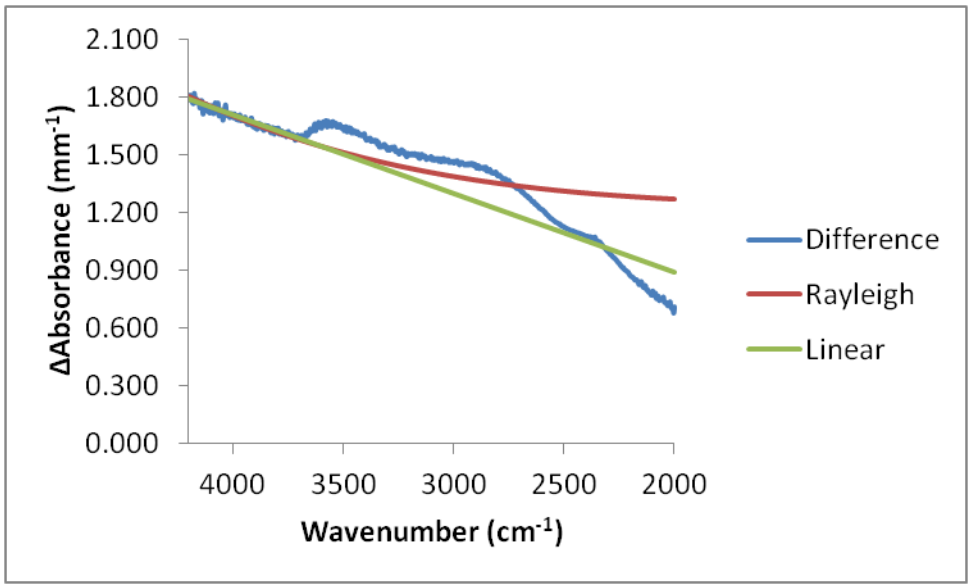

Figure 70. Different correction techniques shown on an uncorrected difference spectra for 1 mol% Cu containing SLS glass treated at 600°C for 52 hours.